SECOND-ORDER SMALL DISTURBANCE THEORY FOR

HYPERSONIC FLOW OVER POWER-LAW BODIES

A Dissertation

Presented to

the Faculty of the School of Engineering and Applied Science

University of Virginia

In Partial Fulfillment

of the Requirements for the Degree

Doctor of Philosophy (Aerospace Engineering)

by

James C. Townsend

December 20, 1974

APPROVAL SHEET

This dissertation is submitted in partial fulfillment of

the requirements for the degree of

Doctor of Philosophy (Aerospace Engineering)

_____
Author

Approved:

_____
Faculty Advisor

_____
Dean, School of Engineering
and Applied Science

_____
(Date)

ABSTRACT .

Beginning with the equations for conservation of mass, conservation of momentum, and conservation of energy for the inviscid, two-dimensional or axisymmetric adiabatic flow of an ideal gas, similarity solutions have been found which give the flow field to order-δ^2 about power-law bodies in the hypersonic limit $M_\infty \to \infty$, where δ is a body slenderness parameter. Some years ago, the hypersonic small disturbance equations were used to obtain "zeroth-order" similarity solutions for flow over power-law bodies. The second-order solutions, which reflect the effects of the second-order terms in the equations, are obtained by applying the method of small perturbations in terms of the body slenderness parameter δ to these zeroth-order solutions. The method is applied by writing each flow variable as the sum of a zeroth-order and a perturbation function, each multiplied by the axial variable raised to a power. When these expanded variables are substituted into the flow equations, a zeroth-order set and a perturbation set of four first-order ordinary differential equations is obtained, and the axial variation drops out. These equations are integrated numerically from the shock, where the boundary conditions are known from the Rankine-Hugoniot relations, toward the body.

The order-δ^2 solutions which are obtained are independent of the slenderness parameter δ and thus are universal

in that they apply for all values of δ for which $\delta^4 \ll 1$. However, except when the body power-law exponent is equal to unity, the velocity functions, which form part of the solution, have singularities at the body surface. These singularities are an effect of the entropy layer caused by the nose bluntness. Since the singularities are not removed by any of several methods tried, the solutions can only be applied away from the body surface. (It is suggested for future work that the singularities probably could be removed by applying the method of matched asymptotic expansions.)

In comparisons with the exact solutions for inviscid flow over wedges and circular cones, the order-δ^2 similarity results give excellent agreement for δ less than about 0.4, corresponding to wedge or cone angles up to about 20°. Over an even larger range, the order-δ^2 surface pressure predictions are superior to the Newtonian pressure law. The order-δ^2 results are a significant improvement over the zeroth-order results for body angles greater than about 12°. In comparisons with experimental shock wave shapes and surface pressure distributions for 3/4-power axisymmetric bodies, the order-δ^2 similarity solutions give good results, considering that Mach number and boundary layer displacement effects are not included in the theory. For body fineness ratios near two, the effects of the order-δ^2 terms are significant only very near the body nose, whereas for a

fineness ratio near unity the order-δ^2 terms has a large
effect over almost the entire body.

The order-δ^2 similarity solutions are developed for
infinite Mach number, but the derivation shows that they are
compatible with shock-strength perturbation solutions,
which introduce Mach number effects. Also, while all results
obtained are for no flow through the body surface (as a
boundary condition), the derivation indicates that small
amounts of blowing or suction through the wall could be
easily accomodated. Finally, it is noted that a correlation
suggested by Hornung for the shock wave shape and body
pressure distribution can be applied exactly to all of the
flow variables in the order-δ^2 similarity solution form.
This finding suggests for future work a possible refinement
of the present derivation, using the local body or shock
wave slope as the small parameter.

ACKNOWLEDGMENTS

TABLE OF CONTENTS

LIST OF FIGURES

FIGURE

PAGE

LIST OF SYMBOLS

a_1, a_2 shock wave displacement constants (equation (7))

B constant in similarity form of stream function (equation (A2))

C_p pressure coefficient, $\dfrac{\bar{p} - \bar{p}_\infty}{\bar{q}_\infty}$

D constant in stream function solution of longitudinal velocity variable (equation (A15))

f body fineness ratio, $\dfrac{\text{length}}{\text{maximum thickness}}$

F similarity pressure function

j exponent in stream function expression (equation (A2))

$\bar{\ell}$ body length

m power law exponent

M_∞ free stream Mach number

p pressure

$\bar{q}_\infty$ free stream dynamic pressure, $\frac{1}{2}\,\bar{\rho}_\infty \bar{u}_\infty^2$

r lateral coordinate

R lateral coordinate of shock wave

u longitudinal velocity

v lateral velocity

v_w flow velocity through body surface (normal to wall)

x longitudinal coordinate

α density ratio at wall, $\dfrac{\rho_w}{\rho_b}$

β alternate shock shape parameter, $\dfrac{2(1-m)}{(1+\sigma)m}$

γ	ratio of specific heats
δ	slenderness parameter, $\dfrac{\bar{R}_o(\bar{\ell})}{\bar{\ell}}$
ε	shock wave strength parameter, $(\delta M_\infty)^{-2}$
η	similarity lateral coordinate
Θ_b	body surface angle
Θ_s	shock wave angle
θ	similarity stream function
μ	similarity lateral momentum function
ν	similarity longitudinal velocity function
ξ	similarity longitudinal coordinate
ρ	density
σ	0 for planar flow, 1 for axisymmetric flow
υ	similarity longitudinal momentum function
φ	similarity lateral velocity function
ϕ_w	similarity velocity through body surface
ψ	similarity density function
$\hat{\psi}$	stream function
ω	entropy function, p/ρ^γ

Subscripts:

a	part of decomposed function multiplied by a_2 (equation (48))
b	body surface
c	part of decomposed function independent of a_2 (equation (48))

s	shock wave
w	flow through the wall
0	zeroth order
1	order ε
2	order δ^2
∞	free stream

A prime denotes the derivative of a function of one variable. A bar over a variable denotes that it has physical dimensions. A tilda over a dependent variable denotes that it is a function of the normalized lateral coordinate r rather than the similarity lateral coordinate η.

CHAPTER I.   INTRODUCTION

A great deal of research has gone into investigating
solutions to the small disturbance equations for hypersonic
flow. One area that has received particular attention is
that of self-similar solutions for power-law profile bodies.
While the effects of shock wave strength have been investi-
gated in connection with these solutions, there apparently
have been no reported efforts to investigate the effects of
neglecting the second-order terms of the complete inviscid
flow equations in order to reduce them to the small distur-
bance form. The purpose of the present study is to determine
the effects of retaining these terms by using a perturbation
analysis to obtain second-order similarity solutions for
power-law bodies.

Since this dissertation will be concerned with finding
a particular set of similarity solutions of the inviscid
flow equations, it is important at the outset to establish
what is meant by similarity solutions in hypersonic flow.
The similar solutions referred to here are solutions for
self-similar flows; i.e. flows for which the flow field
(expressed in suitable coordinates) at any one position
along the body is the same as that at every other position.
(In the corresponding unsteady self-similar flows, the flow
field in suitable coordinates at any one time is the same as
that at every other time.) Inviscid axisymmetric supersonic

1

flow over a cone with an attached shock wave is a classical
example of a self-similar flow and represents a particular
case of the similar solutions discussed herein. For the
cone, the flow field properties (eg. the pressure, the density,
and the velocity components) are themselves constant along
rays from the cone vertex. For the other power-law bodies,
the flow field properties are not constant themselves, but
similarity functions describing these properties are
constant (to the order of the solution) along curved power-
law paths from the nose of the body.

The similar solution approach to solving the flow
equations is valuable because it allows a reduction in the
number of independent variables in the problem. In particular,
for hypersonic flow about power-law bodies, the similarity
approach reduces a system of partial differential equations
to a system of ordinary differential equations. As noted by
Hayes and Probstein (1), generally these flows occur only
for a self-similar fluid (the most practical example of which
is a perfect gas with a constant ratio of specific heats)
and a self-similar shock wave, i.e. one having the same
density ratio across it at every position.

All of the early investigations of similar solutions
related to the present problem were concerned with unsteady
flows. Early in the Second World War, Taylor (2) developed
a similar solution for the flow behind the spherical shock

wave produced by the instantaneous release of energy at a
point (e.g., an atomic explosion). Sakurai (3,4) generalized
Taylor's approach to obtain solutions for cylindrical and
planar shocks as well. He also introduced perturbation
analysis as a means of obtaining solutions for more moderate
shock wave strengths. The equivalence of these unsteady flows
to steady flows in one additional space dimension was pointed
out by Hayes (5). This equivalence applies to the inviscid
flow equations reduced to the hypersonic small disturbance
form, as derived by Van Dyke (6).

Lees (7) found that there are self-similar flow fields
for bodies having power-law profiles, and Lees and Kubota
(8) determined the range of power-law exponents for which
the similarity holds. Kubota (9) obtained numerical solutions
for this case (herein called the "zeroth-order" case); he
also applied a perturbation in the strong shock parameter (as
Sakurai had done for unsteady flow) and numerically obtained
first-order similar solutions for moderately strong shock
waves. Mirels (10) computed additional and more accurate
numerical results for the zeroth-order and moderately-strong
shock wave cases. He also derived approximate analytical
solutions for these cases.

The parallel but independent work of investigators in
the USSR has been thoroughly described by Hayes and
Probstein (1). Beginning at about the same time as Taylor,
Sedov (11) studied the intense spherical explosion problem

in a more general form and developed an analytic solution for it (12). Grodzovskii (13) and Chernyi (14) applied the unsteady results to the steady hypersonic flow problem. Stanyukovich (15) and others investigated a number of related problems.

All of the important developments in the use of hypersonic small disturbance theory to obtain solutions for power-law bodies were treated in a unified way by Mirels (16), who added an analysis of perturbed power-law body shapes. More recently, Freeman (17) investigated the effects of the entropy layer caused by the nose bluntness of the power-law bodies and determined the power-law exponents below which the entropy-layer effects predominate. Again independently, Sychev (18) developed a correction to the power-law body shape to account for the effect of the entropy layer.

A few experimental investigations of the flow field over power-law bodies have been made. Kubota (9) compared his theoretical results to surface pressure distribution and shock wave shapes measurements for 2/3- and 3/4-power bodies, obtaining good agreement for the more slender bodies. Peckham (19) measured pressure distributions and shock wave shapes for a series of power-law bodies, some of which fall in the similar-solution range. Freeman, Cash and Bedder (20) and Beavers (21) also presented detailed shock shape data for series of power-law bodies, registering some disagreement

with Kubota's results. Spencer and Fox (22) present aerodynamic drag and other data for several power-law bodies over a wide Mach number range. Ashby (27) presents aerodynamic data for a similar series of bodies over a range of Reynolds numbers at Mach 6, and Ashby and Harris (28) use method of characteristics and boundary layer computer programs to show the important effect of boundary layer transition on the total drag of those bodies.

Townsend (23) applied the zeroth-order solution of Kubota and Mirels, with their shock-strength parameter perturbation and a boundary layer displacement correction, to the problem of estimating the forces and moments on a half-axisymmetric body under a thin, flat wing. In order to study a range of configurations at a moderately hypersonic Mach number, Townsend applied his method to configurations which are marginally slender, (i.e. to configurations for which the errors arising from body thickness are small but not negligible). This type of application points up two reasons for seeking solutions which include the effects of the second-order terms for body slenderness in the flow equations: (1) to assess the error caused by making the small disturbance assumption, and (2) to improve the accuracy of calculations for marginally slender bodies.

When compared with experimental data for axisymmetric
power-law bodies and for wing — conical-body configurations,
Townsend's method gave good agreement where the basic
assumptions were satisfied. An example series of computations
with variations in the principal parameters at a full-scale
flight condition showed that varying the power-law exponent
has a greater effect on longitudinal stability and trim than
on the lift-drag ratio. The computations for Mach 6 gave
higher maximum lift-drag ratios, higher drag coefficients at
zero lift, but essentially the same stability characteristics
as their counterparts for Mach 12.

In the present study the second-order similarity solu-
tions were obtained by a perturbation method. This method
used expansions of the variables in terms of a small parameter
to obtain higher-order solutions as perturbations from a
known zeroth-order solution. The approach was very similar
to that of Sakurai (4), Kubota (9), and Mirels (16) in their
first-order determinations of the effects of shock wave
strength; but, the small parameter used herein was a body
slenderness parameter rather than the shock strength parameter.
Van Dyke (29) describes the application of perturbation
methods to fluid mechanics, and Van Dyke (30) shows how, in
favorable cases, such solutions can be extended to improve
convergence when the perturbation quantity is not small.

The importance of the results to be obtained from the present study lies in their practical application. The principle area for this is in estimating the aerodynamic characteristics of generalized configurations (e.g., Townsend's (23) family of wing-body combinations). By improving the results of such studies and by better defining their limits of applicability, the present work contributes to their usefulness in suggesting designs (or parts of designs) for such hypersonic vehicles as transports or re-entry spacecraft.

The remainder of this dissertation will describe the development of the solutions and present the results. Chapter II gives the theoretical development. It goes through the transformations of the flow equations required to put them into similarity form, discusses the results of keeping terms of different order, describes the application of the boundary conditions, and develops an alternative formulation of the problem. Chapter III presents the general scheme for solving the equations and deals with the difficulties which arise. Chapter IV discusses the results and their region of validity. Chapter V gives the conclusions reached as a result of this study. The Appendix describes an approximate analytical solution used near the body surface, where the equations are singular.

CHAPTER II. THEORY

A. Transformation of Basic Flow Equations

This section will show how the basic flow equations can be transformed to obtain a separation of variables for the case of hypersonic flow over power-law bodies. The starting point for this process is the system of steady, two-dimensional, inviscid flow equations for a perfect gas in physical variables:

Continuity:
$$\frac{\partial \bar{\rho}\bar{u}}{\partial \bar{x}} + \frac{\partial \bar{\rho}\bar{v}}{\partial \bar{r}} + \sigma \frac{\bar{\rho}\bar{v}}{\bar{r}} = 0$$

Longitudinal momentum:
$$\bar{u} \frac{\partial \bar{u}}{\partial \bar{x}} + \bar{v} \frac{\partial \bar{u}}{\partial \bar{r}} + \frac{1}{\bar{\rho}} \frac{\partial \bar{p}}{\partial \bar{x}} = 0$$

Lateral momentum:
$$\bar{u} \frac{\partial \bar{v}}{\partial \bar{x}} + \bar{v} \frac{\partial \bar{v}}{\partial \bar{r}} + \frac{1}{\bar{\rho}} \frac{\partial \bar{p}}{\partial \bar{r}} = 0$$

Energy:
$$\left(\bar{u} \frac{\partial}{\partial \bar{x}} + \bar{v} \frac{\partial}{\partial \bar{r}} \right) \left(\frac{\bar{p}}{\bar{\rho}^{\gamma}} \right) = 0$$

$$(1)$$

The constant σ in the continuity equation has the value 0 for planar flow (Cartesian coordinates) or the value 1 for axisymmetric flow (cylindrical coordinates). The bars over the variables indicate that they are dimensional quantitites.

Normalization. The initial treatment of these equations follows that of Kubota (9) (also covered by Mirels (16)),

8

except that no terms are dropped. Kubota showed that for slender bodies in hypersonic flow the variables can be normalized using the expressions:

$$x = \frac{\bar{x}}{\bar{\mathcal{l}}} \ , \quad r = \frac{\bar{r}}{\delta\bar{\mathcal{l}}} \ , \quad p = \frac{\bar{p}}{\delta^2\bar{\rho}_\infty\bar{u}_\infty^2}$$

$$\rho = \frac{\bar{\rho}}{\bar{\rho}_\infty} \ , \quad u = \frac{\bar{u} - \bar{u}_\infty}{\delta^2\bar{u}_\infty} \ , \quad v = \frac{\bar{v}}{\delta\bar{u}_\infty} \quad\quad\Biggr\} \ (2)$$

The δ is a body slenderness parameter (to be discussed later) introduced so as to make the dimensionless variables of order unity. These variables are substituted into equations (1) to obtain the normalized flow equations:

Continuity: $\quad \delta^2\frac{\partial\rho u}{\partial x} + \frac{\partial\rho}{\partial x} + \frac{\partial\rho v}{\partial r} + \sigma\frac{\rho v}{r} = 0$

Longitudinal momentum: $\quad \delta^2 u\frac{\partial u}{\partial x} + \frac{\partial u}{\partial x} + v\frac{\partial u}{\partial r} + \frac{1}{\rho}\frac{\partial p}{\partial x} = 0$

Lateral momentum: $\quad \delta^2 u\frac{\partial v}{\partial x} + \frac{\partial v}{\partial x} + v\frac{\partial v}{\partial r} + \frac{1}{\rho}\frac{\partial p}{\partial r} = 0$

$\left. \phantom{\begin{array}{c}1\\1\\1\\1\\1\\1\\1\end{array}}\right\} \ (3)$

Energy: $\quad \left(\delta^2 u\frac{\partial}{\partial x} + \frac{\partial}{\partial x} + v\frac{\partial}{\partial r}\right)\left(\frac{p}{\rho^\gamma}\right) = 0$

Note that each of these equations contains a leading term in δ^2. If the body were sufficiently slender, the order-δ^2 terms could be dropped, leaving the hypersonic small disturbance equations used by other workers. For the present study, however, the equations are retained in the complete form.

Similarity variables. The next step is to put the flow variables into similarity forms. Still following Kubota (9), these will be found by comparison with the flow through an oblique shock wave. The normalized flow variables just behind an oblique shock are (24):

$$p_s = \frac{\bar{p}_s}{\delta^2 \bar{\rho}_\infty \bar{u}_\infty^2} = \frac{1}{\delta^2 \gamma M_\infty^2} \frac{\bar{p}_s}{\bar{p}_\infty}$$

$$= \frac{1}{\gamma \delta^2 M_\infty^2} \left[\frac{2\gamma M_\infty^2 \sin^2\Theta_s - (\gamma-1)}{\gamma + 1} \right]$$

$$\rho_s = \frac{\bar{\rho}_s}{\bar{\rho}_\infty} = \frac{(\gamma+1) M_\infty^2 \sin^2\Theta_s}{(\gamma-1) M_\infty^2 \sin^2\Theta_s + 2}$$

$$u_s = \frac{\bar{u}_s - \bar{u}_\infty}{\delta^2 \bar{u}_\infty} = \frac{1}{\delta^2} \left(\frac{\bar{u}_s}{\bar{u}_\infty} - 1 \right) = \frac{1}{\delta^2} \left[\frac{-2(M_\infty^2 \sin^2\Theta_s - 1)}{(\gamma+1) M_\infty^2} \right]$$

$$v_s = \frac{\bar{v}_s}{\delta \bar{u}_\infty} = \frac{1}{\delta} \left[\frac{2(M_\infty^2 \sin^2\Theta_s - 1)}{(\gamma+1) M_\infty^2} \cot \Theta_s \right]$$

If the shock wave shape is given by $R(x)$, its slope is $\bar{R}'(\bar{x}) \equiv \frac{d\bar{R}}{d\bar{x}} = \delta \frac{dR}{dx} = \delta R'$. The shock wave angle Θ_s is related to slope by $\tan \Theta_s = \bar{R}' = \delta R'$, from which $\sin^2\Theta_s = \frac{\delta^2 R'^2}{1 + \delta^2 R'^2}$. Putting these results into the oblique shock relations gives (for R' of order unity):

$$p_s = \frac{2}{\gamma+1} \left[\frac{R'^2}{1+\delta^2 R'^2} - \frac{\gamma-1}{2\gamma} \epsilon \right]$$

$$= \frac{2}{\gamma+1} R'^2 - \frac{2}{\gamma+1} \delta^2 R'^4 - \frac{\gamma-1}{\gamma+1} \frac{\epsilon}{\gamma} + 0(\delta^4) \qquad (4a)$$

$$\rho_s = \frac{\gamma+1}{\gamma-1} \bigg/ \left[1 + \frac{2}{\gamma-1} \frac{1 + \delta^2 R'^2}{R'^2} \epsilon \right] \qquad (4b)$$

$$= \frac{\gamma+1}{\gamma-1} - \frac{2(\gamma+1)}{(\gamma-1)^2} \frac{\epsilon}{R'^2} + 0(\delta^4)$$

$$u_s = - \frac{2}{\gamma+1} \left[\frac{R'^2}{1+\delta^2 R'^2} - \epsilon \right]$$

$$= - \frac{2}{\gamma+1} R'^2 + \frac{2}{\gamma+1} \delta^2 R'^4 + \frac{2}{\gamma+1} \epsilon + 0(\delta^4) \qquad (4c)$$

$$v_s = \frac{2}{\gamma+1} \left[\frac{R'}{1 + \delta^2 R'^2} - \frac{\epsilon}{R'} \right]$$

$$= \frac{2}{\gamma+1} R' - \frac{2}{\gamma+1} \delta^2 R'^3 - \frac{2}{\gamma+1} \frac{\epsilon}{R'} + 0(\delta^4) \qquad (4d)$$

Here $\epsilon \equiv \dfrac{1}{\delta^2 M_\infty^2}$ is a shock strength parameter; as $\epsilon \to 0$,

$\dfrac{\bar{\rho}_s}{\bar{\rho}_\infty} \to \dfrac{\gamma+1}{\gamma-1}$, the limiting value for shock wave strength. Using

these equations as guides, the flow variables are taken to

have the forms:

$$p = \tilde{F}_0(r) R'^2 + \delta^2 \tilde{F}_2(r) R'^4 + \epsilon \tilde{F}_1(r)$$

$$\rho = \tilde{\psi}_0(r) + \delta^2 \tilde{\psi}_2(r) R'^2 + \epsilon \tilde{\psi}_1(r)(R')^{-2}$$

$$u = \tilde{v}_0(r) R'^2 + \delta^2 \tilde{v}_2(r) R'^4 + \epsilon \tilde{v}_1(r)$$

$$v = \tilde{\phi}_0(r) R' + \delta^2 \tilde{\phi}_2(r) R'^3 + \epsilon \tilde{\phi}_1(r)(R')^{-1}$$

$$\left. \right\} \quad (5)$$

At this point, in order to get an expression for the shock wave shape, consideration is narrowed to flows about power-law bodies. Under the hypersonic small disturbance assumptions, a power-law body ($\bar{r}_b \sim \bar{x}^m$) produces a power-law shock wave ($\bar{R} \sim \bar{x}^m$) for $\frac{2}{3+\sigma} < m \leq 1$. (See Lees and Kubota (8).) Specifically, for $\delta^2 \ll 1$ and $\varepsilon \ll 1$, the "zeroth-order" shock shape about a body $\frac{\bar{r}_b}{\bar{\ell}} = \frac{1}{2f} \left(\frac{\bar{x}}{\bar{\ell}}\right)^m$ is given by $\frac{\bar{R}_0}{\bar{\ell}} = \delta \left(\frac{\bar{x}}{\bar{\ell}}\right)^m$; or, in normalized coordinates, the shock shape about a body $r_b = \frac{1}{2\delta f} x^m$ is $R_0 = x^m$ (Figure 1, parts (a) and (b)). Note that for $m=1$ the body is a wedge (for $\sigma = 0$) or a cone (for $\sigma = 1$), both of which are known to have straight shock waves and therefore satisfy the above relations. For $m < 1$, the power-law body has a small blunt nose, so that the shock wave is detached. Consequently, this type of relation between the body and the shock cannot hold in the immediate vicinity of the nose. The effects of nose bluntness on the flow downstream are confined to a thin layer near the body surface. Freeman (17) found that the effects are less than order M_∞^{-2} for $m > \frac{2(\gamma+1)}{(3+\sigma)\gamma+2}$. (For $\gamma = 7/5$ this amounts to $\frac{24}{31} \approx .77$ for $\sigma = 0$ and to $\frac{24}{38} \approx .63$ for $\sigma = 1$).

The expression for the zeroth-order shock wave shape serves to define the slenderness parameter δ. That is, $\bar{R}_0(x) = \delta\bar{\ell} \left(\frac{\bar{x}}{\bar{\ell}}\right)^m$ evaluated at $\bar{x} = \bar{\ell}$ gives the relation $\delta = \frac{R_0(\bar{\ell})}{\bar{\ell}}$. Thus, δ is the tangent of an angle defined by

(a) Physical coordinate system.

(b) Normalized coordinate system.

(c) Similarity coordinate system.

Figure 1.   Power-law and Zero-order Shock in Physical and Transformed Coordinate Systems.

the shock wave position (Figure 1(a.)) and is, in fact, a "mean shock wave angle" parameter. However, since the zeroth-order case implies $M_\infty \to \infty$ (as will be seen), the shock lies near the body so that the shock wave angle and body slenderness are closely related. The definition of δ is made in terms of the shock for convenience, since the solutions are to be found by integrating from the shock to the body.

To aid in the separation of variables, a shock-oriented coordinate system is now introduced (Figure 1(c)). This system has

$$\xi = x \quad \text{and} \quad \eta = \frac{r}{R_o} \tag{6}$$

so that $r = \eta R_o = \eta x^m = \eta \xi^m$. The body surface is then $r_b = \eta_b \xi^m$, where $\eta_b = \frac{1}{2\delta f}$.

The shock wave shape to be used in equations (5) is the zeroth-order shock with Kubota's (9) shock strength perturbation and a separate perturbation for the body slenderness. It is taken to be

$$R(x) = R_o(1 + \delta^2 a_2 R_o'^2 + \varepsilon a_1 m^2 R_o'^{-2}),$$

where the constants a_1 and a_2 are to be determined as part of the solution. (The factor m^2 is included in the

last term of this equation so that it conforms to the usage of Kubota and Mirels.) Putting in $R_o = \xi^m$,

$$R(\xi) = \xi^m \left[1 + \delta^2 a_2 m^2 \xi^{-2(1-m)} + \varepsilon a_1 \xi^{2(1-m)} \right] \qquad (7)$$

Substituting the derivative of equation (7) into equations (5) and ordering the terms by powers of δ and ε give expressions for the flow variables in the following form (neglecting terms of order δ^4 and of order ε^2):

$$p(\xi,\eta) = F_o(\eta)m^2 \xi^{-2(1-m)} + \delta^2 F_2(\eta)m^4 \xi^{-4(1-m)}$$

$$+ \varepsilon F_1(\eta)m^2$$

$$\rho(\xi,\eta) = \psi_o(\eta) + \delta^2 \psi_2(\eta)m^2 \xi^{-2(1-m)} + \varepsilon\psi_1(\eta) \xi^{2(1-m)}$$

$$u(\xi,\eta) = \nu_o(\eta)m^2 \xi^{-2(1-m)} + \delta^2 \nu_2(\eta)m^4 \xi^{-4(1-m)}$$

$$+ \varepsilon\nu_1(\eta)m^2$$

$$v(\xi,\eta) = \phi_o(\eta)m \xi^{-(1-m)} + \delta^2\phi_2(\eta)m^3 \xi^{-3(1-m)}$$

$$+ \varepsilon\phi_1(\eta) \xi^{(1-m)}$$

$$\left. \right\} (8)$$

The relations between the functions of η and the functions of r in equations (5) are not needed since it is easier to

work with equations (8) directly. These expressions are now ready to be substituted into equations (3) to obtain the transformed flow equations. In taking the derivatives of these variables it is necessary to note that, whereas $\xi = x$ gives the simple relations $\frac{\partial \xi}{\partial x} = 1$ and $\frac{\partial \xi}{\partial r} = 0$, $\eta = rx^{-m}$ gives $\frac{\partial \eta}{\partial x} = -mrx^{-m-1} = -\frac{m\eta}{\xi}$ and $\frac{\partial \eta}{\partial r} = x^{-m} = \xi^{-m}$; thus

$$\left. \begin{aligned} \frac{\partial}{\partial x} &= \frac{\partial \xi}{\partial x} \frac{\partial}{\partial \xi} + \frac{\partial \eta}{\partial x} \frac{\partial}{\partial \eta} = \frac{\partial}{\partial \xi} - \frac{m\eta}{\xi} \frac{\partial}{\partial \eta} \\[2mm] \text{and} \qquad & \\[2mm] \frac{\partial}{\partial r} &= \frac{\partial \xi}{\partial r} \frac{\partial}{\partial \xi} + \frac{\partial \eta}{\partial r} \frac{\partial}{\partial \eta} = \frac{1}{\xi^m} \frac{\partial}{\partial \eta} \end{aligned} \right\} \quad (9)$$

Equations in similarity variables. When the expressions (8) are substituted into the normalized flow equations (3), these become (away from the nose $\xi = 0$):

Continuity: $\left[\psi_0(\phi_0' + \frac{\sigma}{\eta}\phi_0) - (\eta - \phi_0)\psi_0' \right] m\xi^{-1}$

$+ \delta^2 \left\{ \psi_0\phi_2' + (\psi_0' + \frac{\sigma}{\eta}\psi_0)\phi_2 + \left[\phi_0' + \frac{\sigma}{\eta}\phi_0 - 2(\frac{1-m}{m}) \right] \psi_2 \right.$

$- (\eta - \phi_0)\psi_2' - n\nu_0\psi_0' - \left[n\nu_0' + 2(\frac{1-m}{m})\nu_0 \right] \psi_0 \left. \right\} m^3\xi^{-3+2m}$

$+ \varepsilon \left\{ \psi_0\phi_1' + (\psi_0' + \frac{\sigma}{\eta}\psi_0)\phi_1 + \left[\phi_0' + \frac{\sigma}{\eta}\phi_0 + 2(\frac{1-m}{m}) \right] \psi_1 \right.$ (10a)

$- (\eta - \phi_0)\psi_1' \left. \right\} \frac{1}{m} \xi^{1-2m} + 0(\delta^4) = 0;$

Longitudinal momentum:

$$\left[(\eta - \phi_o)\nu_o' + \eta\,\frac{F_o'}{\psi_o} + 2(\tfrac{1-m}{m})(\nu_o + \frac{F_o}{\psi_o})\right] m^3 \xi^{-3+2m}$$

$$+\ \delta^2 \Bigg\{ (\eta - \phi_o)\nu_2' + \eta\,\frac{F_2'}{\psi_o} + 4(\tfrac{1-m}{m})(\nu_2 + \frac{F_2}{\psi_o}) - \nu_o'\phi_2$$

$$-\ \frac{1}{\psi_o^2}\left[\eta F_o' + 2(\tfrac{1-m}{m})F_o\right]\psi_2 + \nu_o\left[\eta\nu_o' + 2(\tfrac{1-m}{m})\nu_o\right]\Bigg\} m^5\xi^{-5+4m} \tag{10b}$$

$$+\ \varepsilon\Bigg\{ (\eta - \phi_o)\nu_1' + \eta\,\frac{F_1'}{\psi_o} - \frac{1}{\psi_o^2}\left[\eta F_o' + 2(\tfrac{1-m}{m})F_o\right]\psi_1$$

$$-\ \nu_o'\phi_1\Bigg\} m^3\xi^{-1} + O(\delta^4) = 0;$$

Lateral momentum:

$$\left[(\eta - \phi_o)\phi_o' - \frac{F_o'}{\psi_o} + (\tfrac{1-m}{m})\phi_o\right] m^2\xi^{-2+m}$$

$$+\ \delta^2\Bigg\{ (\eta - \phi_o)\phi_2' - \frac{F_2'}{\psi_o} + \frac{F_o'}{\psi_o^2}\psi_2 - \left[\phi_o' - 3(\tfrac{1-m}{m})\right]\phi_2$$

$$+\ \left[\eta\phi_o' + (\tfrac{1-m}{m})\phi_o\right]\nu_o\Bigg\} m^4\xi^{-4+3m} \tag{10c}$$

$$+\ \varepsilon\Bigg\{ (\eta - \phi_o)\phi_1' - \frac{F_1'}{\psi_o} + \frac{F_o'}{\psi_o^2}\psi_1 - \left[\phi_o' + (\tfrac{1-m}{m})\right]\phi_1\Bigg\} m^2\xi^{-m}$$

$$+\ O(\delta^4) = 0;$$

Energy: $\left[(\eta - \psi_o)(\gamma \dfrac{\psi_o'}{\psi_o} - \dfrac{F_o'}{F_o}) - 2(\dfrac{1-m}{m})\right] m\xi^{-1}$

$+ \delta^2 \Bigg\{ (\eta - \phi_o) \left[(\gamma \dfrac{\psi_2'}{\psi_o} - \dfrac{F_2'}{F_o}) - (\gamma \dfrac{\psi_2 \psi_o'}{\psi_o^2} - \dfrac{F_2 F_o'}{F_o^2})\right]$

$+ 2(\dfrac{1-m}{m}) (\gamma \dfrac{\psi_2}{\psi_o} - \dfrac{F_2}{F_o}) - (\gamma \dfrac{\psi_o'}{\psi_o} - \dfrac{F_o'}{F_o})\phi_2$

$- \left[2(\dfrac{1-m}{m}) - \eta(\gamma \dfrac{\psi_o'}{\psi_o} - \dfrac{F_o'}{F_o})\right] \nu_o \Bigg\} m^3 \xi^{-3+2m}$

(10d)

$+ \epsilon \Bigg\{ (\eta - \phi_o) \left[(\gamma \dfrac{\psi_1'}{\psi_o} - \dfrac{F_1'}{F_o}) - (\gamma \dfrac{\psi_1 \psi_o'}{\psi_o^2} - \dfrac{F_1 F_o'}{F_o^2})\right]$

$- 2(\dfrac{1-m}{m})(\gamma \dfrac{\psi_1}{\psi_o} - \dfrac{F_1}{F_o}) - (\gamma \dfrac{\psi_o'}{\psi_o} - \dfrac{F_o'}{F_o})\phi_1 \Bigg\} m\xi^{1-2m} + 0(\delta^4) = 0.$

These equations are seen to be ordinary first-order differential equations, linear in the derivatives of the functions defining the pressure, density, and velocity fields. It is noteworthy that although δ appears to the first power in the normalization of variables (equations (2)), only the even powers of δ appear in the final form of the flow equations. Thus, while the solutions to be found are of second order in the body slenderness parameter δ, they could be considered of first order in δ^2. To avoid any ambiguity they will generally be referred to as order-δ^2 solutions. Physically, the absence of lower powers of δ indicates that the error due to a given body thickness is less at hypersonic speeds than at lower speeds, where terms of order δ or $\delta^{3/2}$ appear (Van Dyke (6)).

B. Discussion of Orders of Magnitude

As a result of the normalization procedure (equation (2)), the variables p, ρ, u, and v are of order unity for slender bodies in hypersonic flow. The similarity variables in equations (10) are also considered to be of order unity, but this assumption must be tested by the results obtained. The development so far has been based on δ^2 and ε being small parameters. This section will consider their relative sizes.

Zeroth-order equations. If $\delta^2 \ll 1$ and $\varepsilon \ll 1$, so that all terms containing either one may be neglected, equations (10) are reduced to the zeroth-order equations:

$$\text{Continuity:} \quad \psi_o(\phi_o' + \frac{\sigma}{\eta}\phi_o) - (\eta - \phi_o)\psi_o' = 0$$

$$\text{Longitudinal momentum:} \quad (\eta - \phi_o)v_o' + \eta\frac{F_o'}{\psi_o} + 2(\frac{1-m}{m})(v_o + \frac{F_o}{\psi_o}) = 0$$

$$\text{Lateral momentum:} \quad (\eta - \phi_o)\phi_o' - \frac{F_o'}{\psi_o} + (\frac{1-m}{m})\phi_o = 0$$

$$\text{Energy:} \quad (\eta - \phi_o)(\gamma\frac{\psi_o'}{\psi_o} - \frac{F_o'}{F_o}) - 2(\frac{1-m}{m}) = 0$$

$$(11)$$

These equations represent the case first studied by Kubota (9); they are the same as his equations except that he omitted the longitudinal momentum equation, which is uncoupled from the others. References 9, 10, and 23 contain results of numerically solving Kubota's equations, which are a special case of the present more general treatment.

Equations (11) contain only one parameter, the power-law exponent m. Thus, for two-dimensional flow ($\sigma = 0$) or axisymmetric flow ($\sigma = 1$) of a given gas, the similar solutions $F_o(\eta)$, $\psi_o(\eta)$, $\nu_o(\eta)$, and $\phi_o(\eta)$ each form two families of "universal functions" depending only on the power-law of the body.

As was mentioned in Chapter I, the simultaneous application of the conditions leading to these equations imposes a stringent condition on the Mach number; viz., $\delta^2 \ll 1$ and $\varepsilon \equiv \dfrac{1}{M_\infty^2 \delta^2} \ll 1$ requires $M_\infty \gg 1$. This relation between ε and δ is illustrated in Figure 2, where part (a) shows, for example, that $\varepsilon < .1$ and $\delta^2 < .1$ are both true at Mach 12 only if $\delta \approx .3$. Note, in addition, that dropping the terms in ε removes all Mach number dependence from the equations, which really implies $M_\infty \to \infty$ and illustrates Hayes' "Mach number independence principle" (ref. 1).

Order-ε equations. If, in equations (10), the terms in $\delta^2 \ll 1$ are dropped but the terms in ε are retained, two systems of equations can be obtained by setting the zeroth-order and order-ε terms separately equal to zero. The zeroth-order system is the same as before; the order-ε system is:

Continuity:

$$\psi_o \phi_1' + (\psi_o' + \frac{\sigma}{\eta} \psi_o)\phi_1 - (\eta - \phi_o)\psi_1' + [\phi_o' + \frac{\sigma}{\eta} \phi_o + 2(\frac{1-m}{m})]\psi_1 = 0$$

$$(12a)$$

(a) Relative errors from neglecting terms of order ϵ and of order δ^2.

Figure 2.   Relation Between Body Slenderness Parameter and Shock Strength Parameter
for Several Mach Numbers.

(b) Relative errors from neglecting terms of order ϵ^2 and of order δ^2.

Figure 2. Continued.

(c) Relative errors from neglecting terms of order ϵ^2 and of order δ^4.

Figure 2. Concluded.

Longitudinal momentum: $(\eta - \phi_o)\nu_1' + \eta \dfrac{F_1'}{\psi_o}$

(12b)

$- \dfrac{1}{\psi_o^2}\left[\eta F_o' + 2(\dfrac{1-m}{m})F_o\right]\psi_1 - \nu_o'\phi_1 = 0$

Lateral momentum:

$(\eta - \phi_o)\phi_1' - \dfrac{F_1'}{\psi_o} + \dfrac{F_o'}{\psi_o^2}\psi_1 - \left[\phi_o' + (\dfrac{1-m}{m})\right]\phi_1 = 0$ (12c)

Energy: $(\eta - \phi_o)\left[(\gamma \dfrac{\psi_1'}{\psi_o} - \dfrac{F_1'}{F_o}) - (\gamma \dfrac{\psi_o'}{\psi_o^2}\psi_1 - \dfrac{F_o'}{F_o^2}F_1)\right]$

(12d)

$- 2(\dfrac{1-m}{m})(\gamma \dfrac{\psi_1}{\psi_o} - \dfrac{F_1}{F_o}) - (\gamma \dfrac{\psi_o'}{\psi_o} - \dfrac{F_o'}{F_o})\phi_1 = 0$

These equations are the same as Kubota's (9) first-order
perturbation for shock wave strength, except that (again) he
omitted the longitudinal momentum equation since it is un-
coupled from the rest. They can be solved numerically using
the results of the zeroth-order solutions. The resulting
similarity functions $F_1(\eta)$, $\psi_1(\eta)$, $\nu_1(\eta)$, and $\phi_1(\eta)$ are,
like the zeroth-order functions, universal in that they
depend only on m as a parameter. References 9, 10, and 23
contain the results of the numerical solution. Applying this
shock wave strength perturbation reintroduces the Mach number
dependence and somewhat relieves the requirement that $M_\infty \to \infty$
(see Figure 2(b)), but the body must still be very slender
in order that $\delta^2 \ll 1$.

<u>Order-δ^2 equations</u>. If the terms in δ^2 are kept in equations (10) and all higher order terms are dropped, a case is found which has not been studied previously. This is the case of present interest. Since general similarity solutions are being sought which do not depend on the particular values of δ or ε, each of the three major terms in each of the four conservation equations must be separately equal to zero. As a result of observing this, the terms can be separated into twelve equations in the twelve unknown functions F_o, ψ_o, v_o, ϕ_o, F_1, ψ_1, v_1, ϕ_1, F_2, ψ_2, v_2, and ϕ_2. Eight of these equations are the zeroth-order and order-ε systems of equations found before. The remaining four are the order-δ^2 equations:
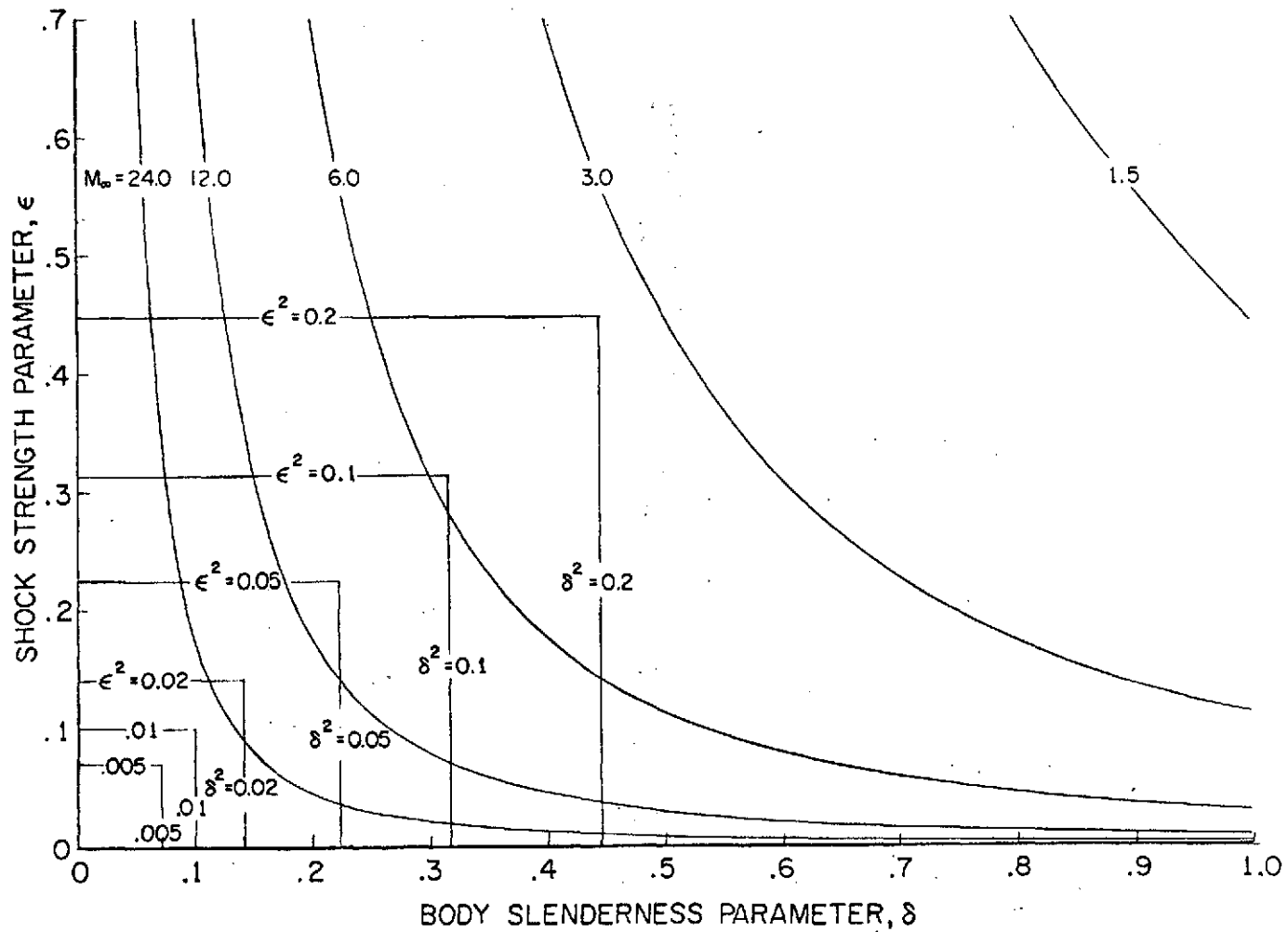
<u>Continuity</u>:
$$\psi_o\phi_2' + (\psi_o' + \frac{\sigma}{\eta}\,\psi_o)\phi_2 - (\eta - \phi_o)\psi_2'$$

$$+ \left[\phi_o' + \frac{\sigma}{\eta}\,\phi_o - 2(\frac{1-m}{m})\right]\psi_2 - \eta v_o\psi_o' - \left[\eta v_o' + 2(\frac{1-m}{m})\,v_o\right]\psi_o = 0 \tag{13a}$$

<u>Longitudinal momentum</u>:
$$(\eta - \phi_o)v_2' + \eta\,\frac{F_2'}{\psi_o}$$

$$+ 4(\frac{1-m}{m})(v_2 + \frac{F_2}{\psi_o}) - \frac{1}{\psi_o^2}\left[\eta F_o' + 2(\frac{1-m}{m})F_o\right]\psi_2 - v_o'\phi_2 \tag{13b}$$

$$+ v_o\left[\eta v_o' + 2(\frac{1-m}{m})\,v_o\right] = 0$$

Lateral momentum:
$$(\eta - \phi_o)\phi_2' - \frac{F_2'}{\psi_o} + \frac{F_o'}{\psi_o^2}\psi_2$$

$$-\left[\phi_o' - 3(\frac{1-m}{m})\right]\phi_2 + \left[\eta\phi_o' + (\frac{1-m}{m})\phi_o\right]\nu_o = 0 \tag{13c}$$

Energy:
$$(\eta - \phi_o)\left[(\gamma\frac{\psi_2'}{\psi_o} - \frac{F_2'}{F_o}) - (\gamma\frac{\psi_o'\psi_2}{\psi_o^2} - \frac{F_o'F_2}{F_o^2})\right]$$

$$+ 2(\frac{1-m}{m})(\gamma\frac{\psi_2}{\psi_o} - \frac{F_2}{F_o}) - (\gamma\frac{\psi_o'}{\psi_o} - \frac{F_o'}{F_o})\phi_2 \tag{13d}$$

$$-\left[2(\frac{1-m}{m}) - \eta(\gamma\frac{\psi_o'}{\psi_o} - \frac{F_o'}{F_o})\right]\nu_o = 0$$

Except for additional terms corresponding to the order-δ^2 terms retained in the normalized equations (3), these equations are very similar to the order-ϵ equations; many of the coefficients are the same, and the only body shape parameter that appears is m. The similarity functions $F_2(\eta)$, $\psi_2(\eta)$, $\nu_2(\eta)$, and $\phi_2(\eta)$, which form the solutions to these equations, will therefore be families of universal functions in the same sense as the other solutions are. Furthermore, just as the order-ϵ equations are independent of the body slenderness perturbation (in δ^2), these equations are independent of the shock wave strength perturbation (in ϵ). Thus, application of these equations to determine the body slenderness perturbation of the zeroth-order small disturbance similar solutions neither requires nor excludes application of the equations for the shock strength

perturbation at the same time. Figure 2(c) shows that with both perturbations applied the expected error for a given Mach number and body slenderness is much less than without them (Figure 2(a)) or with just the shock strength perturbation (Figure 2(b)).

Since the order-ε solutions have been found previously and are not needed to get the order-δ^2 solutions, they will not be considered further. All subsequent development will assume $\varepsilon < \delta^2$, so that $\varepsilon^2 < \varepsilon\delta^2 < \delta^4 \ll 1$; all terms of order δ^4 or smaller will be neglected.

C. Boundary Conditions

This section will deal with the boundary conditions at the shock and at the body surface and with the implications of the body boundary conditions on the solutions near the surface.

Shock wave. The boundary conditions at the shock wave are determined by the oblique shock relations (equation (4)). Using the expression for $R(\xi)$ (equation (7)) these relations become:

$$p_s = \frac{2}{\gamma+1} m^2 \xi^{-2(1-m)} + \delta^2 \frac{2}{\gamma+1}\left[2\left(\frac{3m-2}{m}\right) a_2 - 1\right] m^4 \xi^{-4(1-m)}$$

$$+ \varepsilon \frac{2}{\gamma+1}\left[2\left(\frac{2-m}{m}\right) a_1 - \frac{\gamma-1}{2\gamma m^2}\right] m^2 + 0(\delta^4)$$

$$\rho_s = \frac{\gamma+1}{\gamma-1} - \varepsilon \frac{2}{\gamma+1} \left(\frac{\gamma+1}{\gamma-1}\right) \frac{1}{m^2} \xi^{2(1-m)} + 0(\delta^4)$$

$$u_s = \frac{-2}{\gamma+1} m^2 \xi^{-2(1-m)} - \delta^2 \frac{2}{\gamma+1}\left[2\left(\frac{3m-2}{m}\right) a_2 - 1\right] m^4 \xi^{-4(1-m)} \left.\vphantom{\int}\right\} \quad (14)$$

$$- \varepsilon \frac{2}{\gamma+1}\left[2\left(\frac{2-m}{m}\right) a_1 - \frac{1}{m^2}\right] m^2 + 0(\delta^4)$$

$$v_s = \frac{2}{\gamma+1} m \xi^{-(1-m)} + \delta^2 \frac{2}{\gamma+1}\left[\left(\frac{3m-2}{m}\right) a_2 - 1\right] m^3 \xi^{-3(1-m)}$$

$$+ \varepsilon \frac{2}{\gamma+1}\left[\left(\frac{2-m}{m}\right) a_1 - \frac{1}{m^2}\right] m \xi^{1-m} + 0(\delta^4)$$

Comparing these equations term-by-term with equations (8) determines the boundary conditions for the similarity functions at the shock wave ($\eta = \eta_s$):

$$F_o(\eta_s) = \frac{2}{\gamma+1} \qquad F_1(\eta_s) = \frac{2}{\gamma+1}\left[2\left(\frac{2-m}{m}\right) a_1 - \frac{\gamma-1}{2\gamma m^2}\right]$$

$$\psi_o(\eta_s) = \frac{\gamma+1}{\gamma-1} \qquad \psi_1(\eta_s) = -\frac{\gamma+1}{\gamma-1} \frac{2}{\gamma-1} \frac{1}{m^2} \qquad \left.\vphantom{\int}\right\} \begin{array}{l} (15a) \\ (15b) \end{array}$$

$$v_o(\eta_s) = -\frac{2}{\gamma+1} \qquad v_1(\eta_s) = -\frac{2}{\gamma+1}\left[2\left(\frac{2-m}{m}\right) a_1 - \frac{1}{m^2}\right]$$

$$\phi_o(\eta_s) = \frac{2}{\gamma+1} \qquad \phi_1(\eta_s) = \frac{2}{\gamma+1}\left[\left(\frac{2-m}{m}\right) a_1 - \frac{1}{m^2}\right]$$

$$F_2(\eta_s) = \frac{2}{\gamma+1}[2(\frac{3m-2}{m})a_2 - 1]$$

$$\psi_2(\eta_s) = 0$$

$$\nu_2(\eta_s) = -\frac{2}{\gamma+1}[2(\frac{3m-2}{m})a_2 - 1]$$

$$\phi_2(\eta_s) = \frac{2}{\gamma+1}[(\frac{3m-2}{m})a_2 - 1]$$

$$\left.\begin{array}{c} \\ \\ \\ \\ \end{array}\right\} \quad (15c)$$

Note that the shock wave displacement constants a_1 and a_2 are initially unknown. They depend on the parameter m and are to be found in satisfying the boundary condition at the body surface as part of the solution of the flow equations.

Body surface. The boundary conditions at the body surface are determined by the mass flow through the surface. If $\bar{v}_w$ is the velocity and $\bar{\rho}_w$ is the density of the flow out through the surface (Figure 3), the mass flow balance normal to the surface is given by:

$$\bar{\rho}_b\bar{v}_b \cos \theta_b - \bar{\rho}_b\bar{u}_b \sin \theta_b = \bar{\rho}_w\bar{v}_w \qquad (16)$$

Or, in the normalized variables:

$$v_b = \alpha\, v_w \sec \theta_b + (1 + \delta^2 u_b) \frac{1}{\delta} \tan \theta_b \qquad (17)$$

Figure 3. Vector diagram of flow at the body surface.

where $\alpha = \dfrac{\bar{\rho}_w}{\bar{\rho}_b}$, $v_w = \dfrac{\bar{v}_w}{\delta \bar{u}_\infty}$. Now

$$\left.\begin{aligned}
\tan \theta_b &= \frac{d\bar{r}_b}{d\bar{x}} = \delta \eta_b m x^{-(1-m)} , \\[2mm]
\sec \theta_b &= \left[1 + \delta^2 \eta_b^2 \, m^2 \, x^{-2(1-m)} \right]^{1/2} \\[2mm]
&= 1 + \frac{1}{2} \, \delta^2 \eta_b^2 \, m^2 \, x^{-2(1-m)} + 0(\delta^4) .
\end{aligned}\right\} \quad (18)$$

Putting these into equation (17) along with the expressions in the similarity functions for u and v from equations (8) gives the relation

$$\left[\phi_o(\eta_b) - \eta_b\right] m\xi^{-(1-m)} - \alpha v_w$$

$$+ \delta^2\left\{\left[\phi_2(\eta_b) - \eta_b v_o(\eta_b)\right] m^3\xi^{-3(1-m)} - \alpha v_w \frac{\eta_b^2}{2} m^2\xi^{-2(1-m)}\right\} \quad (19)$$

$$+ \epsilon\ \phi_1(\eta_b)\ m\xi^{-(1-m)} + 0(\delta^4) = 0$$

If the flow through the surface has the particular form $\alpha v_w = \phi_w m\xi^{-(1-m)}$, where ϕ_w is a constant, the boundary conditions at the body surface are (from equation (19))

$$\phi_o(\eta_b) - \eta_b - \phi_w = 0,$$

$$\phi_2(\eta_b) - \eta_b v_o(\eta_b) - \frac{\eta_b^2}{2} \phi_w = 0 , \quad\quad (20)$$

$$\phi_1(\eta_b) = 0$$

While the development of these boundary condition shows that mass flow through the surface can be accommodated without difficulty, the rest of this dissertation will be restricted to the no mass flow conditions, $\phi_w = 0$. The resulting boundary conditions are

$$\phi_o(\eta_b) - \eta_b = 0,$$

$$\phi_2(\eta_b) - \eta_b \nu_o(\eta_b) = 0, \tag{21}$$

$$\phi_1(\eta_b) = 0.$$

Initial magnitude checks. These boundary conditions can be used with the flow equations to provide some initial checks of the order of magnitude of the similarity functions. As stated in Section II-B, these functions have been assumed to be of order unity. From the boundary conditions at the shock (equations (15)), this assumption appears justified there, for γ not too close to one and if a_2 is not too large, except that $\psi_2(\eta_s) = 0$. Having a function become much less than one does not invalidate the procedure used in getting the equations so long as the function does not appear as the denominator of terms that one dropped as being negligibly small, i.e. of order δ^4. Neither ψ_2 nor any other order - δ^2 function is in the denominator of any term that is dropped.

Solutions to the zeroth-order equations given by Kubota (9) indicate that F_o and ϕ_o remain of order one from the shock to the body but that ψ_o goes to zero at the body surface when $m < 1$. This result could affect the validity of the solutions in the region where ψ_o is small

since ψ_o does appear in the denominator of a number of terms of equations (10) - (13). One of these is the zeroth-order lateral momentum equation (11). Applying the boundary condition $\phi_o(\eta_b) - \eta_b = 0$, this equation becomes

$$\frac{F_o'(\eta_b)}{\psi_o(\eta_b)} = (\frac{1-m}{m}) \eta_b,$$

from which $F_o'(\eta_b) = 0$. The zeroth-order longitudinal momentum equation (11) multiplied through by ψ_o is

$$(\eta - \phi_o)\psi_o v_o' + \eta F_o' + 2(\frac{1-m}{m})(v_o\psi_o + F_o) = 0.$$

Using $\phi_o(\eta_b) - \eta_b = 0$ and $F_o'(\eta_b) = 0$, this becomes

$$v_o(\eta_b)\psi_o(\eta_b) + F_o(\eta_o) = 0 . \tag{22}$$

Since $\psi_o(\eta_b) = 0$ and $F_o(\eta_b) \neq 0$, this requires $v_o \to \infty$ as $\eta \to \eta_b$. Thus there is a (non-physical) singularity[*] in the similarity solutions at the surface of the body $\eta = \eta_b$.

One possible way to avoid the singularity at the body surface is to reformulate the problem. The fact that $v_o\psi_o$, which remains finite as $\eta \to \eta_b$, is the zeroth-order similarity form of the longitudinal momentum suggests that

_____

[*]Kubota (9) and Mirels (10,16) do not encounter this problem because they omit the variable v_o entirely. It only occurs in the longitudinal momentum equation, which they do not use, prefering a Bernoulli equation for the velocity.

using momentum components, instead of velocity components, as fundamental variables might remove the singularity. This approach is pursued in the next section.

D. Momentum Variable Formulation

As was noted in the previous section, the zeroth-order longitudinal velocity similarity function v_o is singular at the body surface. However, the product $\psi_o v_o$ remains finite, which suggests that a reformulation of the problem in terms of new variables might remove the singularity and allow the numerical integration to proceed all the way to the body surface. The variables chosen for the reformulation are the longitudinal momentum $\overline{\rho u}$ (which is expected to behave like $\psi_o v_o$ and so remain finite at the body surface), the lateral momentum $\overline{\rho v}$, the pressure $\bar{p}$, and the density $\bar{\rho}$. In terms of these variables, the inviscid flow equations (1) become:

Continuity:
$$\frac{\partial \overline{\rho u}}{\partial x} + \frac{\partial \overline{\rho v}}{\partial r} + \sigma \frac{\overline{\rho v}}{r} = 0 \qquad (23a)$$

Longitudinal momentum:

$$\overline{\rho u}\left(\bar{\rho}\,\frac{\partial \overline{\rho u}}{\partial x} - \overline{\rho u}\,\frac{\partial \rho}{\partial x}\right) + \overline{\rho v}\left(\bar{\rho}\,\frac{\partial \overline{\rho u}}{\partial r} - \overline{\rho u}\,\frac{\partial \bar{\rho}}{\partial r}\right) + \bar{\rho}^2\,\frac{\partial \bar{p}}{\partial x} = 0 \qquad (23b)$$

Lateral momentum:

$$\overline{\rho u}(\bar{\rho}\,\frac{\partial \overline{\rho v}}{\partial x} - \overline{\rho v}\,\frac{\partial \bar{\rho}}{\partial x}) + \overline{\rho v}\,(\bar{\rho}\,\frac{\partial \overline{\rho v}}{\partial r} - \overline{\rho v}\,\frac{\partial \bar{\rho}}{\partial r}) + \bar{\rho}^2\,\frac{\partial p}{\partial r} = 0 \qquad (23c)$$

Energy: $\quad (\overline{\rho u}\,\frac{\partial}{\partial \bar{x}} + \overline{\rho v}\,\frac{\partial}{\partial \bar{r}})\,(\frac{\bar{p}}{\bar{\rho}^\gamma}) = 0 \qquad (23d)$

Normalization. These equations are normalized using the expressions:

$$x = \frac{\bar{x}}{\bar{\ell}} \quad , \quad r = \frac{\bar{r}}{\delta \bar{\ell}} \quad , \quad p = \frac{\bar{p}\,\bar{\rho}_\infty}{\delta^2(\overline{\rho_\infty u_\infty})^2}$$

$$\rho = \frac{\bar{\rho}}{\rho_\infty} \quad , \quad (\rho u) = \frac{\overline{\rho u}}{\overline{\rho_\infty u_\infty}}, \quad (\rho v) = \frac{\overline{\rho v}}{\delta \overline{\rho_\infty u_\infty}} \quad . \qquad (24)$$

(Note that these expressions are the same as equations (2) with the exception that (ρu) here is the same as the previous $\rho(1+\delta^2 u)$.) The normalized forms of the equations (23) are then:

Continuity: $\quad \frac{\partial(\rho u)}{\partial x} + \frac{\partial(\rho v)}{\partial r} + \sigma\,\frac{(\rho v)}{r} = 0 \qquad (25a)$

Longitudinal momentum: $\quad (\rho u)\left[\rho\,\frac{\partial(\rho u)}{\partial x} - (\rho u)\,\frac{\partial \rho}{\partial x}\right]$

$$(25b)$$

$$+ (\rho v)\left[\rho\,\frac{\partial(\rho u)}{\partial r} - (\rho u)\,\frac{\partial \rho}{\partial r}\right] + \delta^2 \rho^2\,\frac{\partial p}{\partial x} = 0$$

Lateral momentum: $(\rho u) \left[\rho \frac{\partial(\rho v)}{\partial x} - (\rho v) \frac{\partial \rho}{\partial x} \right]$ (25c)

$+ (\rho v) \left[\rho \frac{\partial(\rho v)}{\partial r} - (\rho v) \frac{\partial \rho}{\partial r} \right] + \rho^2 \frac{\partial p}{\partial r} = 0$

Energy: $\left[(\rho u) \frac{\partial}{\partial x} + (\rho v) \frac{\partial}{\partial r} \right] (\frac{p}{\rho^\gamma}) = 0$ (25d)

Similarity variables. Just as in the first section of this chapter, the similarity forms of the momentum variables are chosen using the relations for flow through an oblique shock wave as guides. Combining the density and velocity relations used previously (equations (4)) gives the following relations for the normalized variables just behind an oblique shock:

$$(\rho u)_s \equiv \frac{(\overline{\rho u})_s}{\rho_\infty u_\infty} = \frac{(\gamma+1) \, M_\infty^2 \sin^2 \theta_s}{(\gamma-1) \, M_\infty^2 \sin^2 \theta_s - 2} \left[1 - \frac{2(M_\infty^2 \sin^2 \theta_s - 1)}{(\gamma+1) \, M_\infty^2} \right]$$

$$= \frac{(\frac{\gamma+1}{2} + \frac{1}{M_\infty^2}) + \delta^2 R'^2 (\frac{\gamma+1}{2} + \frac{1}{M_\infty^2} - 1)}{(\frac{\gamma-1}{2} - \frac{1}{M_\infty^2} - \frac{1}{M_\infty^2 \delta^2 R'^2})(1 + \delta^2 R'^2)} \qquad (26a)$$

$$= \frac{\gamma+1}{\gamma-1} - \delta^2 \frac{2}{\gamma-1} R'^2 + \varepsilon \frac{2(\gamma+1)}{(\gamma-1)^2} (R')^{-2} + O(\delta^4)$$

$$(\rho v)_s \equiv \frac{(\overline{\rho u})_s}{\delta \overline{\rho_\infty u_\infty}} = \frac{2(\gamma+1) M_\infty^2 \sin^2 \theta_s (M_\infty^2 \sin^2 \theta_s - 1)}{\delta \left[(\gamma-1)M_\infty^2 \sin^2 \theta_s + 2\right](\gamma+1)M_\infty^2 \tan \theta_s}$$

$$= \frac{\left[R'^2 - \frac{1}{M_\infty^2 \delta^2}(1 + \delta^2 R'^2)\right] R'}{\left[\frac{\gamma-1}{2} R'^2 + \frac{1}{\delta^2 M_\infty^2}(1 + \delta^2 R'^2)\right](1 + \delta^2 R'^2)} \qquad (26b)$$

$$= \frac{2}{\gamma-1} R' - \delta^2 \frac{2}{\gamma-1} R'^3 - \varepsilon \frac{2(\gamma+1)}{(\gamma-1)^2}(R')^{-1} + 0(\delta^4)$$

The similarity forms of the momentum variables are taken to be:

$$\left.\begin{array}{l}
\rho u = \tilde{\upsilon}_o(r) + \delta^2 \tilde{\upsilon}_2(r)R'^2 + \varepsilon \tilde{\upsilon}_1(r)(R')^{-2} \\[2mm]
\text{and} \\[2mm]
\rho v = \tilde{\mu}_o(r) R' + \delta^2 \tilde{\mu}_2(r)R'^3 + \varepsilon \tilde{\mu}_1(r)(R')^{-1}
\end{array}\right\} \qquad (27)$$

Using the same perturbed, power-law shock wave shape as before (equation (7)), these become (for $\varepsilon < \delta^2$)

$$\left.\begin{array}{l}
\rho u = \upsilon_o(\eta) + \delta^2 \upsilon_2(\eta) \, m^2 \xi^{-2(1-m)} + \varepsilon \upsilon_1(\eta) \frac{1}{m^2} \xi^{2(1-m)} + 0(\delta^4) \\[3mm]
\text{and} \\[3mm]
\rho v = \mu_o(\eta) \, m\xi^{-(1-m)} + \delta^2 \mu_2(\eta) \, m^3 \xi^{-3(1-m)} + \varepsilon \mu_1(\eta) \frac{1}{m} \xi^{(1-m)} \\[3mm]
+ 0(\delta^4)
\end{array}\right\} (28)$$

The similarity forms of p and ρ are unchanged from the previous formulation (equations (8)). Putting the similarity forms of these variables into the flow equations (25), and using the chain rule for partial derivatives (equations (9)) as before, produces:

Continuity:

$$(\mu_o' - \eta\upsilon_o' + \frac{\sigma}{\eta}\mu_o)\, m\xi^{-1}$$

$$+ \delta^2[\mu_2' - \eta\upsilon_2' - 2(\frac{1-m}{m})\upsilon_2 + \frac{\sigma}{\eta}\mu_2]\, m^3\xi^{2m-3}$$

$$+ \varepsilon[\mu_1' - \eta\upsilon_1' + 2(\frac{1-m}{m})\upsilon_1 + \frac{\sigma}{\eta}\mu_1]\, \frac{1}{m}\xi^{(1-2m)} + 0(\delta^4) = 0$$

(29a)

Longitudinal momentum: $(\eta\upsilon_o - \mu_o)(\upsilon_o\psi_o' - \psi_o\upsilon_o')\, m\xi^{-1}$

$$+ \delta^2\{(\eta\upsilon_o - \mu_o)(\upsilon_o\psi_2' - \psi_o\upsilon_2') +$$

$$[2(\frac{1-m}{m})\upsilon_o^2 - (\eta\upsilon_o - \mu_o)\upsilon_o']\,\psi_2 + (\psi_o\upsilon_o' - \upsilon_o\psi_o')\mu_2$$

$$+ [(\eta\upsilon_o - \mu_o)\psi_o' + \eta(\upsilon_o\psi_o' - \psi_o\upsilon_o') - 2(\frac{1-m}{m})\psi_o\upsilon_o]\upsilon_2$$

$$- \psi_o^2[\eta F_o' + 2(\frac{1-m}{m})F_o]\}\, m^3\xi^{2m-3}$$

(29b)

$$+ \varepsilon\{(\eta\upsilon_o - \mu_o)(\upsilon_o\psi_1' - \psi_o\upsilon_1') - [2(\frac{1-m}{m})\upsilon_o^2$$

$$+ (\eta\upsilon_o - \mu_o)\upsilon_o']\,\psi_1 + (\psi_o\upsilon_o' - \upsilon_o\psi_o')\mu_1$$

$$+ [(\eta\upsilon_o - \mu_o)\psi_o' + \eta(\upsilon_o\psi_o' - \psi_o\upsilon_o')$$

$$+ 2(\frac{1-m}{m})\psi_o\upsilon_o]\upsilon_1\}\, \frac{1}{m}\xi^{(1-2m)} + 0(\delta^4) = 0.$$

Lateral momentum:

$$[(\eta\upsilon_o - \mu_o)(\mu_o\psi_o' - \psi_o\mu_o') + \psi_o^2 F_o' - (\frac{1-m}{m})\,\psi_o\mu_o\upsilon_o]\,m^2\xi^{m-2}$$

$$+ \; \delta^2\{(\eta\upsilon_o - \mu_o)(\mu_o\psi_2' - \psi_o\mu_2') + \psi_o^2 F_2'$$

$$+ \; [2\psi_o F_o' - (\eta\upsilon_o - \mu_o)\mu_o' + (\frac{1-m}{m})\mu_o\upsilon_o]\psi_2$$

$$+ \; [(\eta\upsilon_o - \mu_o)\psi_o' + (\psi_o\mu_o' - \mu_o\psi_o') - 3(\frac{1-m}{m})\,\psi_o\upsilon_o]\mu_2$$

$$+ \; [\eta(\mu_o\psi_o' - \psi_o\mu_o') - (\frac{1-m}{m})\,\psi_o\mu_o]\upsilon_2\}m^4\,\xi^{3m-4} \qquad (29c)$$

$$+ \; \varepsilon\{(\eta\upsilon_o - \mu_o)(\mu_o\psi_1' - \psi_o\mu_1') + \psi_o^2 F_1'$$

$$+ [2\psi_o F_o' - (\eta\upsilon_o - \mu_o)\mu_o' - 3(\frac{1-m}{m})\mu_o\upsilon_o]\psi_1$$

$$+ \; [(\eta\upsilon_o - \mu_o)\,\psi_o' + (\psi_o\mu_o' - \mu_o\psi_o') + (\frac{1-m}{m})\,\psi_o\upsilon_o]\mu_1$$

$$+ \; [\eta(\mu_o\psi_o' - \psi_o\mu_o') - (\frac{1-m}{m})\,\psi_o\mu_o]\upsilon_1\}\,\xi^{-m} + 0(\delta^4) = 0$$

Energy: $[(\eta\upsilon_o - \mu_o)(\gamma F_o\psi_o' - \psi_o F_o') - 2(\frac{1-m}{m})F_o\psi_o\upsilon_o]\ m^3\xi^{2m-3}$

$+ \delta^2\{(\eta\upsilon_o - \mu_o)(\gamma F_o\psi_2' - \psi_o F_2') + [\gamma(\eta\upsilon_o - \mu_o)\psi_o'$

$- 4(\frac{1-m}{m})\ \psi_o\upsilon_o]\ F_2 - (\gamma F_o\psi_o' - \psi_o F_o')\ \mu_2$

$- [(\eta\upsilon_o - \mu_o)\ F_o' - 2(\frac{1-m}{m})(\gamma-1)F_o\upsilon_o]\ \psi_2$

$+ [n(\gamma F_o\psi_o' - \psi_o F_o') - 2(\frac{1-m}{m})\ F_o\psi_o]\ \upsilon_2\}\ m^5\xi^{4m-5}$

(29d)

$+ \varepsilon\{(\eta\upsilon_o - \mu_o)(\gamma F_o\psi_1' - \psi_o F_1') + \gamma(\eta\upsilon_o - \mu_o)\psi_o'F_1$

$- [(\eta\upsilon_o - \mu_o)F_o' + 2(\frac{1-m}{m})\ (\gamma+1)F_o\upsilon_o]\psi_1$

$+ [n(\gamma F_o\psi_o' - \psi_o F_o') - 2(\frac{1-m}{m})\ F_o\psi_o]\upsilon_1$

$- (\gamma F_o\psi_o' - \psi_o F_o')\ \mu_1\}\ m\xi^{-1} + 0(\delta^4) = 0\ .$

Zeroth-order equations. Using the same reasoning as was employed in Section II-B, the coefficients of the zeroth-order term, the order-δ^2 term, and the order-ε term of each of these four equations must be equal to zero. The zeroth-order system of equations which results from recognizing this fact is:

Continuity: $\qquad \mu_o' - \eta \upsilon_o' + \dfrac{\sigma}{\eta} \mu_o = 0$

Longitudinal momentum: $\quad (\eta \upsilon_o - \mu_o)(\upsilon_o \psi_o' - \psi_o \upsilon_o') = 0$

Lateral momentum:

$(\eta \upsilon_o - \mu_o)(\mu_o \psi_o' - \psi_o \mu_o') + \psi_o^2 F_o' - (\dfrac{1-m}{m}) \psi_o \upsilon_o \mu_o = 0$

Energy: $\quad (\eta \upsilon_o - \mu_o)(\gamma F_o \psi_o' - \psi_o F_o') - 2(\dfrac{1-m}{m}) F_o \psi_o \upsilon_o = 0$

$$\left. \right\} \quad (30)$$

The longitudinal momentum equation can be integrated immediately. For $(\eta \upsilon_o - \mu_o) \neq 0$ (i.e. away from the body surface; see next section), it becomes $\upsilon_o \psi_o' - \psi_o \upsilon_o' = 0$, which has the solution, $\upsilon_o = c\psi_o$. Comparing equations (26) and (28), the boundary condition on υ_o at the shock wave is $\upsilon_o(\eta_s) = \dfrac{\gamma+1}{\gamma-1}$. Thus, with $\psi_o(\eta_s)$ given by equation (16), the constant c is

and
$$c = \frac{\upsilon_o(\eta_s)}{\psi_o(\eta_s)} = \frac{(\frac{\gamma+1}{\gamma-1})}{(\frac{\gamma+1}{\gamma-1})} = 1,$$
$$\upsilon_o = \psi_o.$$

(31)

(This result could have been anticipated by making a comparison of the similarity variables for the two formulations as given by equations (8) and (28).)

Using the results just obtained, the three remaining zeroth-order equations may be written:

Continuity:
$$\mu_o' - \eta\psi_o' + \frac{\sigma}{\eta}\mu_o = 0$$

Lateral momentum:

$$(\eta\psi_o - \mu_o)(\mu_o\psi_o' - \psi_o\mu_o') + \psi_o^2[F_o' - (\frac{1-m}{m})\mu_o] = 0 \qquad \left.\begin{array}{c} \\ \\ \\ \\ \end{array}\right\} \quad (32)$$

Energy: $(\eta\psi_o - \mu_o)(\gamma F_o\psi_o' - \psi_o F_o') - 2(\frac{1-m}{m})\psi_o^2 F_o = 0$

Order-δ^2 equations. Also using the result $\upsilon_o = \psi_o$, the order-δ^2 system of equations may be written:

Continuity:
$$\mu_2' - \eta\upsilon_2' - 2(\frac{1-m}{m})\upsilon_2 + \frac{\sigma}{\eta}\mu_2 = 0 \qquad (33a)$$

Longitudinal momentum:

$$(\eta\psi_o - \mu_o)\psi_o(\psi_2' - \upsilon_2') + [2(\frac{1-m}{m})\psi_o^2 - (\eta\psi_o - \mu_o)\psi_o']\psi_2$$

$$\qquad (33b)$$

$$+ [(\eta\psi_o - \mu_o)\psi_o' - 2(\frac{1-m}{m})\psi_o^2]\upsilon_2 - \psi_o^2[\eta F_o' + 2(\frac{1-m}{m})F_o] = 0$$

Lateral momentum: $(\eta\psi_o - \mu_o)(\mu_o\psi_2' - \psi_o\mu_2') + \psi_o^2 F_2'$

$$+ [\psi_o(2F_o' + (\frac{1-m}{m})\mu_o) - (\eta\psi_o - \mu_o)\mu_o']\psi_2$$

$$\qquad (33c)$$

$$+ [(\eta\psi_o - \mu_o)\psi_o' + (\psi_o\mu_o' - \mu_o\psi_o') - 3(\frac{1-m}{m})\psi_o^2]\mu_2$$

$$+ [\eta(\mu_o\psi_o' - \psi_o\mu_o') - (\frac{1-m}{m})\psi_o\mu_o]\upsilon_2 = 0$$

Energy: $(\eta\psi_o - \mu_o)(\gamma F_o \psi_2' - \psi_o F_2') - (\gamma F_o \psi_o' - \psi_o F_o')\mu_2$

$$+ [\gamma(\eta\psi_o - \mu_o)\psi_o' - 4(\frac{1-m}{m})\psi_o^2]F_2$$

(33d)

$$- [(\eta\psi_o - \mu_o)F_o' - 2(\frac{1-m}{m})(\gamma-1)F_o\psi_o]\psi_2$$

$$+ [\eta(\gamma F_o \psi_o' - \psi_o F_o') - 2(\frac{1-m}{m})F_o\psi_o]\upsilon_2 = 0$$

The order-ε equations governing the shock wave strength perturbation are very similar and could be written in the same manner, but since they are not needed here they will not be derived.

Since the physical momentum component variables are simply the products of the density with the velocity components in the usual formulation, the similarity functions of the two formulations are simply related. Noting that the normalized momentum variable (ρu) is equivalent to $\rho(1 + \delta^2 u)$ in the previous formulation, the relations between the similarity functions are:

$$\upsilon_o = \psi_o, \quad \mu_o = \psi_o\phi_o, \quad \upsilon_2 = \psi_2 - \psi_o\upsilon_o, \quad \text{and} \quad \mu_2 = \phi_o\psi_2 + \psi_o\phi_2$$

(34)

Boundary conditions. To determine the boundary conditions for the momentum variables, equations (28) must be

compared to the expanded form of equations (26). Putting the shock wave shape (equation (7)) into equation (26) and expanding gives

$$(\rho u)_s = \frac{\gamma+1}{\gamma-1} - \delta^2 \frac{2}{\gamma-1} m^2 \xi^{-2(1-m)} + \varepsilon \frac{2(\gamma+1)}{(\gamma-1)^2} \frac{1}{m^2} \xi^{2(1-m)} + 0(\delta^4)$$

(35)

$$(\rho v)_s = \frac{2}{\gamma-1} m\xi^{-(1-m)} + \delta^2 \frac{2}{\gamma-1} [a_2(\frac{3m-2}{m}) - 1]m^3\xi^{-3(1-m)}$$

$$+ \varepsilon \frac{2}{\gamma-1} [(\frac{2-m}{m})a_1 + \frac{\gamma+1}{\gamma-1}] \frac{1}{m} \xi^{(1-m)} + 0(\delta^4)$$

The term-by-term comparison of these equations with equations (28) gives

$$\mu_0(\eta_s) = \frac{2}{\gamma-1}, \quad \upsilon_2(\eta_s) = -\frac{2}{\gamma-1}, \quad \mu_2(\eta_s) = \frac{2}{\gamma-1} [(\frac{3m-2}{m})a_2 - 1]$$

(36)

The boundary conditions at the shock on ψ_0, ψ_2, F_0, and F_2 are the same as given by equation (15). The boundary conditions at the body are determined by the mass flow through the surface, as in the previous formulation, Section II-C. In this case, when equation (16) is normalized in terms of the momentum variables it becomes:

$$(\rho v)_b = (\rho v)_w \sec \theta_b + \frac{1}{\delta} (\rho u)_b \tan \theta_b$$

(37)

Putting in the similarity functions (equations (28)), noting $\upsilon_o = \psi_o$, and the relations for $\tan \theta_b$ and $\sec \theta_b$ (equations (18)), the mass flow balance becomes:

$$[\mu_o(n_b) - n_b\psi_o(n_b)]m\xi^{-(1-m)} + \delta^2[\mu_2(n_b) - n_b\upsilon_2(n_b)]m^3\xi^{-3(1-m)}$$

$$+ \varepsilon[\mu_1(n_b) - n_b\upsilon_1(n_b)]\frac{1}{m}\xi^{(1-m)} - (\rho v)_w[1 + \delta^2\frac{1}{2}n_b^2m^2\xi^{-2(1-m)}]$$

$$+ 0(\delta^4) = 0.$$

If the mass flow through the surface has the form $(\rho v)_w = \mu_w m\xi^{-(1-m)}$, where μ_w is a constant ($\mu_w = 0$ for no flow), the zeroth-order and order-δ^2 boundary conditions are

$$\mu_o(n_b) - n_b\psi_o(n_b) = \mu_w,$$

$$\tag{38}$$

$$\mu_2(n_b) - n_b\upsilon_2(n_b) = \frac{1}{2}n_b^2\mu_w .$$

For no mass flow through the body surface, which is the case of present interest, these boundary conditions become

$$\mu_o(n_b) - n_b\psi_o(n_b) = 0, \quad \mu_2(n_b) - n_b\upsilon_2(n_b) = 0 \tag{39}$$

The boundary conditions can be used with the flow equations as in the previous formulation to provide some

initial checks of the order of magnitude of the similarity variables. At the shock wave, the boundary conditions (equations (35)) indicate the variables are of order unity there. At the body, the zero-order boundary condition (equation (39)) produces the same results from the zero-order energy equation (32) as before; i.e. $\psi_o(\eta_b) = 0$. Thus the boundary condition at the body (equation (39)) becomes $\mu_o(\eta_o) = \eta_b \psi_o(\eta_b) = 0$; but $\mu_o(\eta_b)/\psi_o(\eta_b) = \eta_b$ in agreement with equations (34) and (21).

The development above shows that it should be possible to get order-δ^2 similarity solutions using the momentum variable formulation, and that this formulation avoids the singularity in the zeroth-order longitudinal velocity at the body surface. Whether the formulation is successful in avoiding singularities in the order-δ^2 variables must be determined from the numerical solutions to be obtained.

E. Correlation of Solutions

Hornung (26) suggested a method to nondimensionalize experimental data so that shock wave shapes and pressure distributions for a given body power-law exponent would each form a single correlation curve. The basis of his correlation is to nondimensionalize the shock coordinates by a length scale $\bar{D}$ defined such that the body shape is given

by

$$\frac{\bar{r}_b}{\bar{D}} = \left(\frac{\bar{x}}{\bar{D}}\right)^m$$

For $r_b = \eta_b x^m$, $\bar{D} = (\delta \eta_b)^{\frac{1}{1-m}} \bar{\ell}$.

When this correlation is applied to the order-δ^2 similarity
solution shock-wave shape, given by

$$\frac{\bar{R}}{\delta \bar{\ell}} = \left(\frac{\bar{x}}{\bar{\ell}}\right)^m \left[1 + \delta^2 a_2 m^2 \left(\frac{\bar{x}}{\bar{\ell}}\right)^{-2(1-m)}\right]$$

the shock shape becomes

$$\frac{\bar{R}}{\bar{D}} = \frac{1}{\eta_b}\left(\frac{\bar{x}}{\bar{D}}\right)^m \left[1 + a_2 \left(\frac{m}{\eta_b}\right)^2 \left(\frac{\bar{x}}{\bar{D}}\right)^{-2(1-m)}\right]$$

Since this equation does not contain the slenderness parameter
δ, it gives a single curve for any given value of the body
power-law exponent m; i.e., the order-δ^2 similarity
solution produces a single correlation curve independent
of the value of the slenderness parameter δ.

Hornung suggested that pressure data would correlate in
much the same way if it were plotted as $\bar{p}/\bar{\rho}_\infty \bar{u}_\infty^2$ vs $\bar{x}/\bar{D}$,
where $\bar{D}$ is the same non-dimensionalizing scale length
as used for the shocks. In fact, the order-δ^2 solutions
show that not only the pressure, but also the other flow
variables correlate when $\bar{x}/\bar{D}$ is the longitudinal distance.
The pressure, density and velocity components from
equations (8) can be written

$$\frac{\bar{p}}{q_\infty} = 2\delta^2 p = 2\delta^2 \left[F_o m^2 (\frac{\bar{x}}{\bar{\ell}})^{-2(1-m)} + \delta^2 F_2 m^4 (\frac{\bar{x}}{\bar{\ell}})^{-4(1-m)} \right]$$

$$= 2 \left[F_o m^2 \delta^2 (\delta\eta_b)^{-2} (\frac{\bar{x}}{\bar{D}})^{-2(1-m)} + F_2 m^4 \delta^4 (\delta\eta_b)^{-4} (\frac{\bar{x}}{\bar{D}})^{-4(1-m)} \right]$$

$$= 2F_o (\frac{m}{\eta_b})^2 (\frac{\bar{x}}{\bar{D}})^{-2(1-m)} + 2F_2 (\frac{m}{\eta_b})^4 (\frac{\bar{x}}{\bar{D}})^{-4(1-m)},$$

$$\frac{\bar{\rho}}{\rho_\infty} = \rho = \psi_o + \delta^2 \psi_2 m^2 (\frac{\bar{x}}{\bar{\ell}})^{-2(1-m)}$$

$$= \psi_o + \psi_2 (\frac{m}{\eta_b})^2 (\frac{\bar{x}}{\bar{D}})^{-2(1-m)},$$

$$\frac{\bar{u}}{u_\infty} = 1 + \delta^2 u = 1 + \delta^2 \left[\nu_o m^2 (\frac{\bar{x}}{\bar{\ell}})^{-2(1-m)} + \delta^2 \nu_2 m^4 (\frac{\bar{x}}{\bar{\ell}})^{-4(1-m)} \right]$$

$$= 1 + \nu_o (\frac{m}{\eta_b})^2 (\frac{\bar{x}}{\bar{D}})^{-2(1-m)} + \nu_2 (\frac{m}{\eta_b})^4 (\frac{\bar{x}}{\bar{D}})^{-4(1-m)}$$

and

$$\frac{\bar{v}}{u_\infty} = \delta v = \delta \left[\phi_o m (\frac{\bar{x}}{\bar{\ell}})^{-(1-m)} + \delta^2 \phi_2 m^3 (\frac{\bar{x}}{\bar{\ell}})^{-3(1-m)} \right]$$

$$= \phi_o \frac{m}{\eta_b} (\frac{\bar{x}}{\bar{D}})^{-(1-m)} + \phi_2 (\frac{m}{\eta_b})^3 (\frac{\bar{x}}{\bar{D}})^{-3(1-m)} .$$

Since none of these contains δ explicitly, each one forms
a single curve for a given value of the body power-law
exponent m, independent of the body slenderness. Thus it
should be possible to correlate experimental velocity
component and density distributions, as well as the pressure
distributions, by plotting them against the normalized
coordinate $\bar{x}/\bar{D}$.

The regularity of the correlation form for expressing the physical variables in terms of the similarity functions suggests a possible refinement of the similarity formulation. By using the local zeroth-order shock wave slope, expressed as

$$\tau = \left(\frac{\bar{R}}{D}\right)' = \frac{m}{\eta_b}\left(\frac{\bar{x}}{D}\right)^{-(1-m)} \; ,$$

as the small parameter instead of the average shock wave slope $\delta = \bar{R}_o(\bar{\ell})/\bar{\ell}$ (Figure 1, p. 13), it should be possible to improve the formulation. In particular, this change would facilitate the estimation of error in the nose region, where the local shock slope increases rapidly. While it has not been possible to include it in the present study, such a reformulation would provide a good starting point for further work on similarity solutions in hypersonic flow.

CHAPTER III   SOLUTION OF EQUATIONS

A.   General Scheme of Solution

Either the velocity-variable or the momentum-variable similarity form of the flow equation ((11) and (13) or (32) and (33)) with the boundary conditions at the shock wave (equations (15) or (35)) and at the body surface (equations (21) or (39)) is sufficient to completely determine a solution for the flow field. However, since there is no general analytic form for the solution in either formulation, it must be found numerically for each case (i.e. for each value of the power-law exponent m with σ set equal to either zero or one). The general scheme for obtaining the numerical solution is to begin at the shock $\eta = \eta_s$, where the boundary conditions are known, and to integrate the similarity functions numerically toward the body, which is known to be reached when the zeroth-order boundary condition is satisfied; i.e., $\eta = \dot{\eta}_b$ when

$$\phi_o(\eta) = \eta \quad \text{or} \quad \frac{\mu_o(\eta)}{\psi_o(\eta)} = \eta \ .$$

The derivatives of the similarity functions, used for this integration, are found by solving the flow equations for them algebraically. Thus, from the zeroth-order equations (11), the derivatives are

50

$$F_O'(\eta) = \frac{\psi_O}{\gamma - (\eta - \phi_O)^2 \frac{\psi_O}{F_O}} \left\{ \gamma \left(\frac{1-m}{m}\right) \phi_O - (\eta - \phi_O) \left[\gamma \frac{\sigma}{\eta} \phi_O - 2\left(\frac{1-m}{m}\right) \right] \right\}$$

$$\psi_O'(\eta) = \frac{\psi_O}{\gamma} \left\{ \frac{F_O'}{F_O} + 2\left(\frac{1-m}{m}\right) / (\eta - \phi_O) \right\}$$

$$\nu_O'(\eta) = \frac{-1}{\eta - \phi_O} \left\{ \eta \frac{F_O'}{\psi_O} + 2\left(\frac{1-m}{m}\right)(\nu_O + \frac{F_O}{\psi_O}) \right\}$$

$$\phi_O'(\eta) = \frac{1}{\eta - \phi_O} \left\{ \frac{F_O'}{\psi_O} - \left(\frac{1-m}{m}\right) \phi_O \right\}$$

$$\left. \right\} (40)$$

The derivatives of the order-δ^2 functions, from equations (13), are

$$\phi_2'(\eta) = \left\{ \left[(\eta - \phi_O) \frac{\psi_O}{F_O} \left(3 \frac{1-m}{m} - \phi_O'\right) - \gamma \frac{\sigma}{\eta} - \frac{F_O'}{F_O} \right] \right.$$

$$+ (\eta - \phi_O)\left(\frac{\psi_2}{\psi_O} - \frac{F_2}{F_O}\right) \frac{F_O'}{F_O} + 2\left(\frac{1-m}{m}\right) \frac{F_2}{F_O} + \gamma \eta \nu_O' \tag{41a}$$

$$+ \left. \left[(\eta - \phi_O) \frac{\psi_O}{F_O} \left(\eta \phi_O' + \frac{1-m}{m} \phi_O\right) + \eta \frac{F_O'}{F_O} + 2(\gamma+1)\left(\frac{1-m}{m}\right) \right] \right\}$$

$$\Big/ \left\{ \gamma - (\eta - \phi_O)^2 \frac{\psi_O}{F_O} \right\}$$

$$F_2' = \psi_O \left\{ (\eta - \phi_O)\phi_2' + \left[3\left(\frac{1-m}{m}\right) - \phi_O'\right] \phi_2 \right.$$

$$\left. + \left[\eta \phi_O' + \left(\frac{1-m}{m}\right)\phi_O\right]\nu_O \right\} + \frac{F_O'}{\psi_O} \psi_2 \tag{41b}$$

$$\psi_2' = \frac{1}{\eta - \phi_o} \left\{ \left[\phi_o' + \frac{\sigma}{\eta} \phi_o - 2\left(\frac{1-m}{m}\right) \right] \psi_2 + \psi_o \phi_2' \right.$$

$$\left. + \left(\psi_o' + \frac{\sigma}{\eta} \psi_o \right) \phi_2 - 2\left(\frac{1-m}{m}\right) \nu_o \psi_o - \eta (\nu_o \psi_o' + \psi_o \nu_o') \right\} \tag{41c}$$

$$\nu_2' = \frac{1}{\eta - \phi_o} \left\{ \nu_o' \phi_2 - \frac{\eta}{\psi_o} F_2' - 4\left(\frac{1-m}{m}\right) \nu_2 \right.$$

$$\left. + \frac{F_o}{\psi_o} \left[\left(2\frac{1-m}{m} + \eta \frac{F_o'}{F_o} \right) \frac{\psi_2}{\psi_o} - 4\left(\frac{1-m}{m}\right) \frac{F_2}{F_o} \right] \right\} \tag{41d}$$

Similarly, the derivatives of the similarity functions for the momentum variable formulation are, from equations (32) and (33):

$$F_o' = \frac{\gamma\left(\frac{1-m}{m}\right)\mu_o + \left(\eta - \frac{\mu_o}{\psi_o}\right)\left[2\left(\frac{1-m}{m}\right)\psi_o - \gamma \frac{\sigma}{\eta}\mu_o \right]}{\gamma - \left(\eta - \frac{\mu_o}{\psi_o}\right)^2 \frac{\psi_o}{F_o}}$$

$$\psi_o' = \frac{1}{\gamma}\left[\frac{\psi_o}{F_o} F_o' + 2\left(\frac{1-m}{m}\right)\psi_o / \left(\eta - \frac{\mu_o}{\psi_o}\right) \right] \tag{42}$$

$$\mu_o' = \frac{\mu_o}{\psi_o}\psi_o' + \left[F_o' - \left(\frac{1-m}{m}\right)\mu_o \right] / \left(\eta - \frac{\mu_o}{\psi_o}\right)$$

and

$$F_2' = \left\{ (\eta - \frac{\mu_o}{\psi_o}) \left[4(\frac{1-m}{m})\psi_o - \gamma(\eta - \frac{\mu_o}{\psi_o})\psi_o' \right] \frac{F_2}{F_o} \right.$$

$$+ 2(\frac{1-m}{m})(\eta - \frac{\mu_o}{\psi_o})(\psi_2 + \upsilon_2) + \gamma \left[3(\frac{1-m}{m}) - \frac{\sigma}{\eta}(\eta - \frac{\mu_o}{\psi_o}) \right] \mu_2$$

$$+ (\eta - \frac{\mu_o}{\psi_o}) \frac{F_o'}{F_o} \left[(\eta - \frac{\mu_o}{\psi_o})\psi_2 + (\eta\upsilon_2 + \mu_2) \right] \tag{43a}$$

$$+ \frac{\gamma}{\psi_o} \left[(\mu_o' - \frac{\mu_o}{\psi_o}\psi_o')(\eta\upsilon_2 - \psi_2) + \gamma(\frac{1-m}{m})\frac{\mu_o}{\psi_o}(\psi_2 - \upsilon_2) \right.$$

$$\left. - (2F_o + (\eta - \frac{\mu_o}{\psi_o})(\eta\psi_o' - \mu_o'))\,\psi_2 \right] - \gamma\eta \left[\eta F_o' - 2(\frac{1-m}{m})F_o \right] \right\}$$

$$\psi_2' = \frac{1}{\gamma F_o} \left\{ \psi_o F_2' + F_o'\psi_2 - \left[\gamma\psi_o' - 4(\frac{1-m}{m})\frac{\psi_o}{(\eta - \frac{\mu_o}{\psi_o})} \right] F_2 \right.$$

$$\tag{43b}$$

$$\left. + \left[(F_o' - \gamma F_o \frac{\psi_o'}{\psi_o})(\eta\upsilon_2 - \mu_2) + 2(\frac{1-m}{m})\frac{\gamma-1}{\gamma}\frac{(\psi_2 - \upsilon_2)}{(\eta - \frac{\mu_o}{\psi_o})} \right] \right\}$$

$$\upsilon_2' = \psi_2' - \left[\frac{\psi_o'}{\psi_o} - \frac{2(\frac{1-m}{m})}{(\eta - \frac{\mu_o}{\psi_o})} \right](\psi_2 - \upsilon_2) - \frac{\eta F_o' + 2(\frac{1-m}{m})F_o}{(\eta - \frac{\mu_o}{\psi_o})} \tag{43c}$$

$$\mu_2' = \eta\upsilon_2' - \frac{\sigma}{\eta}\mu_2 + 2(\frac{1-m}{m})\upsilon_2 \tag{43d}$$

Two major difficulties must be overcome in order to apply the scheme of integrating either equations (40) and (41) or equations (42) and (43) from the shock to the body. One difficulty is the singularity at the body surface apparent from the fact that the denominators of some of the terms of these equations approach zero as the independent variable η approaches the surface value η_b^*. It was overcome by using an approximate analytic solution, developed by Mirels (10) and described in Section B of the Appendix to calculate the value of η_b and the zeroth-order similarity functions in the region very near the body surface. For reasons explained in Appendix Section C, the second-order variables are calculated at the body by extrapolation of the order-δ^2 similarity functions. The extrapolation techniques used are described in the next section. The second of the two major difficulties is associated with the fact that the problem is a two-point boundary value problem. This difficulty is manifest in the need to choose initially the correct value of the shock wave displacement parameter a_2 (equation (7)) in order to satisfy the order-δ^2 boundary condition at the body surface when $\eta = \eta_b$ at the end of the integration. The steps taken to deal with this difficulty are described in Section C below.

$^*\phi_0 - \eta \to 0$ as $\eta \to \eta_b$ from equation (21).

B. <u>Extrapolation of Order-δ^2 Functions</u>

Two simple extrapolation techniques were used to carry the order-δ^2 similarity functions the short distance from the last computed point to the body surface.[*] For the velocity-variable formulation the extrapolation used for each of the functions F_2, ψ_2, ϕ_2, and ν_2 was a cubic function of η passing through three computed points of the function and having zero curvature at the body surface. The points used to define the curve were the last computed point and two previously computed points. The number of steps between the points was the next integer larger than the distance between the last point and the body divided by the last step size.

For the momentum-variable formulation, the functions F_2 and ν_2 were extrapolated linearly to the body surface using the last computed point and slopes. The order-δ^2 stream function θ_2 and its derivative were also calculated at the last point, using the momentum-variable form of equation (A9), and θ_2 was also extrapolated linearly. The values obtained were then used in equations (34) and (A8) to calculate $\psi_2(\eta_b)$ and $\mu_2(\eta_b)$.

C. <u>Methods for Determining the Constant a_2</u>

Since the constant a_2 is initially undetermined, the value of the order-δ^2 shock wave similarity ordinate

[*] The results are insensitive to the technique (Section IV-B).

$\eta_s = 1 + \delta^2 a_2 m^2 \, \xi^{-2(1-m)}$ is unknown and cannot be used to begin the integration toward the body surface. Also, this shock ordinate varies with the longitudinal distance ξ, so that its use would require a separate solution for every ξ value. The use of the zeroth-order shock ordinate $\eta = 1$ as the starting point for the integration avoids these two problems in determining the initial value of η_s but requires that the boundary conditions be transferred to $\eta = 1$ from $\eta = \eta_s$, the order-δ^2 shock position, where they are known. This transfer is made by using the Taylor series expansions of the similarity forms of the flow variables about the point $\eta = \eta_s$ in the same way as Kubota (9) and Mirels (10) did for the order-ϵ perturbation. The Taylor series expansion of a general function $g(\eta)$ about η_s is

$$g(\eta) = g(\eta_s) + \left[\frac{dg}{d\eta}\right]_{\eta_s} (\eta - \eta_s) + \left[\frac{d^2 g}{d\eta^2}\right]_{\eta_s} \frac{(\eta - \eta_s)^2}{2!} + \dots$$

Applying this expansion to equations (8)(with terms of order ϵ neglected) and evaluating at $\eta = 1$ give

$$p(\xi,1) = F_0(\eta_s) m^2 \xi^{-2(1-m)} + \delta^2 [F_2(\eta_s) - a_2 F_0'(\eta_s)] m^4 \xi^{-4(1-m)}$$
$$+ 0(\delta^4) \tag{44a}$$

$$\rho(\xi,1) = \psi_0(\eta_s) + \delta^2 [\psi_2(\eta_s) - a_2 \psi_0'(\eta_s)] m^2 \xi^{-2(1-m)} + 0(\delta^4) \tag{44b}$$

$$u(\xi,1) = \nu_o(n_s)m^2\xi^{-2(1-m)} + \delta^2[\nu_2(n_s) - a_2\nu_o'(n_s)]m^4\xi^{-4(1-m)} \quad (44c)$$

$$+ 0(\delta^4)$$

$$v(\xi,1) = \phi_o(n_s)m\xi^{-(1-m)} + \delta^2[\phi_2(n_s) - a_2\phi_o'(n_s)]m^3\xi^{-3(1-m)} \quad (44d)$$

$$+ 0(\delta^4)$$

Similarly applying the Taylor series expansion to equations (28) gives

$$(\rho u)(\xi,1) = \nu_o(n_s) + \delta^2[\nu_2(n_s) - a_2\nu_o'(n_s)]m^2\xi^{-2(1-m)} + 0(\delta^4)$$

$$\tag{45}$$

$$(\rho v)(\xi,1) = \mu_o(n_s)m\xi^{-(1-m)} + \delta^2[\mu_2(n_s) - a_2\mu_o'(n_s)]m^3\xi^{-3(1-m)}$$

$$+ 0(\delta^4)$$

Evaluating equations (8) at $n = 1$ directly and comparing the results to equations (44) and (45) yields boundary condition transfer relations of the form:

$$F_o(1) = F_o(n_s), \qquad F_2(1) = F_2(n_s) - a_2F_o'(n_s),$$

$$\psi_o(1) = \psi_o(n_s), \qquad \psi_2(1) = \psi_2(n_s) - a_2\psi_o'(n_s),$$

etc.

Putting equations (40) in for the derivatives and applying the boundary conditions at η_s (equations (16)) gives the transferred boundary conditions at $\eta = 1$:

$$
\left.
\begin{aligned}
&F_0(1) = \phi_0(1) = \frac{2}{\gamma+1}, \ \psi_0(1) = \frac{\gamma+1}{\gamma-1}, \ \nu_0(1) = \frac{-2}{\gamma+1} \\[2mm]
&F_2(1) = \frac{2}{\gamma+1} \left\{ 2\left[\left(\frac{3m-2}{m}\right) - \left(\frac{1-m}{m}\right)\left(\frac{2\gamma-1}{\gamma-1}\right) + \frac{\sigma\gamma}{\gamma+1}\right]a_2 - 1 \right\} \\[2mm]
&\psi_2(1) = -\frac{2}{\gamma-1}\left[3\left(\frac{1-m}{m}\right)\left(\frac{\gamma+1}{\gamma-1}\right) - \sigma\right]a_2 \\[2mm]
&\nu_2(1) = -\frac{2}{\gamma+1}\left\{ 2\left[\left(\frac{3m-2}{m}\right) - \left(\frac{1-m}{m}\right)\frac{1}{\gamma-1} + \frac{\sigma\gamma}{\gamma+1}\right]a_2 - 1 \right\} \\[2mm]
&\phi_2(1) = \frac{2}{\gamma+1}\left\{ \left[\left(\frac{3m-2}{m}\right) - 3\left(\frac{1-m}{m}\right) + 2\frac{\sigma\gamma}{\gamma+1}\right]a_2 - 1 \right\}
\end{aligned}
\right\} \quad (46)
$$

Similarly for the momentum variables (equations (42) and(36):

$$
\begin{aligned}
&\upsilon_0(1) = \frac{\gamma+1}{\gamma-1}, \quad \mu_0(1) = \frac{2}{\gamma-1} \\[2mm]
&\upsilon_2(1) = -\frac{2}{\gamma-1}\left\{ \left[3\left(\frac{1-m}{m}\right)\left(\frac{\gamma+1}{\gamma-1}\right) - \sigma\right]a_2 + 1 \right\} \qquad (47) \\[2mm]
&\mu_2(1) = \frac{2}{\gamma-1}\left\{ \left[\left(\frac{3m-2}{m}\right) - 3\left(\frac{1-m}{m}\right)\left(\frac{\gamma+1}{\gamma-1}\right) + 2\sigma\right]a_2 - 1 \right\}
\end{aligned}
$$

Iteration method. These transferred boundary conditions provide a definite starting position for the integration toward the body, but the constant a_2 must still be determined. There are two methods for determining a_2. The more obvious one is to guess the value of a_2, integrate toward the body (using the method given in the previous section to reach the surface), test the order-δ^2 boundary condition at the surface, and repeat using improved guesses until the surface boundary condition is satisfied closely enough. The improved gusses for this iteration method were made using the method of chords, a finite difference approximation to the well known Newton-Raphson method. (Note that the amount by which the boundary condition is not satisfied corresponds to the mass flow through the surface according to equations (20) or (38).)

Decomposition method. The other method for determining a_2 takes advantage of the linearity of the equations in the order-δ^2 functions, which allows superposition of solutions. It was used by Sakurai (4), Kubota (9), and Mirels (10) in obtaining their results and is applied in a similar manner here. Each of the order-δ^2 similarity functions is decomposed into a linear combination in the parameter a_2; e.g.

$$F_2(\eta) = F_{2a}(\eta)a_2 + F_{2c}^{\bullet}(\eta),$$

(48)

$$\psi_2(\eta) = \psi_{2a}(\eta)a_2 + \psi_{2c}(\eta), \text{ etc.}$$

Splitting each of the equations obtained in this way into two separate equations, by setting the term containing a_2 and the other term each equal to zero, produces a system of equations in the subscript-a functions and a system in the subscript-c functions. The system in the subscript-c functions is identical to the original system of equations (13) or (33). The system in the subscript-a functions is the same except that the inhomogeneous terms (i.e. the terms that do not contain an order-δ^2 function or its derivative) do not appear. These two systems of equations have two different sets of boundary conditions. In order to obtain them, the boundary conditions at $\eta = 1$ (equations (46) or (47)) are decomposed by comparisons with equation (48), giving

$$F_{2a}(1) = \frac{4}{\gamma+1}\left[(\frac{3m-2}{m}) - (\frac{1-m}{m})(\frac{2\gamma-1}{\gamma-1}) + \frac{\sigma\gamma}{\gamma+1}\right], \quad F_{2c}(1) = -\frac{2}{\gamma+1} \quad \text{(49a)}$$

$$\psi_{2a}(1) = -\frac{2}{\gamma-1}\left[3(\frac{1-m}{m})(\frac{\gamma+1}{\gamma-1}) - \sigma\right], \quad \psi_{2c}(1) = 0 \quad \text{(49b)}$$

$$v_{2a}(1) = -\frac{4}{\gamma+1}\left[(\frac{3m-2}{m}) - (\frac{1-m}{m})(\frac{1}{\gamma-1}) + \frac{\sigma\gamma}{\gamma+1}\right], \quad v_{2c}(1) = \frac{2}{\gamma+1} \quad \text{(49c)}$$

$$\phi_{2a}(1) = \frac{2}{\gamma+1}\left[\left(\frac{3m-2}{m}\right) - 3\left(\frac{1-m}{m}\right) + 2\frac{\sigma\gamma}{\gamma+1}\right], \quad \phi_{2c}(1) = -\frac{2}{\gamma+1} \quad (49d)$$

or,

$$\upsilon_{2a}(1) = -\frac{2}{\gamma-1}\left[3\left(\frac{1-m}{m}\right)\left(\frac{\gamma+1}{\gamma-1}\right) - \sigma\right], \quad \upsilon_{2c}(1) = -\frac{2}{\gamma-1}$$

$$(50)$$

$$\mu_{2a}(1) = \frac{2}{\gamma-1}\left[\left(\frac{3m-2}{m}\right) - 3\left(\frac{1-m}{m}\right)\left(\frac{\gamma+1}{\gamma-1}\right) + 2\sigma\right], \quad \mu_{2c}(1) = -\frac{2}{\gamma-1}$$

These decomposed variables are then substituted into the order-δ^2 flow equations, so that the continuity equation (13), for example, becomes:

$$\left\{\psi_o\phi'_{2a} + (\psi'_o + \frac{\sigma}{\eta}\psi_o)\phi_{2a} - (\eta - \phi_o)\psi'_{2a}\right.$$

$$\left. + [\phi'_o + \frac{\sigma}{\eta}\phi_o + 2(\frac{1-m}{m})]\psi_{2a}\right\}a_2$$

$$+ \left\{\psi_o\phi'_{2c} + (\psi'_o + \frac{\sigma}{\eta}\psi_o)\phi_{2c} - (\eta - \phi_o)\psi'_{2c}\right.$$

$$\left. + [\phi'_o + \frac{\sigma}{\eta}\phi_o + 2(\frac{1-m}{m})]\psi_{2c} - \eta\upsilon_o\psi'_o\right.$$

$$\left. - [\eta\upsilon'_o + 2(\frac{1-m}{m})\upsilon_o]\psi_o\right\} = 0$$

Beginning at $\eta = 1$ with these boundary conditions, the decomposed system of equations (in either the velocity variables or the momentum variables) is integrated toward

the body. Near the surface the method given in Section III-B is used to obtain values for the decomposed functions at the surface. The boundary condition at the surface, expressed in terms of these surface values of the decomposed functions, is (from equation (21))

$$\phi_{2a}(\eta_b)a_2 + \phi_{2c}(\eta_b) - \eta_b\nu_o(\eta_b) = 0$$

or (from equation (39))

$$[\mu_{2a}(\eta_b) - \eta_b\nu_{2a}(\eta_b)]a_2 + [\mu_{2c}(\eta_b) - \eta_b\nu_{2c}(\eta_b)] = 0$$

Thus, in the velocity-variable formulation, the value of a_2 is found from the relation

$$a_2 = \frac{\eta_b\nu_o(\eta_b) - \phi_{2c}(\eta_b)}{\phi_{2a}(\eta_b)} \tag{51}$$

In the momentum formulation, a_2 is

$$a_2 = - \frac{\eta_b\nu_{2c}(\eta_b) - \mu_{2c}(\eta_b)}{\eta_b\nu_{2a}(\eta_b) - \mu_{2a}(\eta_b)} \tag{52}$$

The value of a_2 is now used to recombine the decomposed similarity functions using relations such as equations (48).

Once these functions have been computed for any value of the body power-law exponent m (with $\sigma = 0$ or 1), they

can be used to calculate the complete flow field about
any such body as long as it is slender enough that $\delta^4 << 1$
and the Mach number is large enough that $\epsilon \equiv \dfrac{1}{M_\infty^2 \delta^2} << 1$.

D. Description of the Numerical Method

The equations derived in the previous sections of this
dissertation have been programmed for numerical solution on
the CDC 6600 digital computer at the NASA Langley Research
Center. Three separate programs were written, correspond-
ing to three of the different methods of obtaining solutions
which have been discussed. Two of these programs integrate
the velocity-function equations (40) and (41); one uses the
iterative and the other the decomposition method for obtain-
ing the value of a_2. The third program integrates the
momentum function equations (42) and (43) and determines a_2
by the iterative method. All three of these computer pro-
grams use a standard integration subroutine employing the
fourth-order Runga-Kutta formula supplemented by a Richard-
son's extrapolation. This subroutine halves or doubles the
integration step size automatically in order to meet a
specified local truncation error.

For the present computations the initial step size (in
η) was 2^{-8} (.00390625), and the maximum allowable step size
was 2^{-7} (.0078125). Generally the step size decreased to
less than 2^{-15} near the body. At each step estimates of

η_b and F_o (η_b) were computed by the method given in Appendix Section B (equations (A18)). When both estimates agreed to within 1.0×10^{-9} on successive steps, the estimates were accepted as the actual values of η_b and F_o (η_b) and the values of the other functions at the body were computed from the approximate analytic solution given in Appendix Section B or the extrapolations given in Section III-B. The iterative programs used a "method of chords" algorithm to compute improved estimates of the values of a_2. (This is a finite difference approximation to the well-known Newton-Raphson method). The iteration was considered to have converged when the order-δ^2 boundary condition at the surface (equation (21) or (39)) was satisfied to within 0.5×10^{-10}.
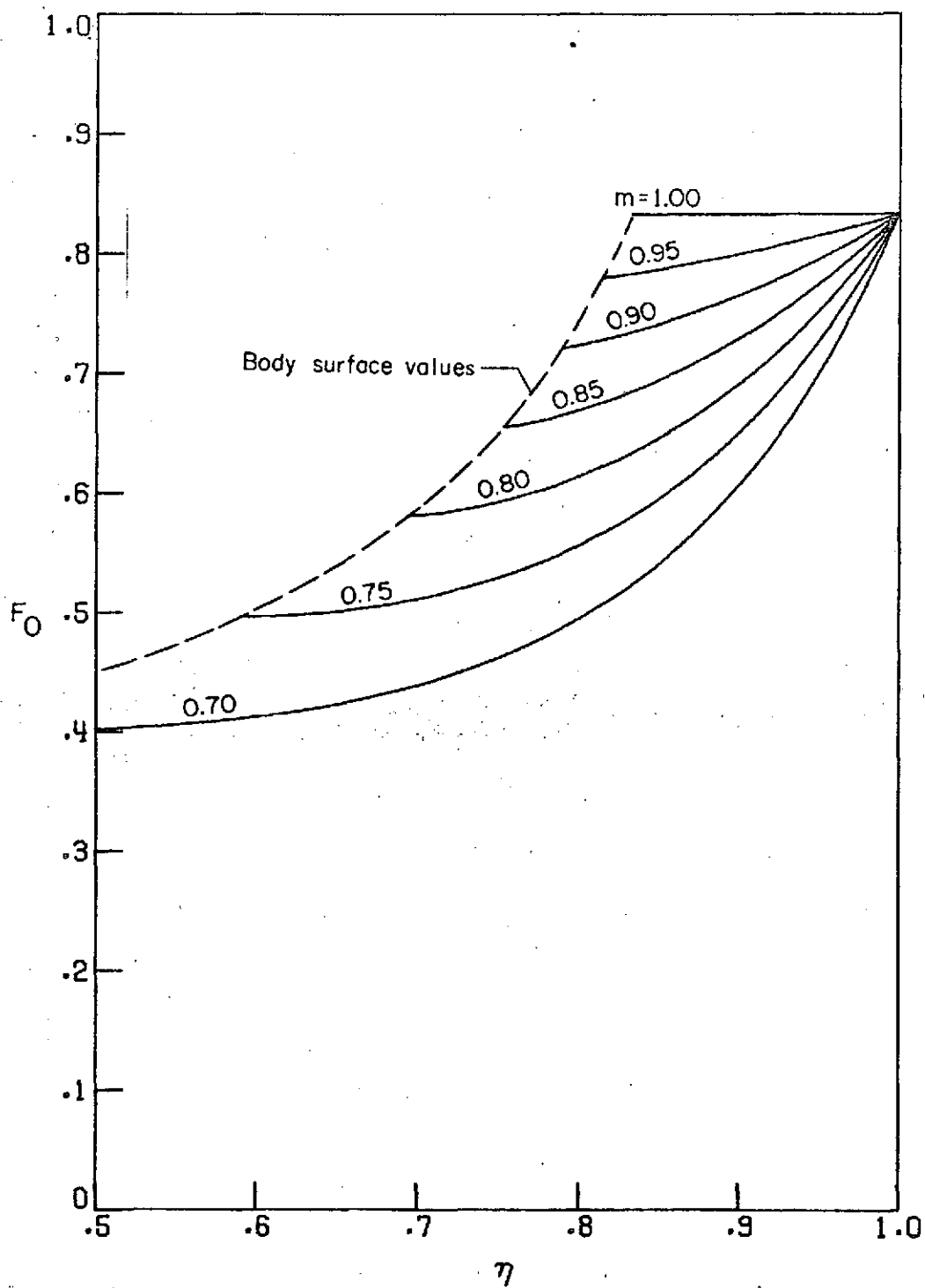
CHAPTER IV.   DISCUSSION OF RESULTS

A.   Zero - Order Functions

The methods given in the last chapter have been used to
compute the zeroth-order and order-δ^2 similarity functions
for a number of cases, which will be presented and discussed
in this chapter. Unless otherwise noted, these cases are all
for $\gamma = 1.4$, representing air as an ideal gas. The Figures
presenting the functions were plotted by Calcomp plotting
machines directly from the computed results. The slight
waviness which may be noticeable at some points in the
Figures is a result of this computer-aided plotting process;
however, the curves at all points on the plots are accurate
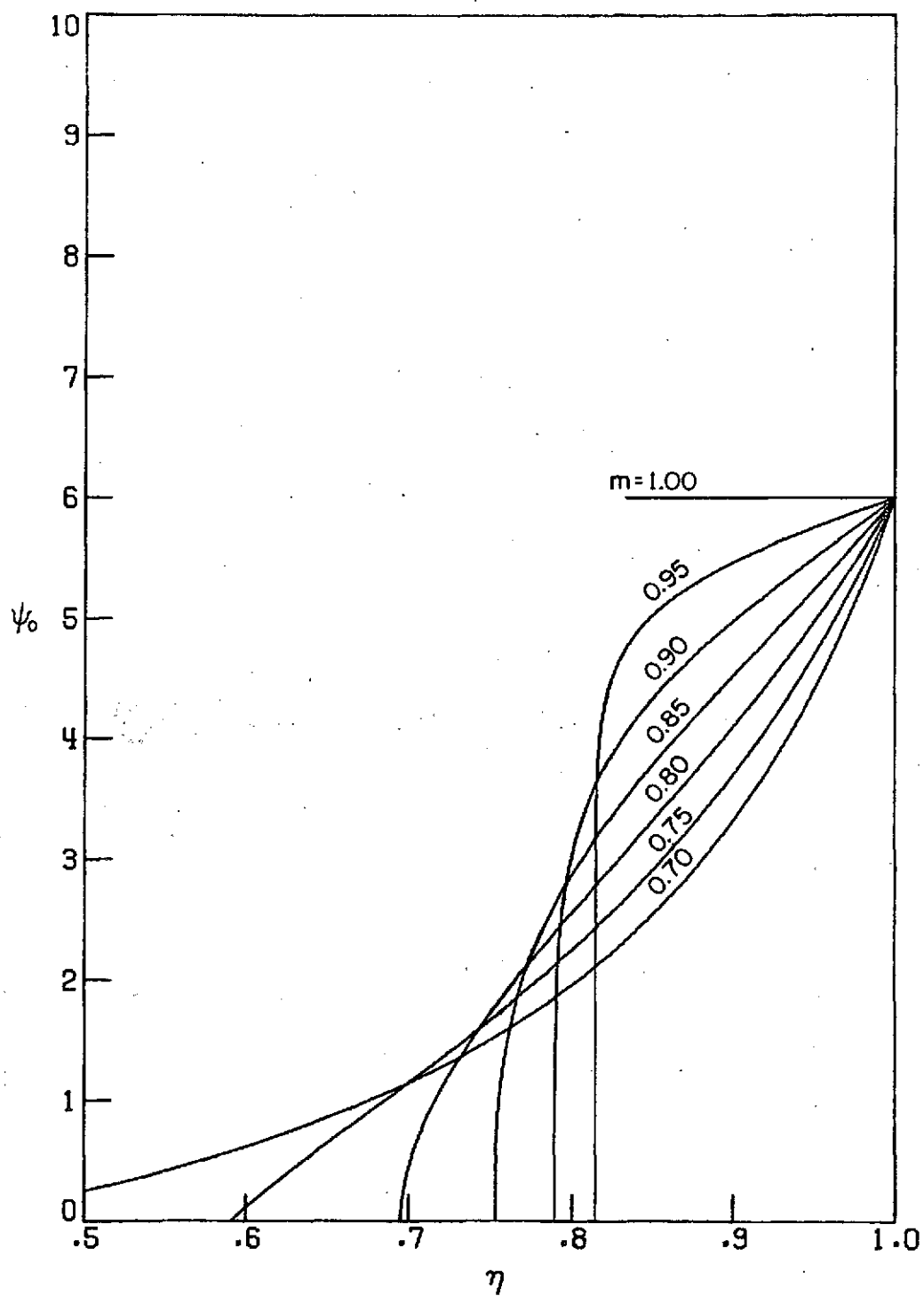to within 0.1 percent of the full scale values.

The zeroth-order similarity functions F_o, ψ_o, ϕ_o and
v_o are shown for several values of the power-law exponent
m in Figure 4 for two-dimensional flow ($\sigma = 0$) and Figure 5
for axially symmetric flow ($\sigma = 1$). These functions agree
with the same functions calculated by Kubota (9), Mirels
(10,16), and Townsend (23).

The pressure function F_o and the lateral-velocity
function ϕ_o are seen to be smooth and well-behaved from
the zero-order shock location ($\eta = 1$) to the body surface.
Note that the body surface values of ϕ_o lie on the line
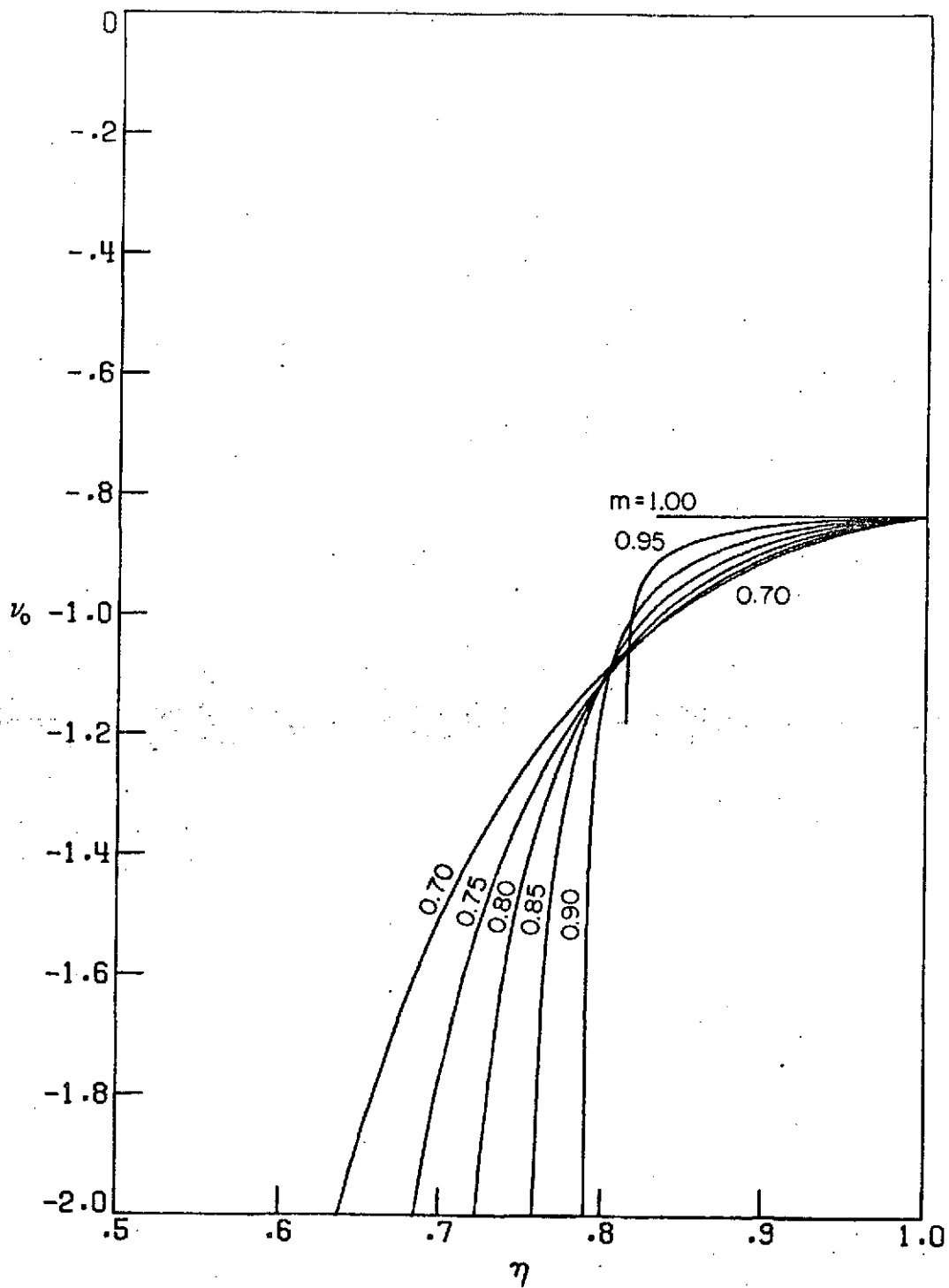$\phi_o = \eta$ in accordance with the zeroth-order boundary condition

(a) Pressure function, $F_O(\eta)$.

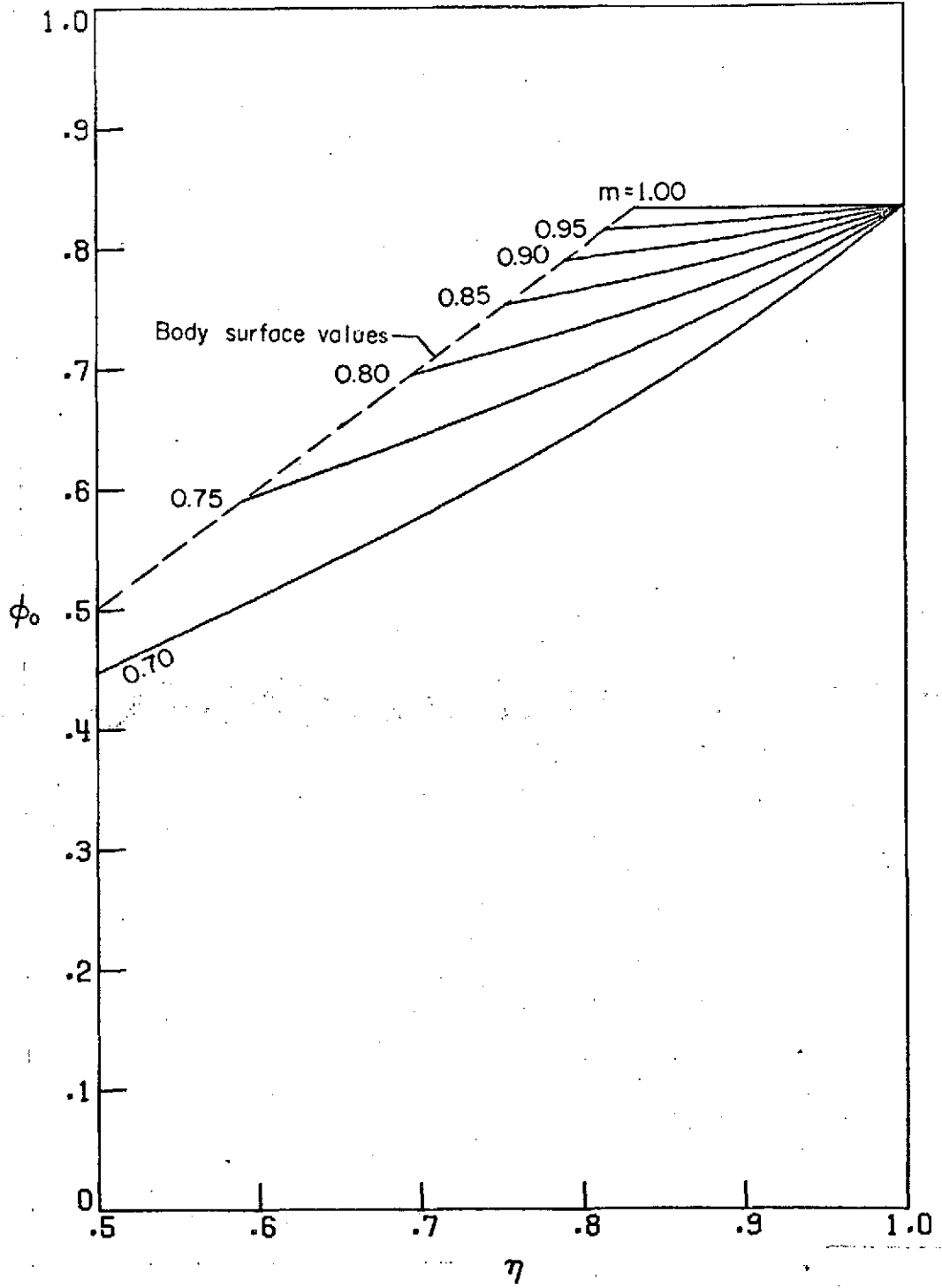Figure 4. Zeroth-order Similarity Functions for Two-Dimensional Flow ($\sigma = 0$).

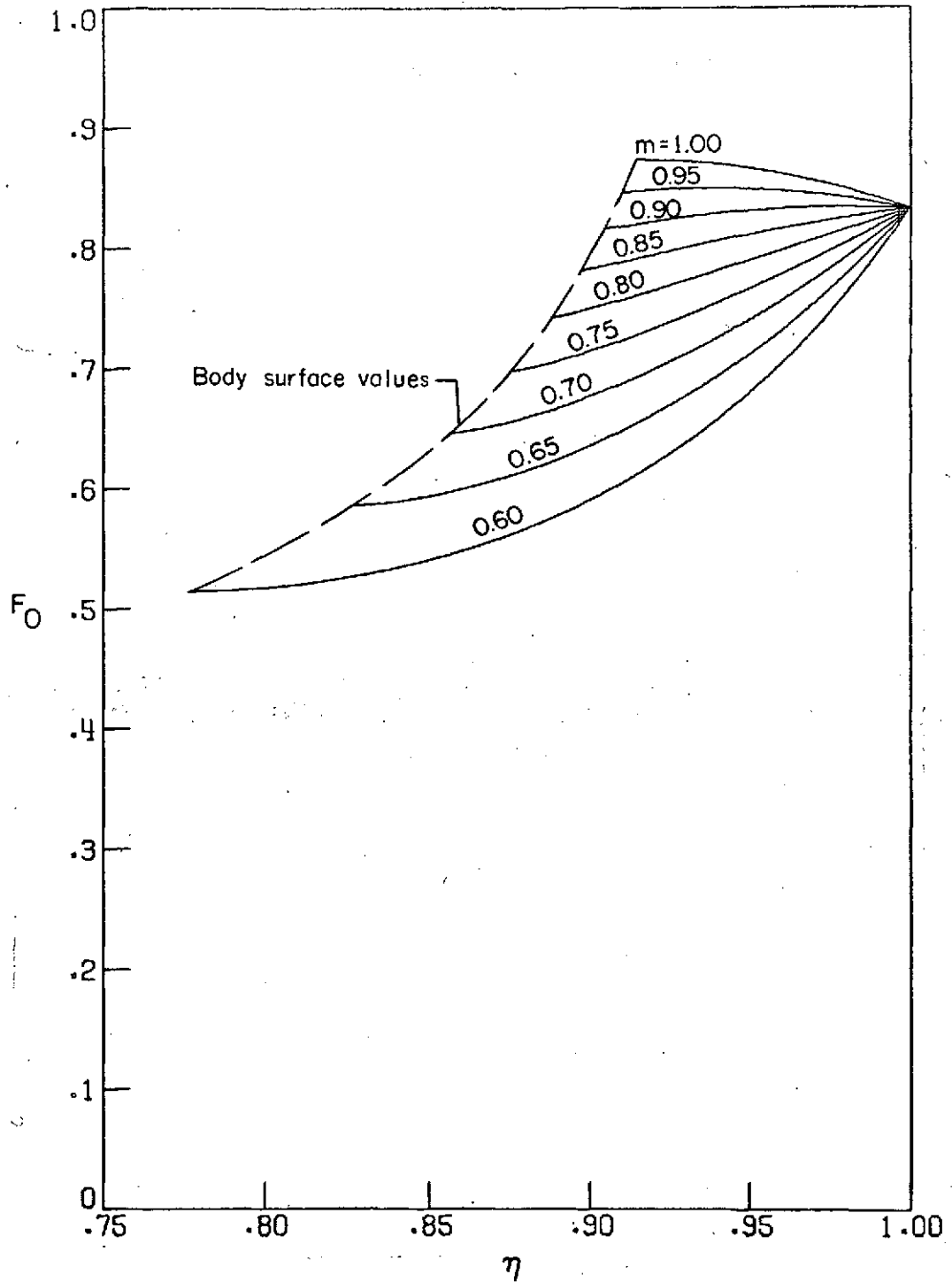(b) Density function, $\psi_0(\eta)$.

Figure 4. Continued.

(c) Longitudinal velocity function, $v_o(\eta)$.

Figure 4. Continued.
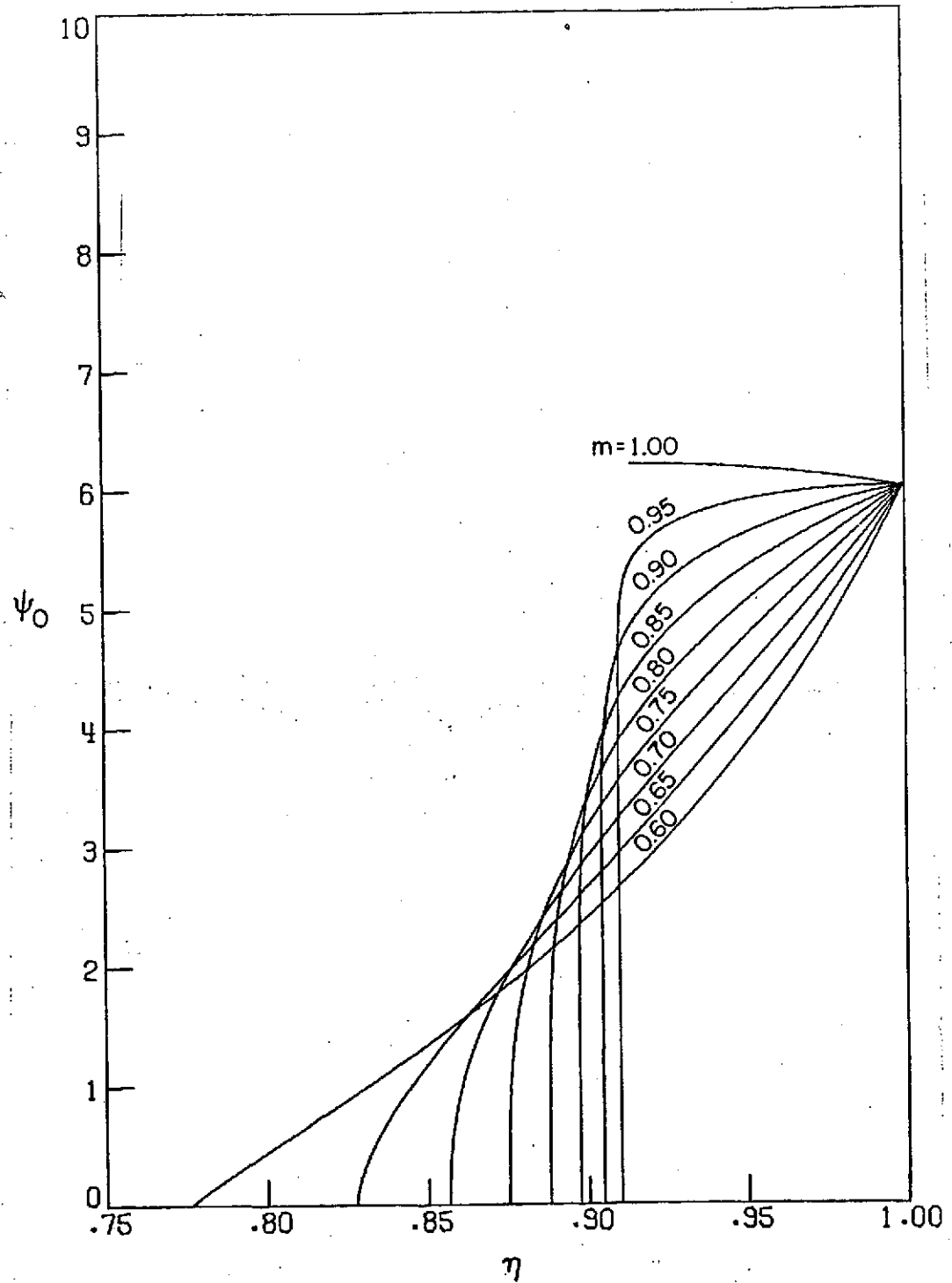
(d) Lateral velocity function, $\phi_o(\eta)$.
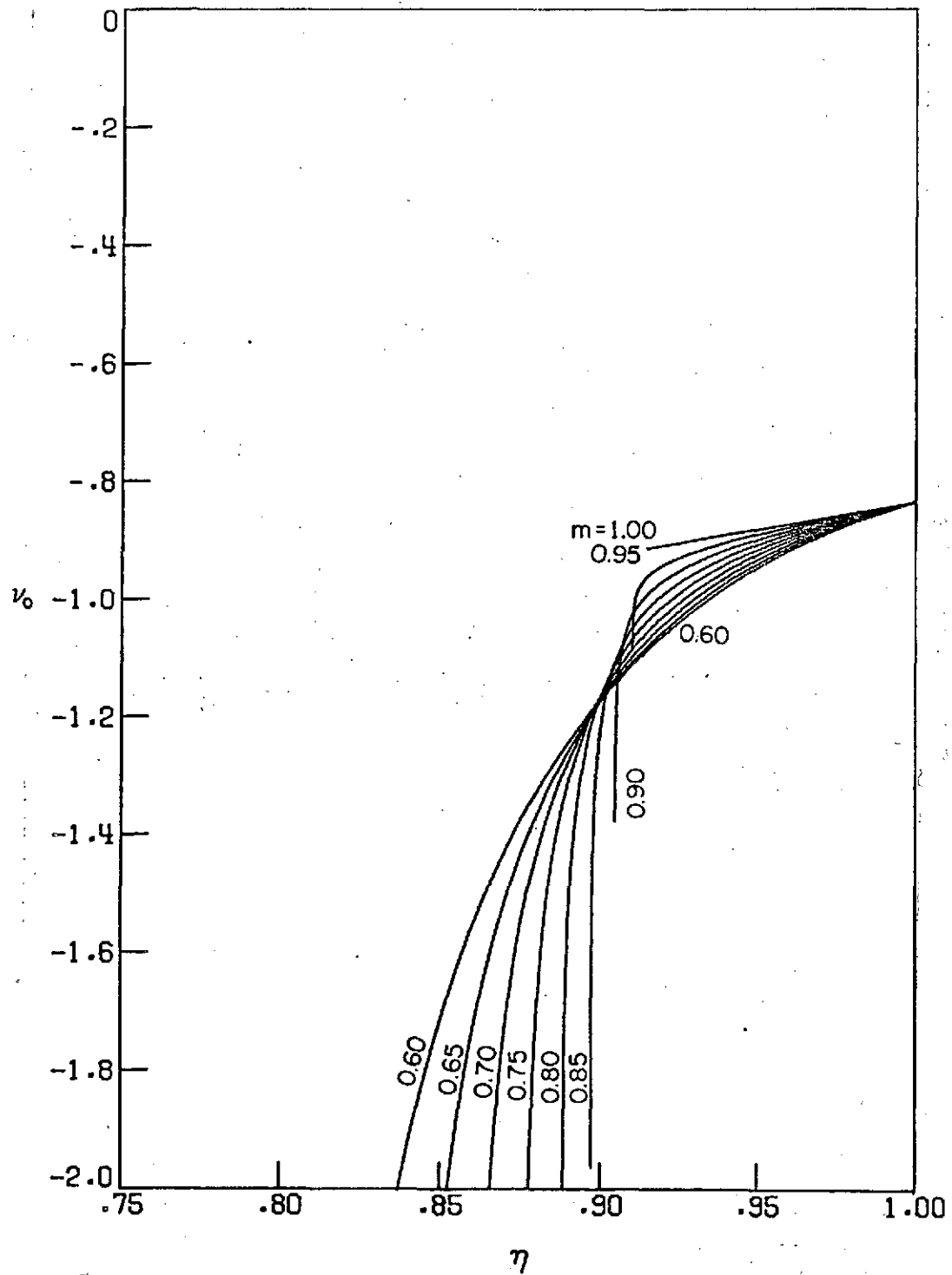
Figure 4. Concluded.

(a) Pressure function, $F_0(\eta)$.

Figure 5. Zeroth-order Similarity Functions for Axisym-
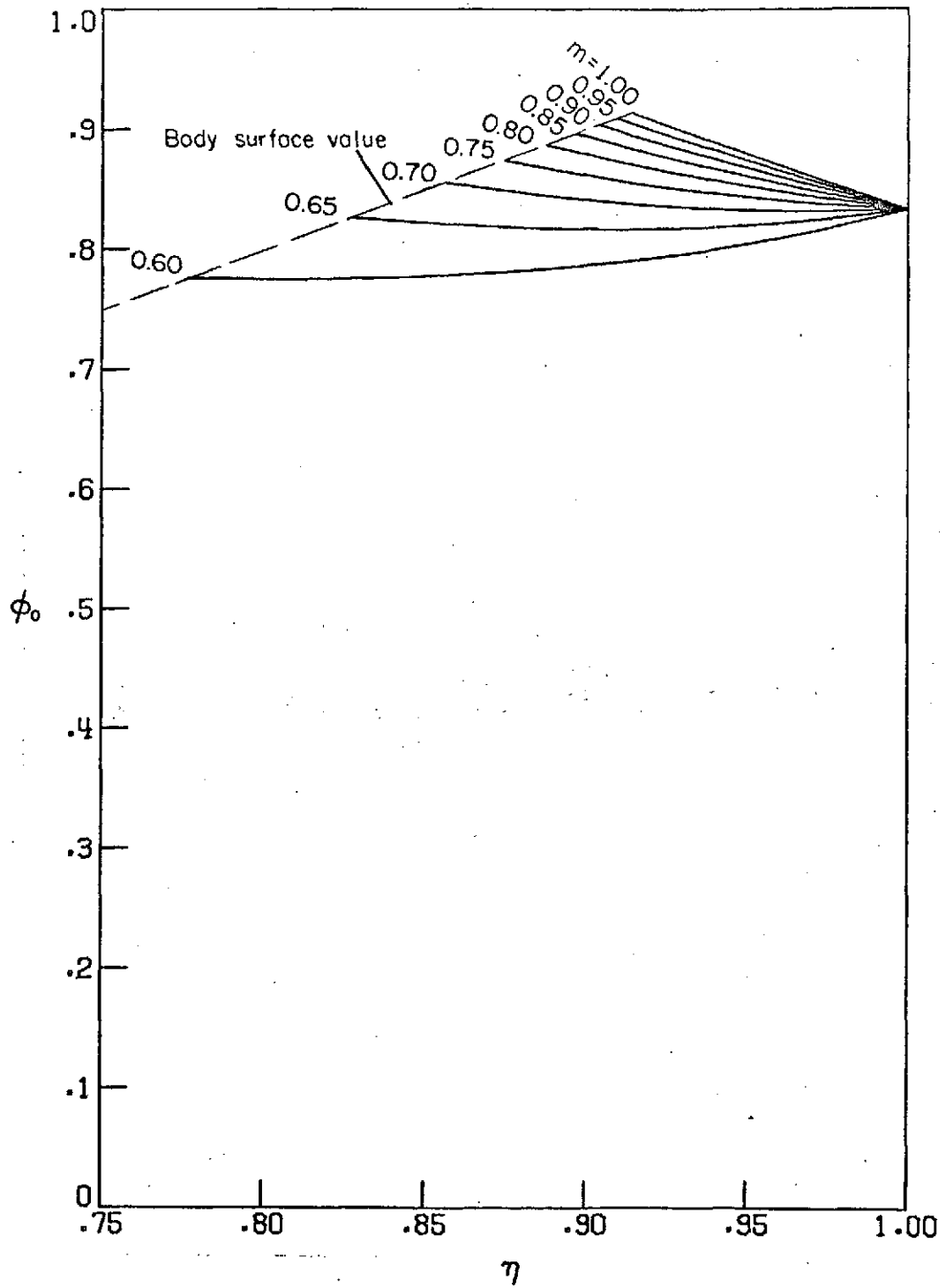metric Flow ($\sigma = 1$).

(b) Density function, $\psi_o(\eta)$.

Figure 5. Continued.

(c) Longitudinal velocity function, $\nu_o(\eta)$.

Figure 5. Continued.

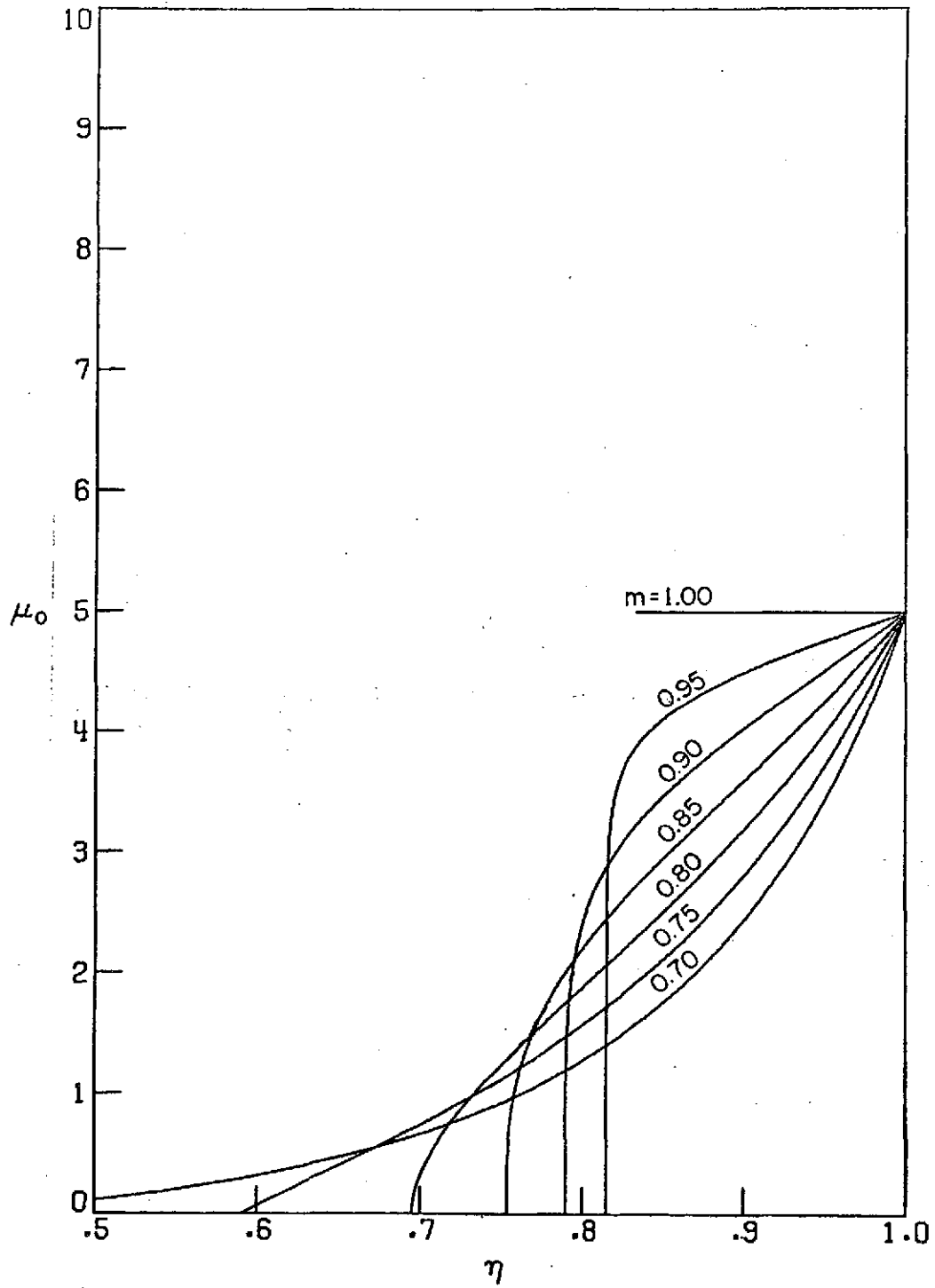(d) Lateral velocity function, $\phi_0(\eta)$.

Figure 5. Concluded.

(equation (21)). As expected from the discussion in Section II-C, the density function ψ_0 and the longitudinal velocity function ν_0 exhibit different types of singular behavior at the body surface for $m \neq 1$: ψ_0 goes to zero, and ν_0 goes toward minus infinity. From the Figure it appears that the effects of these singularities are confined to a thin layer near the body surface, at least for values of m near 1.

The zeroth-order lateral momentum function μ_0 is shown in Figure 6 for both the planar and axisymmetric cases. As indicated in Section II-D, the longitudinal momentum function ν_0 is the same as the density function ψ_0, and the pressure and density functions, F_0 and ψ_0 are the same as in the velocity-variable formulation. In the separate calculations made for the momentum-variable formulations, these functions came out essentially identical to the previous calculations, Figures 4 and 5. The function μ_0 is seen in Figure 6 to behave like ψ_0, in agreement with the comparison of methods in equations (34). Thus the reformulation in terms of momentum variables was successful in avoiding the unlimited growth of ν_0 near the body surface.
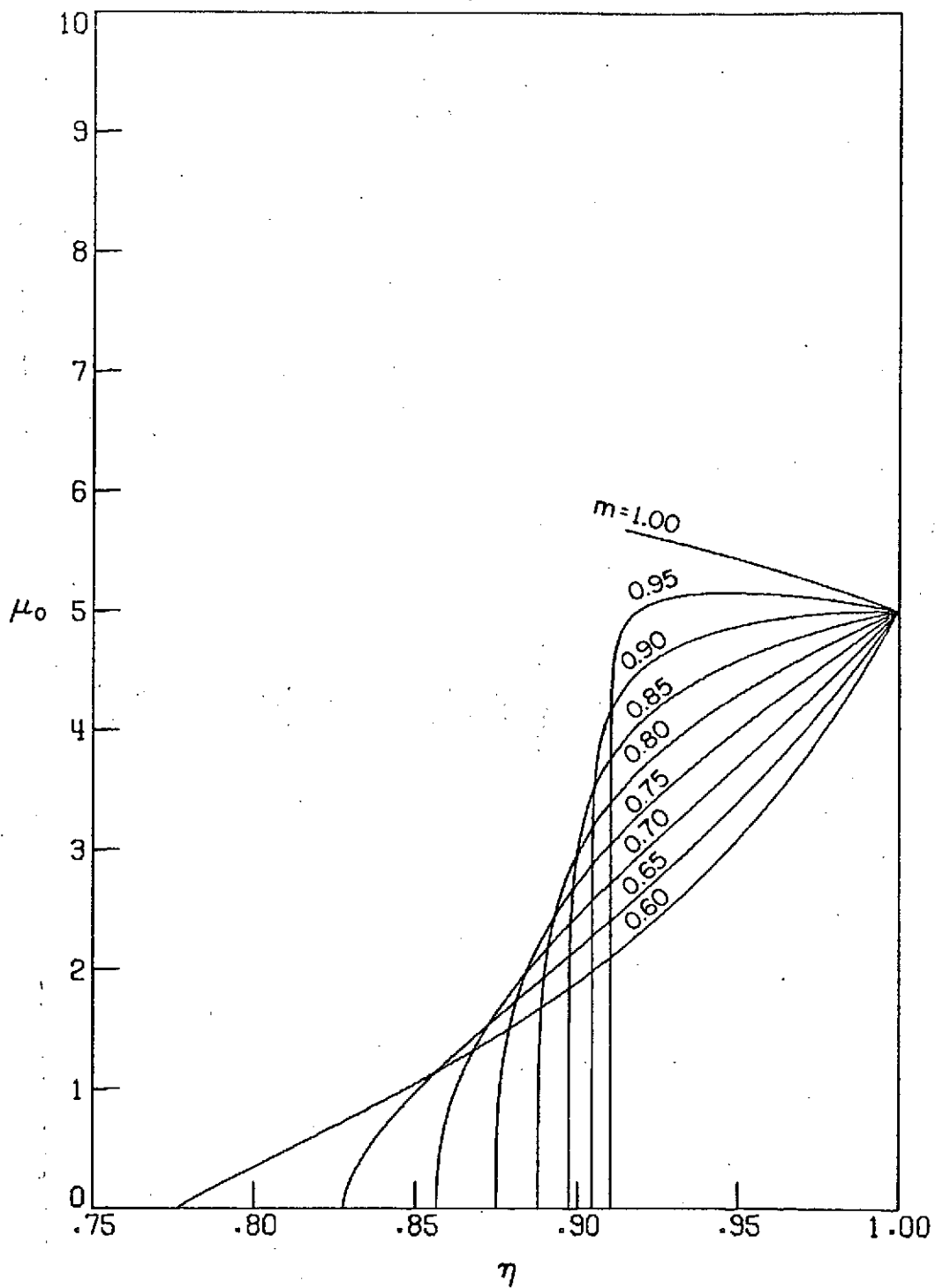
B. Shock Displacement Constant

The variation of the calculated order-δ^2 shock wave displacement constant a_2 with the power-law exponent m is shown in Figure 7(a) for both two-dimensional and

(a) Two-dimensional flow ($\sigma = 0$).

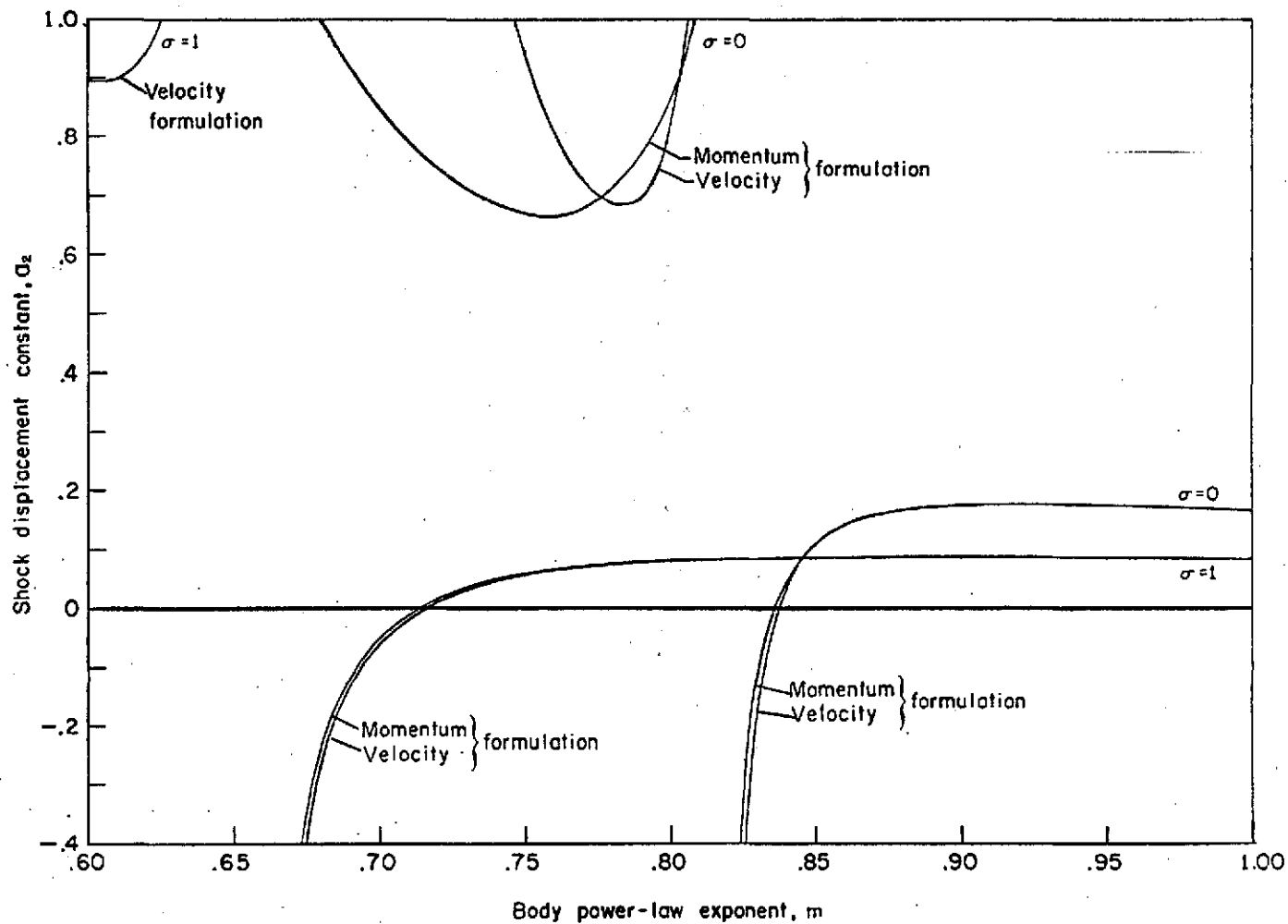Figure 6. Zeroth-Order Lateral Momentum Function, $\mu_o(\eta)$.

(b) Axisymmetric flow ($\sigma = 1$).
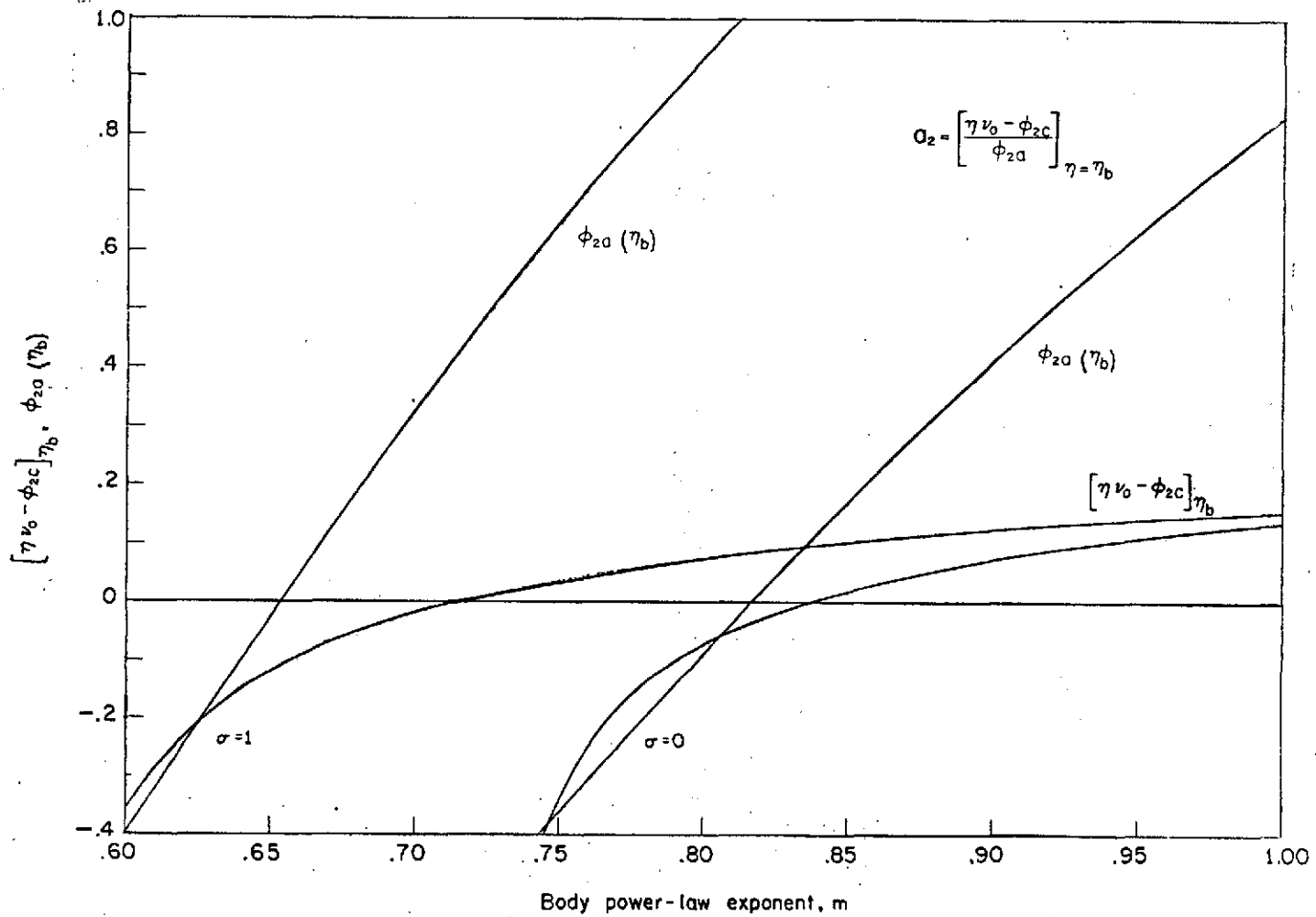
Figure 6. Concluded.

axisymmetric bodies. The calculations made using the iterative method for obtaining a_2 gave essentially the same values as were obtained by the decomposition method (equations (48) - (52)). As can be seen in the Figure, the momentum-variable formulation results for a_2 differ only slightly from the results of the velocity-variable formulation. However, all of the results are characterized by a singular discontinuity in a_2 which has no physical counterpart in the actual flow about power-law bodies. This singularity, which occurs near $m = .817$ for $\sigma = 0$ and near $m = .653$ for $\sigma = 1$, represents a rapid decrease in the distance from the shock to the body as the power-law decrease, followed by a jump to a large distance at the discontinuity. Since this behavior is physically unrealistic, it must be an artifact of the mathematical processes (analytical and numerical) used to obtain the solutions.

Figure 7(b) shows that the singularity is associated with a zero in the denominator of equation (51). (This is the equation used in the decomposition method to determine the value of a_2 satisfying the order-δ^2 boundary condition at the surface.) Since there is a nearby zero in the numerators of this equation, it is probable that the singularity in the quotient a_2 occurs because the zeros in the numerator and denominator, which should coincide, are displaced relative to one another. (Coincidence of the

(a) Computed values for a_2.

Figure 7. Variation of Shock Displacement Constant a_2 with Body Power-Law Exponent m.

(b) Numerator and denominator of expression for a_2 (equation (51)).

Figure 7. Concluded.

zeros would make a_2 mathematically indeterminate at that point but would allow a continuous variation of a_2 with m, from which the value at the indeterminate point could be inferred.) The most likely causes of such a zero displacement are accumulated truncation errors from the numerical integration and errors in the extrapolation from the last integration point to the body surface. Any error occurring in these processes is aggravated by the fact that the numerator of equation (51) is the small difference of two nearly equal extrapolated numbers. For example, with $\sigma = 0$ and $m = .83$, $\eta_b = .73327$ and the extrapolated values $v_o(\eta_b) = -9.9910$ and $\phi_{2c}(\eta_b) = -7.3153$ give the numerator $-.0108$ with a relative error about 1000 times that of the individual functions; that is, an 0.1% error in $v_o(\eta_b)$ and $\phi_{2c}(\eta_b)$ would become a 100% error in the numerator of equation (51).

To test this line of reasoning, additional calculations were made reducing the step size, reducing the range of the extrapolation, and finally, extrapolating the whole numerator of equations (51) rather than just the separate parts. The results of these calculations indicate that the value of a_2 is sensitive to these changes for power-law exponents less than that at the singularity; but, the position of the singularity and the values of a_2 for m greater than that at the singularity were virtually unaffected. Thus, removing
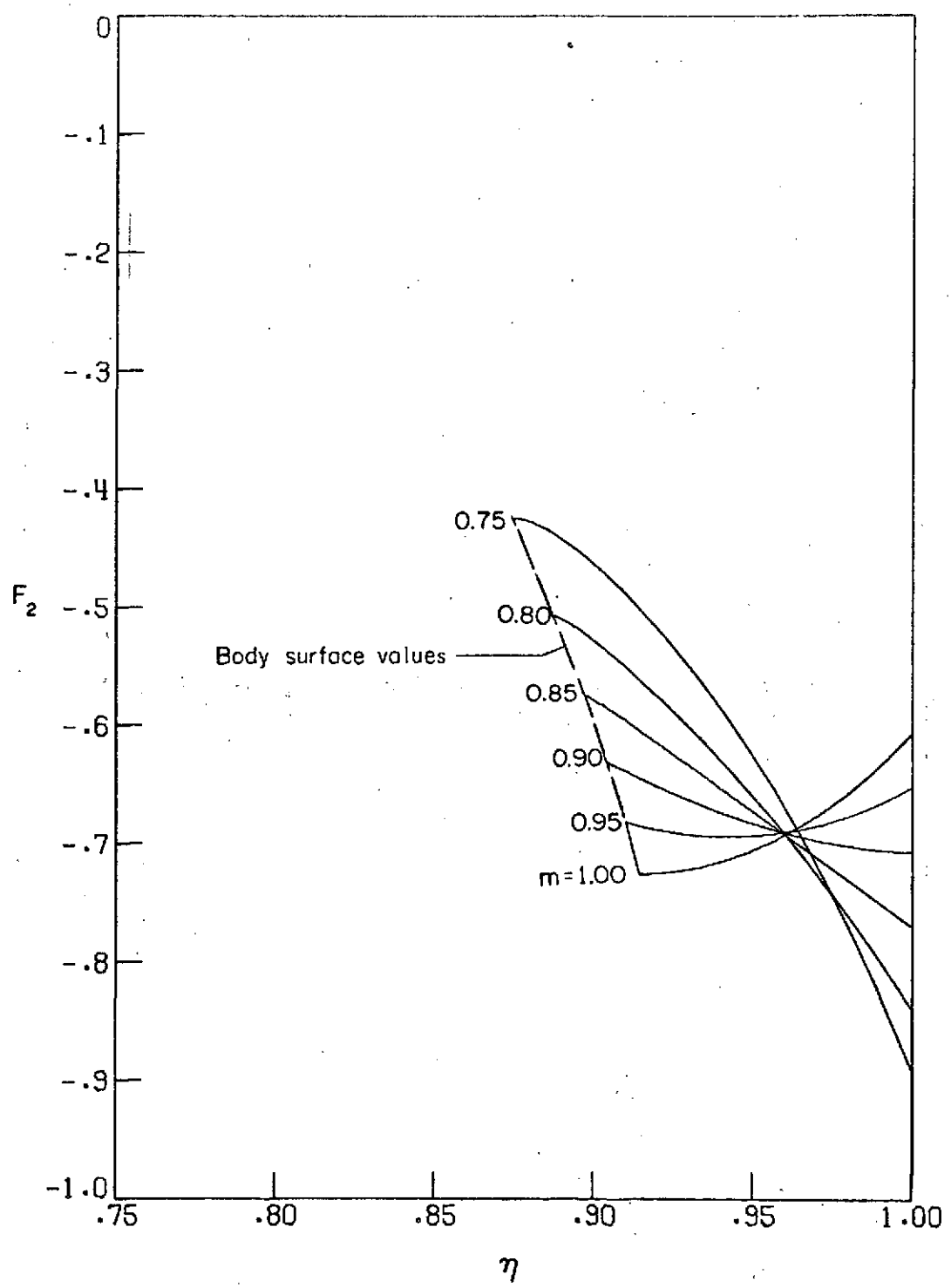
the singularity would require a more radical change in the mathematical process than simply changing parameters in the numerical integration and extrapolation schemes. This conclusion is supported by the results shown in Figure 7(a) where the singularity itself appears to be unaffected by the change to the momentum variable formulation and change in extrapolation mode, although there are large changes in the computed value of a_2 for m less than that at the singularity. Note that, while it is associated with the zero in the denominator of equation (51) from the decomposition method for determining a_2, the singularity in a_2 occurs at exactly the same place when the iteration method is used.

The results of the present calculations should be good for body power-law exponents above those for which there is a significant influence from the singularity. Based on Figure 7, the range for good results is about $.85 \leq m \leq 1.0$ for the two-dimensional flow ($\sigma = 0$) and $.75 \leq m \leq 1.0$ for the axisymmetric flow ($\sigma = 1$). Note that this is a more restricted range than that for similarity solutions ($\frac{2}{3+\sigma} < m \leq 1$, Lees and Kubota (8)) or to avoid first-order entropy-layer effects ($\frac{2(\gamma+1)}{(3+\sigma)\gamma+2} < m \leq 1$, Freeman (17)).

C. Order-δ^2 Functions
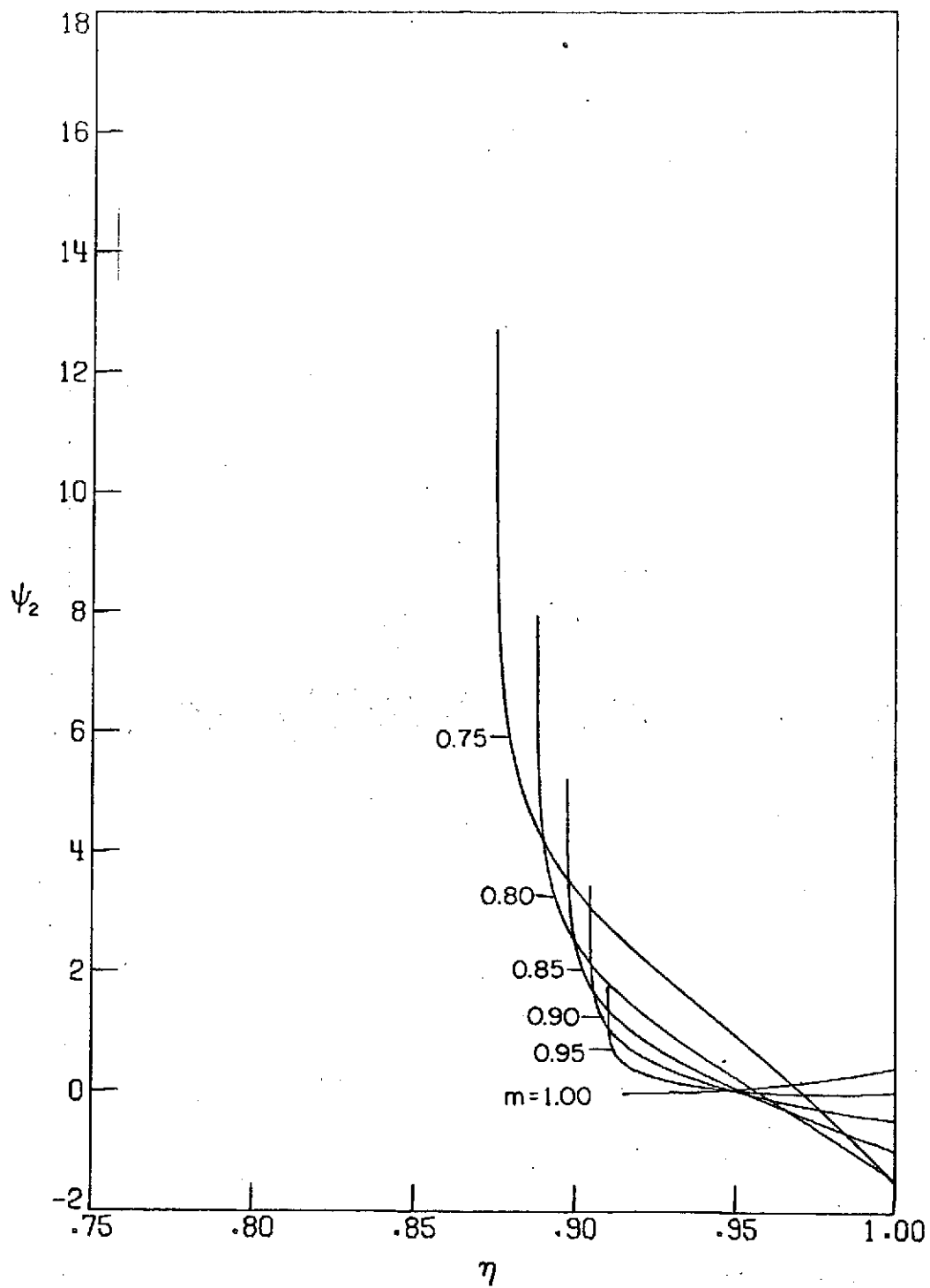
The order-δ^2 similarity functions F_2, ψ_2, υ_2, and μ_2 from the momentum-variable formulation, computed for axisymmetric flow ($\sigma = 1$) using iteration, are shown in Figure 8. These functions are seen to have some differences in behavior from the zeroth-order functions described in Section IV-A. The most obvious difference is that the curves describing these functions do not all emanate from a single point at $\eta = 1$. The variation at $\eta = 1$ is due to the variation of the boundary conditions at the shock with the body power-law m and to the transfer of the boundary conditions from the shock to $\eta = 1$. As was noted Section B of Chapter III, the values of these order-δ^2 functions at the body surface were found using a linear extrapolation from the last computed point of the numerical integration. The range of the extrapolation was less than .00002 in η for all the cases shown except for $m = 1.0$, for which the extrapolation was made over an η distance of less than .001.

The order-δ^2 similarity functions F_2, ψ_2, ν_2, and ϕ_2 from the velocity variable formulation and using the cubic extrapolation to obtain the surface values are shown in Figure 9 for axisymmetric flow ($\sigma = 1$). The results shown were obtained using the decomposition technique for calculating the shock displacement constant a_2 (equations (48) - (52)), but essentially identical results were also obtained

(a) Pressure function, $F_2(\eta)$.

Figure 8. Order-δ^2 Similarity Functions from the Momentum-Variable Formulation for Axisymmetric Flow ($\sigma = 1$).

(b) Density function, $\psi_2(\eta)$.

Figure 8. Continued.

(c) Longitudinal momentum function, $\upsilon_2(\eta)$.

Figure 8. Continued.

(d) Lateral momentum function, $\mu_2(\eta)$.
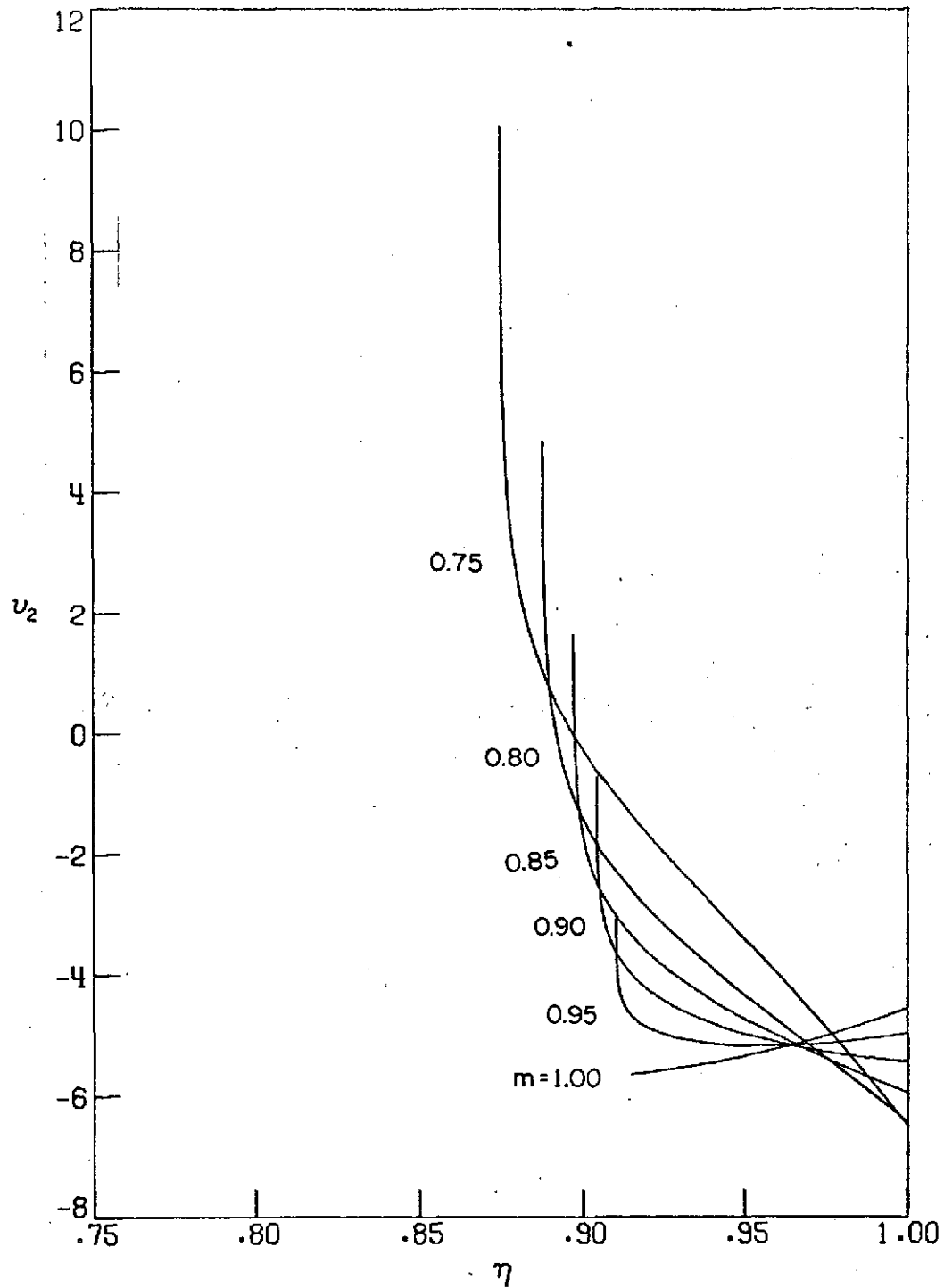
Figure 8.   Concluded.

(a) Pressure function, $F_2(\eta)$.

Figure 9.   Order-δ^2 Similarity Functions from the Velocity-
Variable Formulation for Axisymmetric Flow ($\sigma = 1$).

(b) Density function, $\psi_2(\eta)$.

Figure 9. Continued.

(c) Longitudinal velocity function, $v_2(\eta)$.

Figure 9. Continued.

(d) Lateral velocity function, $\phi_2(\eta)$.

Figure 9. Concluded.

using iteration. The two functions F_2 and ψ_2, which are
the same in both the velocity-variable and momentum-variably
formulations, are practically the same in Figure 9 as in
Figure 8. However, for power-law exponents less than those
shown there are differences which become large as m de-
creases, corresponding to the behavior of the constant a_2
(Figure 7).

The same comparison between methods of computing the body
surface values of the order-δ^2 similarity functions that was
made above for the axisymmetric bodies can be made for the
two-dimensional bodies ($\sigma = 0$). The momentum-variable
similarity functions for these bodies computed using the
linear extrapolation technique are shown in Figure 10. The
velocity-variable similarity functions computed using the
cubic extrapolation technique are shown in Figure 11. These
two sets of functions exhibit the same type of agreement as
the functions for axisymmetric bodies (Figures 8 and 9).

All of the order-δ^2 velocity and momentum functions
show singular behavior at the body surface for m < 1. It
was in anticipation of such behavior for v_0 that the
momentum-variable formulation was undertaken (Section II-D).
While the reformulation was successful in avoiding the un-
limited growth of v_0 at the body, it did not avoid the same
type of behavior by the order-δ^2 functions. Because of this
failure to eliminate the singularities and because it does

(a) Pressure function, $F_2(\eta)$.

Figure 10. Order-δ^2 similarity functions from the velocity-variable formulation for two-dimensional flow ($\sigma = 0$).
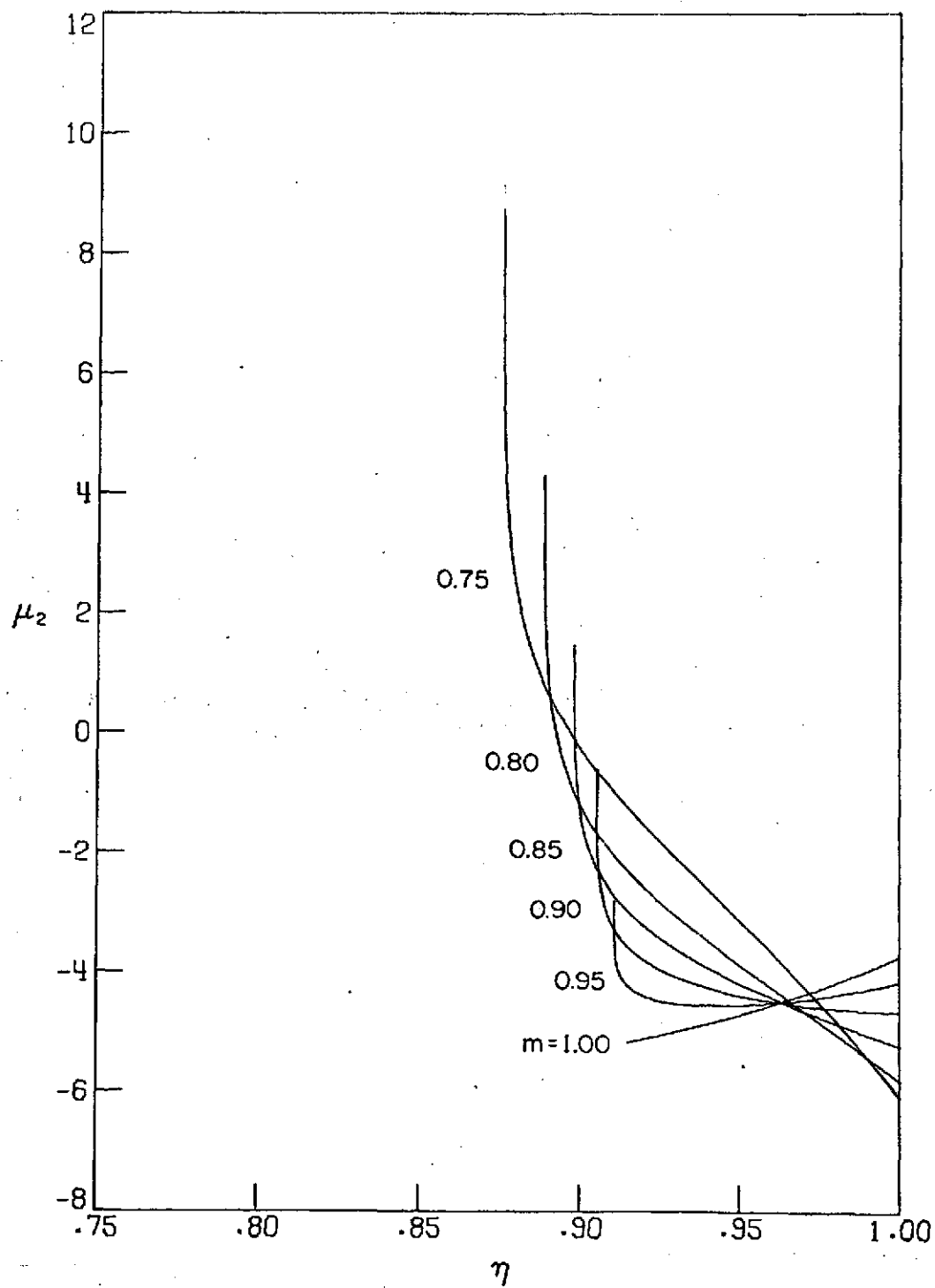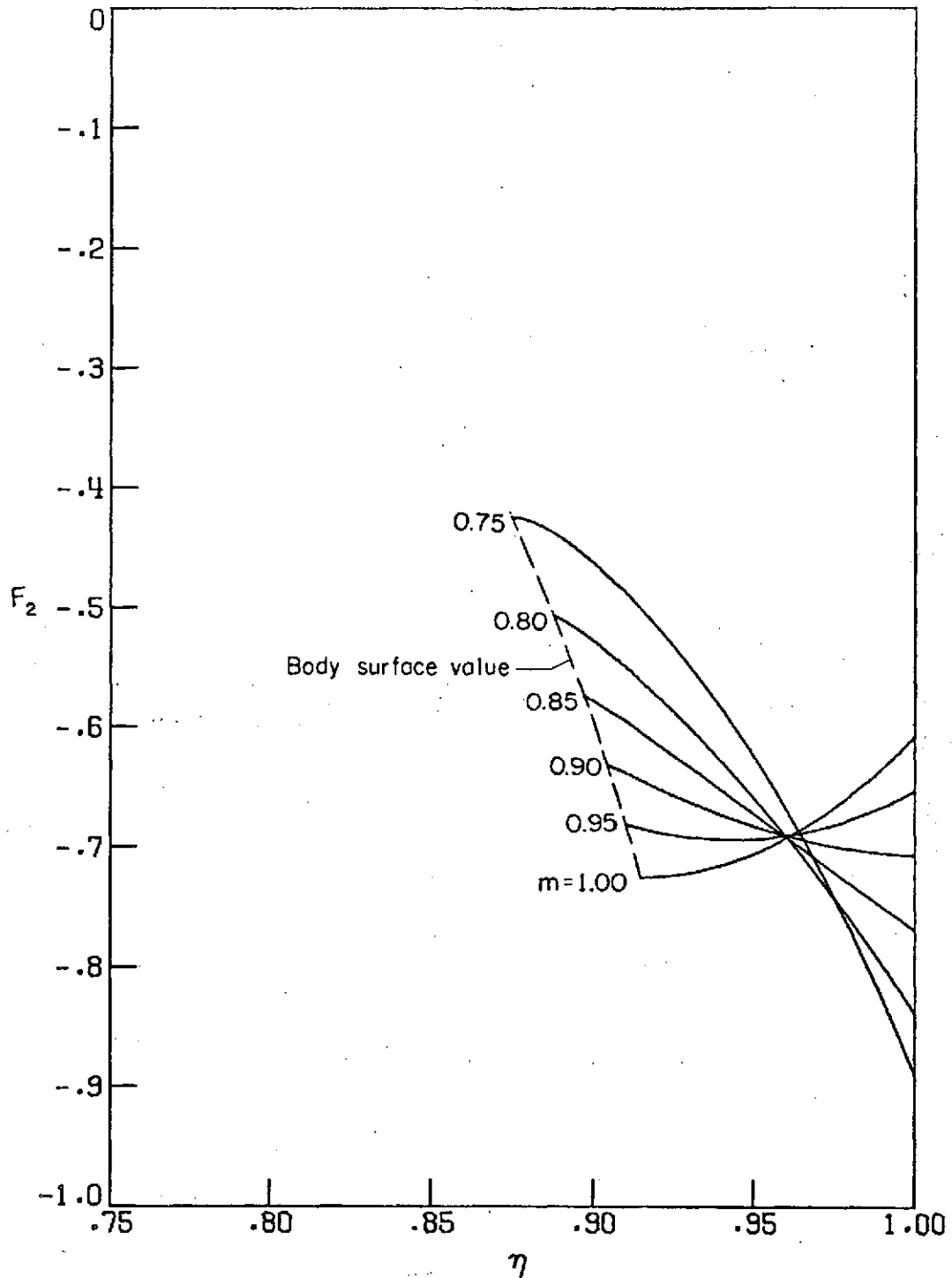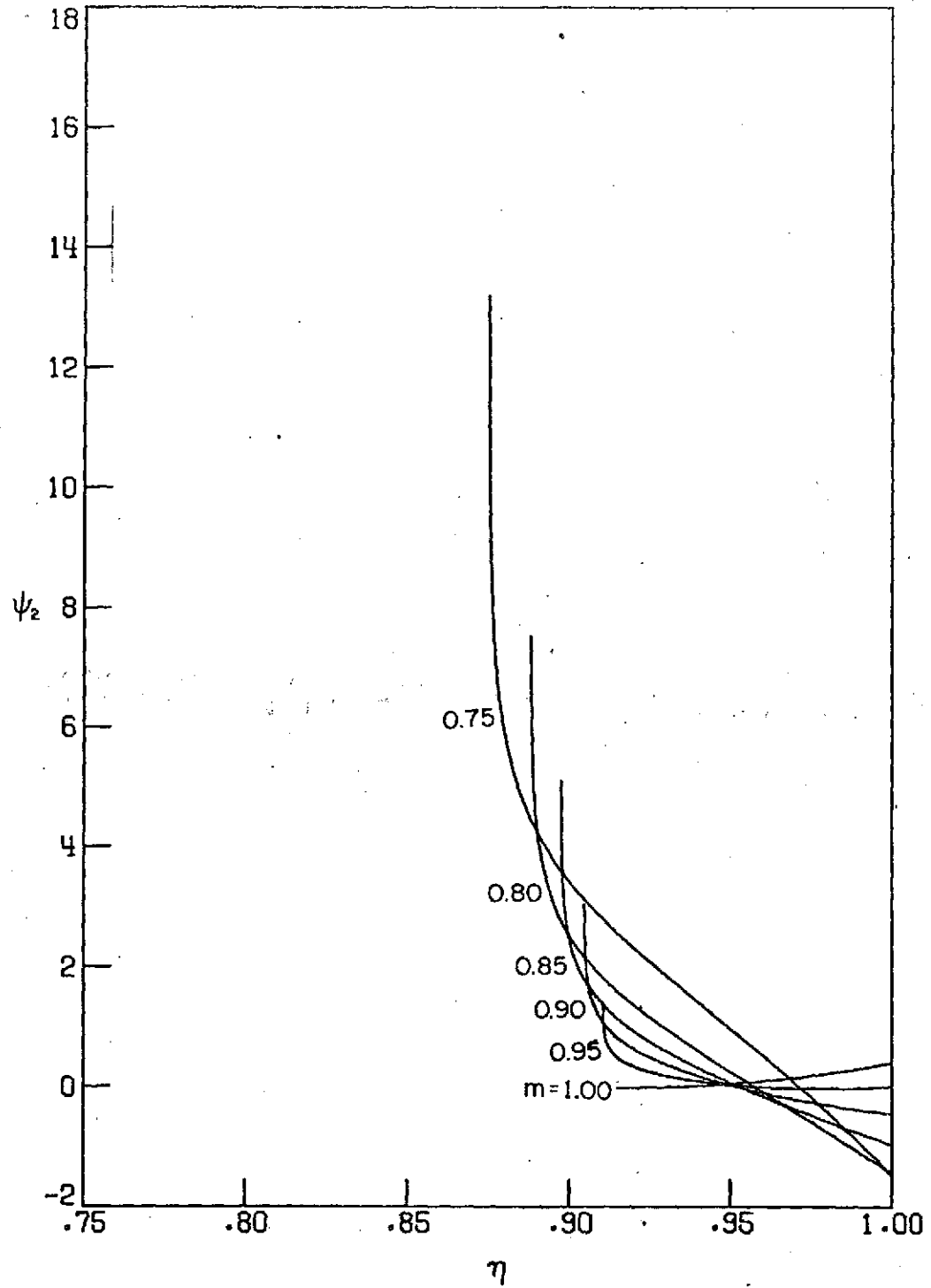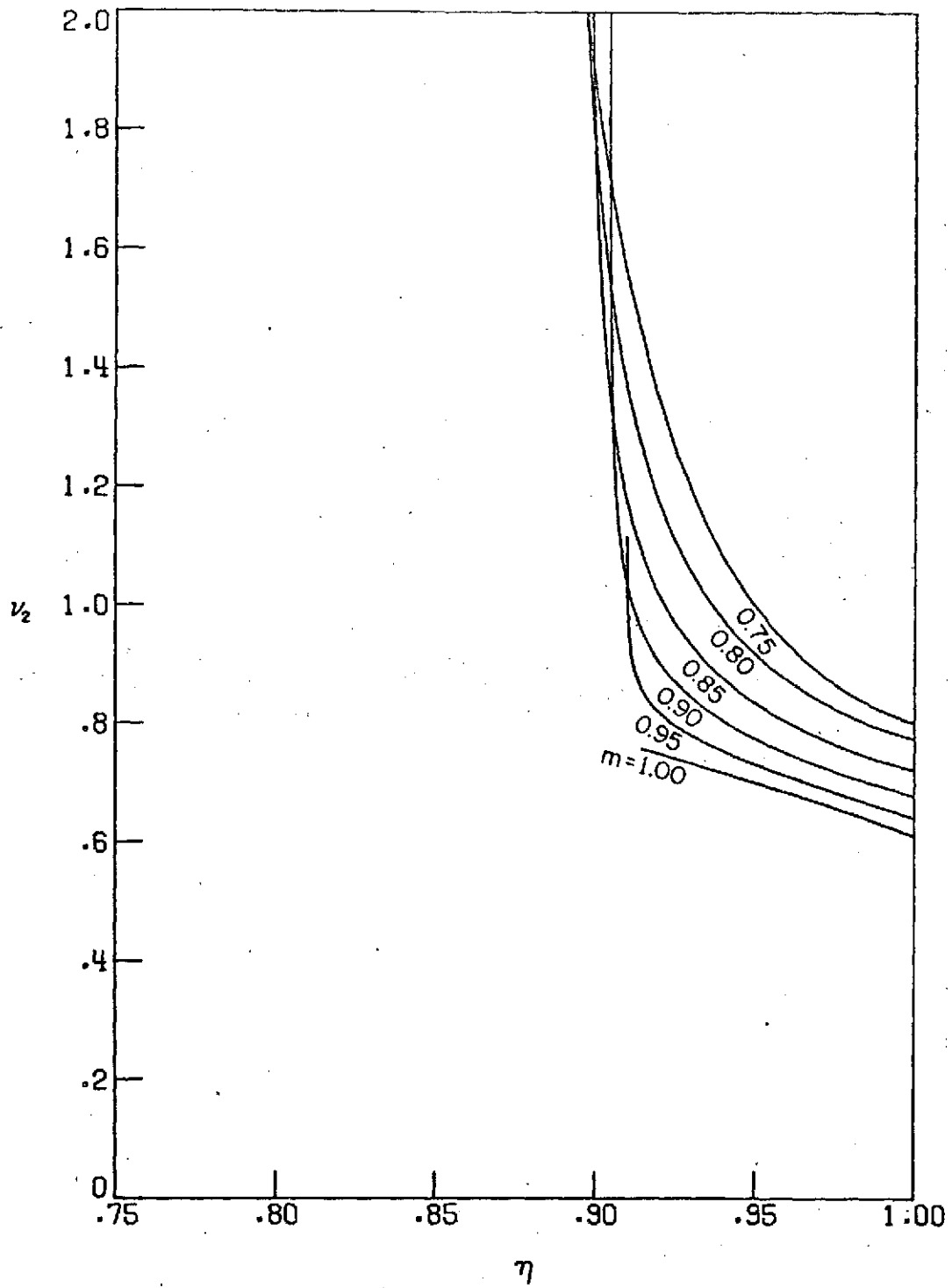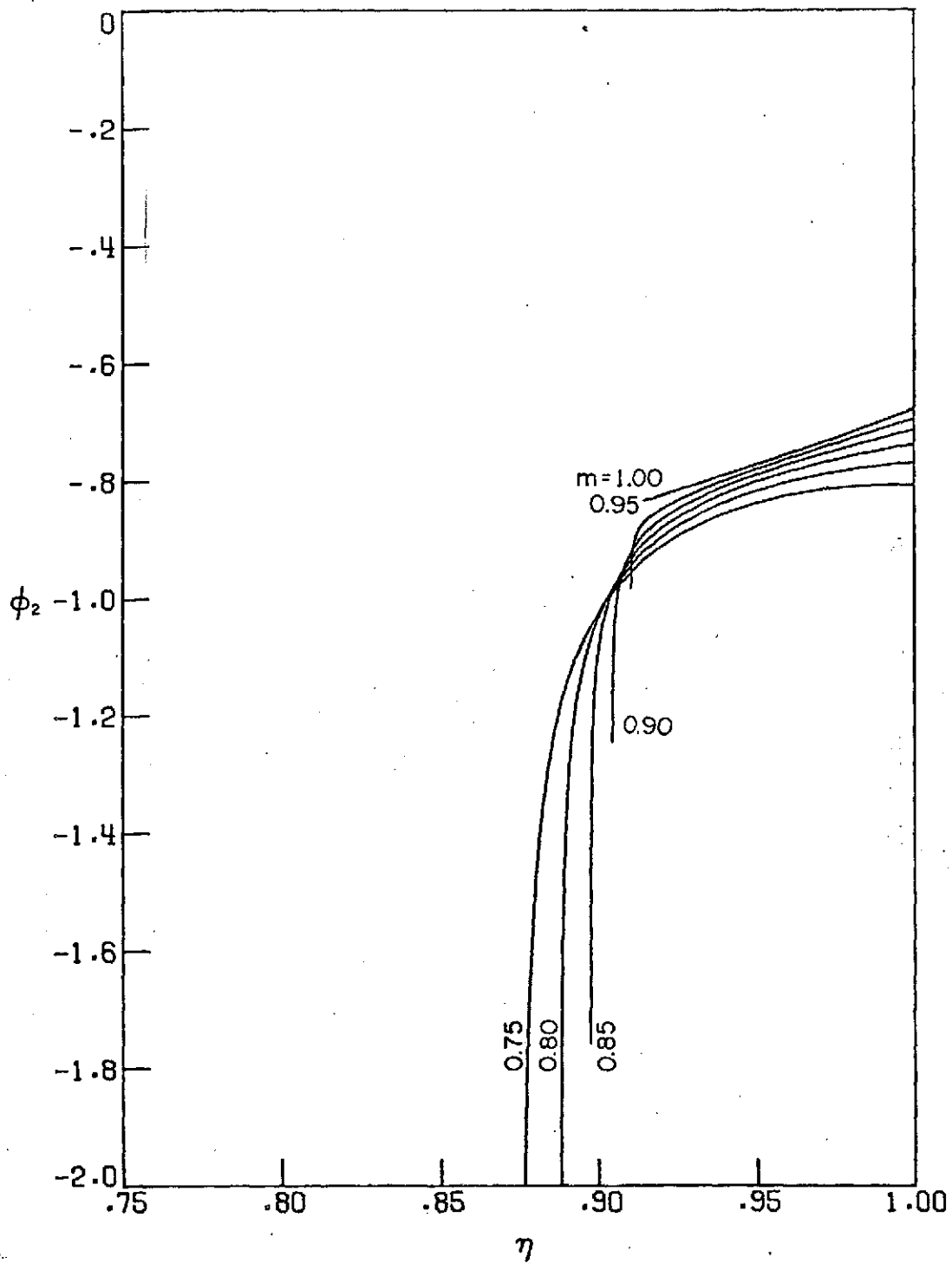
(b) Density function, $\psi_2(\eta)$.

Figure 10. Continued.

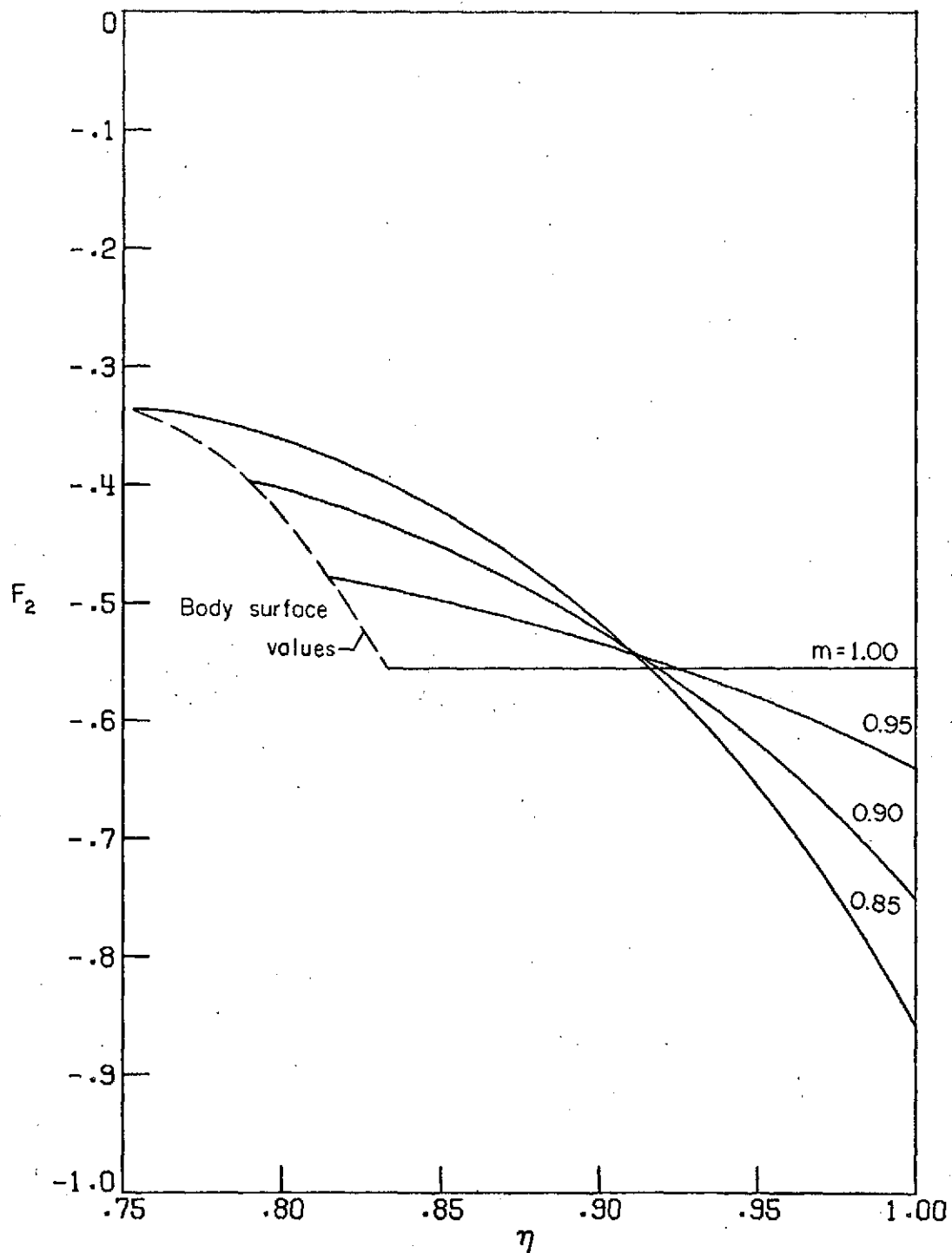(c) Longitudinal velocity function, $\nu_2(\eta)$.

Figure 10.   Continued.

(d) Lateral velocity function, $\phi_2(\eta)$.

Figure 10. Concluded.

(a) Pressure function, $F_2(\eta)$.

Figure 11. Order δ^2 similarity functions from the momentum-variable formulation for two-dimensional flow ($\sigma = 0$).

(b) Density function, $\psi_2(\eta)$.

Figure 11. Continued.

(c) Longitudinal momentum function, $\upsilon_2(\eta)$.

Figure 11. Continued.

(d) Lateral momentum function, $\mu_2(\eta)$.

Figure 11.   Concluded.

not improve on the results of the order-δ^2 velocity-variable
formulation in either quality or range of application, the
momentum-variable formulation of the flow equations has very
little advantage over the more conventional velocity-variable
formulation. It has, however, provided a useful check of
the numerical results.

The singularity at the body surface is thought to be an
entropy layer effect caused by the blunt nose of the body
for $m < 1$. The effect is confined to a very narrow region
since the very high curvature in the nose area (infinite at
$\bar{x} = 0$) reduces the body slope rapidly. For example, when
$m = .80$ and $\delta = .5$, the slope decreases from infinite to
less than 1.0 before $\bar{x}/\bar{\ell} = .006$.

As noted previously, Mirels (10, 16) recognized the
singularity at the body surface and avoided calculating the
longitudinal velocity function, which exhibits the singular
behavior. In addition, Mirels (10) developed an approximate
analytic solution which is valid at the surface and used it
to obtain surface values of the zeroth-order functions (see
Appendix, Section A). The attempt to extend the approximate
analytic solution to order δ^2 is also discussed in the
Appendix.

Van Dyke (29, p. 185) notes the same singular behavior
in a small disturbance solution at the surface for hypersonic
flow over a blunted wedge and observes that it occurs because

the zero-order solution "is not a valid first approximation in the entropy layer." He uses the method of matched asymptotic expansions to obtain a uniformly valid analytic solution for the blunted wedge. Adaptation of that method to the similarity solution problem for power-law bodies probably would extend the solutions to the body surface; but, the application is not straightforward since the similar solutions are not analytic and therefore do not give the order of the singularities which occur.

The effect of the singularity at the body surface, then, is to make the order-δ^2 solution inapplicable at the body surface except for the particular case $m = 1$, for which the body does not have a blunt nose. But, the singularity should not affect the solution away from the surface, where the similarity functions are of order unity, so long as the constant a_2 is correctly determined. Furthermore, the behavior of the order-δ^2 similarity function for the pressure (F_2) is quite regular all the way to the surface. Thus, the body surface pressure can be calculated using this function; however, the results must be suspect until checked against experiment or more exact results.

It is because of the singular behavior of the similarity functions that the numerical integration cannot proceed all the way to the body surface. Neither do the extrapolations follow the singular functions in giving values at the surface; so, the calculated surface values of these functions do not represent the actual values of the singular functions, which go to either plus or minus infinity at the surface. To the extent that they are useful for determining the value of a_2, the extrapolations can be considered as providing a limiting process for this constant.

D. Region of Validity of the Solutions

Three basic assumptions were required in order to obtain the hypersonic similarity solutions for power-law bodies: (1) the body is slender enough that terms of order δ^4 are negligible compared to unity; (2) the shock wave about the body is strong enough that terms of order $\varepsilon \equiv 1/\delta^2 M_\infty^2$ are negligible compared to unity; and (3) the Mach number is large compared to unity. (The second of these can be relaxed to $\varepsilon^2 \ll 1$ if the first-order solution in ε is applied.) However, even when these three assumptions are met overall for a particular power-law body, they generally are not all met in particular local regions.

The first assumption, $\delta^4 \ll 1$, is obviously violated in the nose region of all blunt bodies, such as the power-law

bodies for $m < 1$. Thus, the similarity solutions cannot be expected to apply at the nose of these bodies. But, the order-δ^2 solutions should be particularly useful in providing an improved solution a moderate distance behind the nose. As mentioned in the previous section, the violation of the slender body assumption by the blunt nose is also the cause of the singularities in the order-δ^2 functions at the body surface. Therefore, because the first assumption is violated at the nose, the order-δ^2 solution does not apply at the body surface.

The strong shock assumption, $\varepsilon \ll 1$, is violated wherever the shock wave angle approaches the Mach angle, $\sin^{-1}(1/M_\infty)$. Unless the Mach number is extremely large, the shock wave will become weak far downstream from the nose of the body, and the similarity solutions will not apply in that region.

The similarity solutions apply, then, in an intermediate region from behind the nose to somewhere in the vicinity of the base of the body, and, in the case of the order-δ^2 solution, only outside of the singularity at the body surface. The boundaries of this region depend on the Mach number and on the power-law exponent and slenderness of the body. Decreasing the Mach number or increasing the slenderness of the body tends to weaken the shock; decreasing the power-law exponent increases the nose bluntness but weakens the shock at the rear of the body. In any case, the boundaries of the

region in which the solutions apply are not sharply defined.
They depend on the accuracy required in the results of each
particular problem and must be ultimately determined by
comparison with experimental results.

E.   Comparison With Other Solutions

The only exact solutions available for comparison with the
similarity solutions are those for flow over cones and
wedges, corresponding to a power-law exponent of $m = 1$.
Since the zeroth-order and order-δ^2 similarity solutions do
not contain any Mach number dependence, the most appropriate
comparison is at the hypersonic limit, $M_\infty \to \infty$. (To include
Mach number effects the order-ϵ solution would have to be
used also.) Results from the similarity solutions, in terms
of the physical flow variables, are compared in Figure 12
with the exact solutions for flow over a range of wedge
angles at infinite Mach number. This flow, of course, is
uniform behind the straight oblique shock wave, as indicated
by the solutions for $m = 1$ in Figure 4, pages 66 - 69,
and Figures 10 and 11, pages 92 - 99. In Figure 13, results
from the similarity solutions are compared with the exact
solutions for flow over circular cones. Parts (a) of
Figures 12 and 13 show the variation of the shock wave angle
with the body surface angle, and include exact results from
references 24 and 25 for several Mach numbers in addition to

(a) Shock wave angle, θ_S.

Figure 12.   Comparison of Similarity Solution for m = 1
with Exact Solution for Flow Over a Wedge at
$M_\infty = \infty$.

(b) Pressure, $\bar{p}/\bar{q}_\infty$.

Figure 12. Continued.

(c) Magnitude and direction of the velocity vector.

Figure 12. Continued.

(d) Velocity components.

Figure 12.   Concluded.

(a) Shock wave angle.

Figure 13.   Comparison of Similarity Solution for m = 1
            with Exact Solutions for Flow Over a Circular
            Cone at $M_\infty = \infty$.

(b) Surface pressure, $\bar{p}_b/\bar{q}_\infty$.
Figure 13. Continued.

(c) Magnitude and direction of the velocity
vector at the body surface.

Figure 13.   Continued.

(d) Surface velocity components.

Figure 13. Concluded.

$M_\infty = \infty$. The similarity results are found from
$\tan \theta_s = \bar{R}' = \delta R'$, where $\delta = \dfrac{1}{2\eta_b f} = \dfrac{\tan \theta_b}{\eta_b}$, and R' is
found from equation (7) with $m = 1$. The other parts of
the figures show the variations with the body surface angle
of the pressure coefficient $\bar{p}/\bar{q}_\infty$, the velocity
$\bar{V}/\bar{u}_\infty = \sqrt{\bar{u}^2 + \bar{v}^2}/\bar{u}_\infty$, and the velocity components $\bar{u}/\bar{u}_\infty$
and $\bar{v}/\bar{u}_\infty$ in the uniform flow behind the shock wave (Figure
12) and at the body surface (Figure 13). These similarity
results are found from equations (8) with $m = 1$. The exact
results are found from the oblique shock relations in the
two-dimensional case and from the charts of reference 24 in
the axisymmetric case.

These Figures show that for $m = 1$ the zeroth-order
similarity solution agrees well with the exact solution for
body surface angles up to about $\theta_b = 12^\circ$, while the order-δ^2
solution agrees well up to body angles of about $\theta_b = 20^\circ$.
As can be seen at the bottom of the Figures, these cone or
wedge angles correspond to slenderness parameter values of
about $\delta \approx .2$ and $\delta \approx .4$. The similarity results for the
magnitude of the velocity show good agreement for even
larger body angles (Figures 12(c) and 13(c)). Since the
error in the velocity components is larger (Figures 12(d)
and 13(d)), it must come largely from error in predicting
the direction of the velocity vector. This error in
direction is shown in the upper part of Figures 12(c) and
13(c), where it is compared to the curves $\delta^2 \theta_b$ and $-\delta^4 \theta_b$.

These curves represent the order of error expected from neglecting terms of order δ^2 and of order δ^4, respectively. The error actually occurring is seen to be very close to that which was expected. It should be noted that this error in the direction of the velocity vector corresponds to an error in satisfying the boundary condition that there should be no flow through the body surface. That is, the velocity component normal to the surface, $\bar{v}_w = \bar{V} \sin\left[\tan^{-1}(\frac{v_b}{u_b}) - \theta_b\right]$, should be zero (Figure 3, p. 30). Figures 12(c) and 13(c) show that this boundary condition is satisfied to order δ^2 by the order-δ^2 similarity solution for $m = 1$.

In Parts (b) of Figures 12 and 13, the pressure coefficients are compared also with the Newtonian prediction: $\bar{p}/\bar{q}_\infty = 2 \sin^2\theta_b$. The Newtonian prediction is much more accurate for the conical flows (Figure 13(b)) than for the wedge flows (Figure 12(b)); however, even in the conical case the order-δ^2 similarity solution is closer to the exact solution for moderately small values of the similarity parameter, i.e. $\delta \leq 0.5$.

In Figure 14, the variation of the flow variables from the shock to the body is shown for three values of the power-law exponent, $m = .75$, $.85$ and 1.0. The pressure, density and velocity components, calculated from the axisymmetric zeroth-order and order-δ^2 similarity solutions, are shown at $\bar{x}/\bar{l} = .5$ for a similarity parameter value of

$\delta = 0.4$. The exact solution for a cone at Mach 20 with $\theta_b = 20^\circ$ (reference 25) is also shown in Figure 14(a) for comparison with the case $m = 1.0$. Although the conical bodies are not the same ($\theta_b = 20^\circ$ corresponds to $\delta = .3978$), the order-δ^2 similarity results agree well with the Mach 20 solution shown for all the variables except the density. As can be seen by the symbols representing the exact solution for $M_\infty \to \infty$ at the shock wave, the density is the only one of the flow variables that is much affected by the difference between $M_\infty = 20$ and $M_\infty \to \infty$. The similarity solutions for the density agree exactly with the infinite Mach number solution at the shock. The order-δ^2 solution for the other variables differ from the exact, infinite-Mach number solution at the shock by amounts which are of order δ^4, as expected from the approximation to the oblique shock relations used (equations (4)). On the other hand, the zeroth-order similarity solution is not accurate for a cone of this thickness; it is off by an amount of order δ^2, which is 16% for $\delta = .4$. Note that the zeroth-order results stop at $\eta = 1$, which is the zeroth-order shock wave location. The order-δ^2 results at the shock are given by equations (15); the integrated solution begins at $\eta = 1$, with the results in the region $1 < \eta < \eta_s$ given by the Taylor series expansion as discussed in Section III-C.

(a) Power-law exponent m = 1.0 (conical body).

Figure 14. Variation of Flow Variables from Body to Shock at $\bar{x}/\bar{l} = 0.5$ for Axisymmetric Flow with $\delta = 0.4$.

Zero-order similarity solution
Order-δ² similarity solution
Newtonian
Tangent-cone, $M_\infty = \infty$

(b) Power-law exponent m = 0.85.

Figure 14.   Continued.

(c) Power-law exponent m = 0.75.

Figure 14. Concluded.

For body power-law exponents other than $m = 1$ there is no exact solution available for comparison with the order-δ^2 solution. However, there are some simple empirical methods for estimating the pressure on general bodies. Two of these methods will be used for comparisons. One is the Newtonian law $C_p = 2 \sin^2\theta_b$. As discussed by Hayes and Probstein (1), it corresponds to the limits $\gamma \to 1.0$ and $M_\infty \to \infty$; but, it is widely used for more general hypersonic flows in this or modified form. The other empirical prediction is the tangent-cone method, which takes as the pressure at any point on a body the pressure on the cone having the same surface angle as the body point. This method also is most accurate for $M_\infty \to \infty$, since then the shock layer is very thin with little pressure change across it. Hayes and Probstein (1) give a thorough discussion of these two methods and their limitations. Only one limitation will be mentioned here: these methods give only the body surface pressure and are not complete flow field solutions, as are the similarity solutions.

The calculated flow fields for bodies having $m = .85$ and $m = .75$ are shown in Figures 14(b) and (c). In these cases the order-δ^2 solution is again a major correction to the zeroth-order solution. However, the singularities in some of the order-δ^2 similarity functions show up here at the body surface. Because of the singularities, the

order-δ^2 values of the density and the velocity components

are probably unrealistic close to the surface. Fortunately,

the pressure is well behaved all the way to the body surface,

so that surface pressure coefficients can be calculated.

The surface pressures calculated from the similar

solutions are seen in Figures 14(a), (b) and (c) to agree

fairly well with the empirical predictions of the Newtonian

and tangent-cone methods. However, as m goes from 1.0 to

0.85 to 0.75 the order-δ^2 similarity solution pressure

drops faster than the tangent-cone and Newtonian pressures,

so that the agreement becomes progressively worse. Whether

the similarity solution or the empirical methods give a

better representation of the actual pressure changes with body

power law must be determined by comparison with experiment

as in the following section.

F.   Comparison with Experimental Results

There is only a limited amount of useful experimental

data on the hypersonic flow fields about power-law bodies.

This data consists mainly of measured shock wave shapes and

surface pressure distributions for 3/4- and 2/3-power bodies

of a few different fineness ratios. In this section the

similarity solution predictions for shock wave shape and

surface pressure for axisymmetric bodies with power-law

exponent of m = 0.75 will be compared with the experimental

‌

results of Kubota (9) and Peckham (19). No comparison is
made with results for smaller power-law exponents since
valid order-δ^2 similarity solutions were not obtained in
those cases. Also, no comparisons are made with experimen-
tal total drag measurements (e.g. those of reference 22)
because of the uncertainty in calculating the skin friction
contribution.

Shock shape. Because the shock displacement constant
a_2 is so small, the order-δ^2 shock wave shape is only
slightly different from the zeroth-order shape, an example
of which is shown in Figure 1, page 13. For example,
$a_2 = .0582$ when $m = .75$ in axisymmetric flow (Figure 7,
page 78, $\sigma = 1$); thus, even for $\delta = 0.4$, the order-δ^2
term in equation (7) for the shock shape $\bar{R}/\bar{\ell}$ amounts to
only about .003 at the base of the body ($\bar{x}/\bar{\ell} = 1.0$). There-
fore the order-δ^2 shock wave shape cannot be expected to be
much closer to the experimentally measured shock shape than
is the zeroth-order shape.

The zeroth-order and order-δ^2 shock wave shape predic-
tions are compared to the shock shape data for $m = .75$
from references 9 and 19 in Figure 15. These data are pre-
sented in the correlation form used by Peckham (19) after a
suggestion by Hornung (26).

The chart contains the following plotted text and labels:

Vertical axis: Dimensionless shock radius, $\bar{R}/\bar{D}$ (values: 1, 10, 100)

Horizontal axis: Dimensionless axial coordinate, $\bar{x}/\bar{D}$ (values: 1, 10, 100, 1000)

Legend:

Experiment

	$\bar{D}/\bar{l}$	δ	f	
O	.0555	0.555	2.06	$M_\infty = 7.7$ (ref 9)
□	.00306	0.269	4.25	
◇	.0292	0.327	1.75	$M_\infty = 6.85$ (ref 19)
△	.0195	0.286	2.00	

Theory

— — Zero-order similarity solution

—·— Order-δ^2 similarity solution

Body surface

$$\frac{\bar{r}_b}{\bar{D}} = \left(\frac{\bar{x}_b}{\bar{D}}\right)^{.75}$$

15. Shock wave shape correlation for axisymmetric 3/4-power bodies.

The experimental data for the shock shapes are seen to correlate well with one another but to fall somewhat above the similarity solution predictions. This difference between experiment and theory is largely due to the difference in Mach numbers (6.85 and 7.7 for experiment, $M_\infty \to \infty$ for theory). It is comparable to the shift in shock location with Mach number for cones (Figure 13(a), page 109). The experimental results correlate together because their Mach numbers are relatively close. An additional cause for the difference between the experiment and theory is the outward displacement of the flow by the growth of the viscous boundary layer on the experimental bodies.

The effect of the order-δ^2 term in the similarity solution for the shock wave shape is seen in Figure 15 to increase as $\bar{x}/\bar{D}$ decreases. This is expected since small values of $\bar{x}/\bar{D}$ correspond either to small values of $\bar{x}/\bar{\ell}$ or to large values of $\bar{D}/\bar{\ell}$, that is, either to points near the nose of the body where the slope is larger or to bodies which are less slender and thus have larger δ values. Note that the agreement of experiment with theory is better in this region of smaller $\bar{x}/\bar{D}$ values, as would be expected since the shock location is closer to that for infinite Mach number for larger body slopes. The slope of Kubota's data for $\bar{D}/\bar{\ell} = .0555$ (circles in Figure 15) agrees very well with the slope of the order-δ^2 similarity solution;

this agreement in the slope on a log-log plot indicates good agreement of the power-law exponent of the physical shock wave shape.

Additional shock wave shape data from hypersonic flows over power-law bodies is presented by Freeman, Cash and Bedder (20) (m = .75, M_∞ = 8.8) and by Beaver (21) (m = .85, M_∞ = 7.0). Although they apparently correlate in the same way as the data in Figure 15, these data are not presented here because they fall in ranges of very large $\bar{x}/\bar{D}$ values, for which the order-δ^2 term of the shock wave shape equation is negligible. For these large $\bar{x}/\bar{D}$ values the strong shock assumption, corresponding to $\varepsilon \equiv 1/(M_\infty \delta)^2 << 1$, may not be satisfied. (See Section II-B). For example, $\varepsilon \approx .36$ for the 3/4-power bodies of reference 20. Thus the first-order solution in ε would have to be applied to obtain useful results.

Pressure distribution. The pressure distributions obtained by Kubota (9) and Peckham (19) are shown in Figure 16 for the same 3/4-power bodies as used for the shock wave shapes in Figure 15. In addition to the zeroth-order and order-δ^2 similarity solution predictions, the two empirical pressure distributions are presented. As seen in Figure 16, the similarity solutions as well as the two empirical methods give pressure distributions in good agreement with the experimental data for the three bodies having

Figure 16. Comparison of similarity solutions with experimental pressure distributions; m = .75 (Theory is for same values of δ as experiment; tangent-cone for same Mach number).

fineness ratios $f \equiv \bar{\ell}/2r_b(\bar{\ell})$ of about two. For these cases
the order-δ^2 similarity solution is very nearly the same as
the zeroth-order solution except at the front of the body.
The Newtonian prediction falls slightly higher than the
similarity solutions back of the nose region, but curves
representing these three methods are below the data points.
Since at hypersonic speeds the viscous boundary layer
tends to displace the flow outward, raising the pressure
above that which would occur for inviscid flow, the theore-
tical inviscid pressure levels are expected to fall slightly
below those actually measured. For example, by applying a
boundary layer displacement correction to the zeroth-order
similarity solution for the pressure on his fineness ratio
2.13 body, Kubota (9) obtained excellent agreement with his
experimental data (squares in Figure 16). Since the tangent-
cone pressure distribution falls slightly above the experi-
mental data for the three higher-fineness-ratio bodies, the
other methods are somewhat preferable for these cases.

It is in the case of the body having a fineness ratio
of nearly one, however, that a real difference between the
methods appears. In particular, the difference between the
zeroth-order and order-δ^2 pressure distributions becomes
substantial. The zeroth-order result lies above the
experimental data by an amount which increases rapidly
toward the front of the body. On the other hand, the order-δ^2

result lies below the data by an amount which, for most of the body, is only moderately larger than that for the finer bodies. This amount is on the order of the expected boundary layer displacement effect. It is only at the front of the body that the order-δ^2 result begins to diverge markedly from the experimental pressure distribution. Since the value of the slenderness parameter is $\delta = 0.555$ for this case*, it is not surprising that the order-δ^2 similarity solution should begin to fail as the body surface angle increases at the front of the body. This is about the same value of δ as the limit for good results in the wedge and cone cases (Figures 12 and 13, pages 105-112). The Newtonian method gives excellent agreement with the experimental data in this case, but this must be somewhat fortuitous in that no correction was made to account for the boundary layer displacement effect. The tangent-cone method again lies somewhat above the experimental data.

---

*Kubota's (9) value $\delta = .485$ shown with his data corresponds to $\delta\eta_b = .485$ as used herein.

CHAPTER V.   CONCLUSIONS

Beginning with the equations for conservation of mass, conservation of momentum, and conservation of energy for the inviscid, two-dimensional or axisymmetric adiabatic flow of an ideal gas, similarity solutions have been found which give the flow field to order-δ^2 about power-law bodies in the hypersonic limit $M_\infty \to \infty$, where δ is a body slenderness parameter. On the basis of this investigation the following conclusions can be made:

1. The order-δ^2 solutions are independent of the slenderness parameter δ. Thus the functions expressing the solutions are universal in that they apply for all values of δ for which $\delta^4 \ll 1$. The relations between these similarity functions and the physical flow variables are relatively simple.

2. For the purpose of obtaining the similarity solutions the flow equations can be formulated in terms of the longitudinal and lateral momenta as basic variables instead of the corresponding velocity components, and the similarity functions can be obtained. However, the expected advantage of avoiding singular behavior of the equations at the body surface does not materialize.

3. In the present formulations the value of a_2, the shock displacement constant in the order-δ^2 solution, goes

through plus and minus infinity at about $m = .817$ in the two-dimensional case and $m = .653$ in the axisymmetric case, where m is the body power-law exponent. Because the singularity does not correspond to actual flow conditions it must arise through the mathematical development. Since the singularity was not removed by any of the variations in solution procedure tried, the present results are limited to a range judged relatively free of effects from the singularity ($.85 \leq m \leq 1.0$ for two-dimensional flow, $.75 \leq m \leq 1.0$ for axisymmetric flow).

4. In comparisons with the exact solutions for inviscid flow over wedges and circular cones, the order-δ^2 similarity results give excellent agreement for δ less than about .4, corresponding to wedge or cone angles up to about 20°. Over an even larger range, the order-δ^2 surface pressure predictions were superior to the Newtonian pressure law. The order-δ^2 results were a significant improvement over the zeroth-order results for body angles greater than about 12°.

5. In comparisons with experimental shock wave shapes and surface pressure distributions for 3/4-power axisymmetric bodies, the order-δ^2 similarity solutions gave good results, considering that Mach number and boundary layer displacement effects are not included in the theory. For body fineness ratios near two, the effects of the order-δ^2 terms are significant only very near the body nose, whereas for a

fineness ratio near unity the order-δ^2 terms had a large effect over almost the entire body. These good results for the surface pressure were obtained despite the singular behavior of some other variables at the surface.

6. While the order-δ^2 similarity solutions were developed for the hypersonic limit $M_\infty \to \infty$, the derivation shows that they are compatible with the order-ε solutions of Kubota (9) and Mirels (16), where $\varepsilon \equiv 1/(M_\infty \delta)^2$. The order-$\varepsilon$ solutions introduce Mach number effects.

7. While all present results were obtained for no flow through the body surface as a boundary condition, it appears from the derivation that small amounts of blowing or suction through the wall could be easily accommodated.

8. It was noted that the correlation suggested by Hornung (26) for the shock wave shape and body pressure distribution can be applied exactly to all of the flow variables in the order-δ^2 similarity solution form. This finding suggests a method of correlating for future experimental data. The form of correlation also suggests a possible refinement of the derivation of the order-δ^2 similarity results, using the local body or shock wave slope as the small parameter.

BIBLIOGRAPHY

1. Hayes, Wallace D.; and Probstein, Ronald F.: <u>Hypersonic</u>
    <u>Flow Theory</u>. (Second edition). Academic Press,
    New York, 1966.

2. Taylor, G. I.: The Formulation of a Blast Wave by a
    Very Intense Explosion. Proc. Roy. Soc. London,
    Ser. A, Vol. 201, 1950, pp. 159-186.

3. Sakarai, Akira: On the Propagation and Structure of a
    Blast Wave, I. J. Phys. Soc. Japan, Vol. 8, no. 5,
    Sept. - Oct. 1953, pp. 662-669.

4. Sakarai, Akira: On the Propagation and Structure of a
    Blast Wave, II. J. Phys. Soc. Japan, Vol. 9, no. 2,
    March - April 1954, pp. 256-266.

5. Hayes, W. D.: On Hypersonic Similitude. Quart. of
    Appl. Math. Vol. 5, no. 1, April 1947, pp. 105-106.

6. Van Dyke, Milton, D.: A Study of Hypersonic Small-
    Disturbance Theory. NACA Rept. 1194, 1954.

7. Lees, L.: Inviscid Hypersonic Flow over Blunt Nosed
    Slender Bodies. GALCIT Hypersonic Research Project,
    Memo No. 31, Feb. 1956.

8. Lees, Lester; and Kubota, Toshi: Inviscid Hypersonic
    Flow over Blunt-Nosed Slender Bodies. J. Aero.
    Sci., Vol. 24, no. 3, March 1957, pp. 195-202.

9. Kubota, Toshi: Investigation of Flow around Simple
    Bodies in Hypersonic Flow GALCIT Hypersonic Res.
    Proj. Memo 40, June 25, 1957. Also, Inviscid Hyper-
    sonic Flow over Blunt-Nosed Slender Bodies. GALCIT
    Publication No. 417, 1957.

10. Mirels, Harold: Approximate Analytical Solutions for
    Hypersonic Flow over Slender Power Law Bodies. NASA
    TR R-15, 1959.

11. Sedov, L. I.: On Certain Unsteady Motions of a
    Compressible Fluid. Prikl. Mat. Mekh., Vol. 9, 1945,
    pp. 293-311. Transl. no. T-57, The Rand Corp.,
    Santa Monica, Calif., 1956, cited by Hayes and
    Probstein (1).

12. Sedov, L. I.: Propagation of Strong Blast Waves.
    Prikl. Mat. Mekh., Vol. 10, 1946, pp. 241-250, cited
    by Hayes and Probstein (1).

13. Grodzovskii, G. L.: Certain Peculiarities of the
    Flow around Bodies at High Supersonic Velocities. Izv.
    Akad Nauk SSSR, Otd. Tekhn. Nauk, no. 6, 1957, pp.
    86-92.(Transl. by Morris D. Friedman, Inc.)

14. Chernyi, G. G.: Introduction to Hypersonic Flow. (R. F.
    Probstein, transl. and ed.) Academic Press, New York,
    1961.

15. Stanyakovich, K. P.: Unsteady Motion of Continuous Media.
    (J. G. Adashko, transl., and M. Holt, ed.), Pergamon
    Press, New York, 1960.

16. Mirels, Harold: Hypersonic Flow over Slender Power-Law
    and Related Bodies. Advances in Applied Mechanics,
    Vol. VII, Academic Press, New York, 1962, pp. 1-54, 317-19.

17. Freeman, N. C.: Asymptotic Solutions in Hypersonic Flow:
    An Approach to Second-Order Solutions of Hypersonic
    Small Disturbance Theory. Research Frontiers in Fluid
    Dynamics (R. J. Seeger and G. Temple, eds.) Interscience
    Monographs and Texts in Physics and Astronomy, Vol. XV,
    John Wiley and Sons, 1965, pp. 284-307.

18. Sychev, V. V.: On the Theory of Hypersonic Flow over
    Blunt-Nosed Slender Bodies. Advances in Aeronautical
    Science, vol. 3 (Th. von Kármán, chmn. ed. comm.),
    Macmillan Co., New York, 1962, pp. 87-102.

19. Peckham, D. H.: Measurements of Pressure Distribution
    and Shock-Wave Shape on Power-Law Bodies at a Mach
    Number of 6.85. Aeronautical Research Council C.P.
    871, April 1965.

20. Freeman, N. C., Cash, R. F., and Bedder, D.: An
    Experimental Investigation of Asymptotic Hypersonic
    Flows. J. Fluid Mech., Vol. 18, no. 3, March
    1964, pp. 379-384.

21. Beavers, G. S.: Shock Wave Shapes on Hypersonic
    Axisymmetric Power-Law Bodies. AIAA J., Vol. 7,
    no. 10, Oct. 1969, pp. 2038-2040.

22. Spencer, Bernard, Jr., and Fox, Charles H., Jr.:
    Hypersonic Aerodynamic Performance of Minimum-Wave-
    Drag Bodies. NASA TR R-250, 1966.

23. Townsend, James C.: Hypersonic Aerodynamic Characteristics of a Family of Power-Law, Wing-Body Configurations. NASA TN D-7427, 1973.

24. Equations, Tables, and Charts for Compressible Flow. NACA Report 1135, 1953.

25. Sims, Joseph L.: Tables of Supersonic Flow around Right, Circular Cones at Zero Angle of Attack. NASA SP-3004, 1964.

26. Hornung, H. G.: Inviscid Flow over Plane Power Law Bodies. J. Fluid Mech., vol. 27, no. 2, Feb. 1967, pp. 315-336.

27. Ashby, George C., Jr.: Longitudinal Aerodynamic Performance of a Series of Power-Law and Minimum Drag Bodies at Mach 6 and Several Reynolds Numbers. NASA TM X-2713, August 1974.

28. Ashby, George C., Jr.; and Harris, Julius, E.: Boundary-Layer Transition and Displacement-Thickness Effects on Zero-Lift Drag of a Series of Power-Law Bodies at Mach 6. NASA TN D-7723, September 1974.

29. Van Dyke, Milton: Perturbation Methods in Fluid Mechanics. Academic Press, New York, 1964.

30. Van Dyke, Milton: Extension, Analysis, and Improvement of Perturbation Series. Tenth Naval Hydrodynamics Symp., M.I.T., Cambridge, MA, June 27, 1974.

APPENDIX.   ASYMPTOTIC SOLUTION IN TERMS OF
STREAM FUNCTIONS

A.   Stream Function Formulation

This Appendix describes the development of an asymptotically valid analytic solution to the flow equations in terms of a similarity-function form of the stream function.   The solution is basically the zeroth-order solution of Mirels (10,16) with order-δ^2 terms added.   It is developed from the velocity-variable formulation, which Mirels used, but the results can be easily related to the momentum-variable formulation also.

By definition, the stream function must satisfy the continuity equation (3), which may be rewritten

$$\frac{\partial}{\partial x} [\rho(1 + \delta^2 u)] + \frac{\partial}{\partial r} (\rho v) + \sigma \frac{\rho v}{r} = 0.$$

If

$$\rho(1 + \delta^2 u) = \frac{1}{r^\sigma} \frac{\partial \hat{\psi}}{\partial r}$$

and

$$\rho v = - \frac{1}{r^\sigma} \frac{\partial \hat{\psi}}{\partial x}$$

(A1)

then $\hat{\psi}(x,r)$ is a stream function.   It can be put into the similarity form

134

135

$$\hat{\psi}(\xi,\eta) = \frac{\theta_o(\eta)}{1+\sigma}\,\xi^{(1+\sigma)m} + \delta^2 B\theta_2(\eta)\xi^j \tag{A2}$$

where the zeroth-order term was given by Mirels (10) and the constants B and j in the order-δ^2 term are to be determined by comparison with the similarity form of the flow variables (equation (8)). Putting the stream function defining relations (A1) into similarity form (using equation (A2) and the chain rule equations (9)):

$$\rho(1+\delta^2 u) = \frac{\theta_o'}{(1+\sigma)\eta^\sigma} + \delta^2 B\,\frac{\theta_2'}{\eta^\sigma}\,\xi^{j-(1+\sigma)m}$$

and

$$\rho v = -\left[\theta_o - \frac{\eta}{1+\sigma}\theta_o'\right]\frac{m}{\eta^\sigma}\,\xi^{-(1-m)} - \delta^2 B\left[\frac{j}{m}\theta_2 - \eta\theta_2'\right]\frac{m}{\eta^\sigma}\,\xi^{j-(1+\sigma m)} \tag{A3}$$

The comparable relations from equations (8), omitting the order-ε terms, are

$$\rho(1+\delta^2 u) = \psi_o + \delta^2(\psi_2 + \nu_o\psi_o)m^2\xi^{-2(1-m)} + 0(\delta^4)$$

and

$$\rho v = \psi_o\phi_o m\xi^{-(1-m)} + \delta^2(\phi_o\psi_2 + \psi_o\phi_2)m^3\xi^{-3(1-m)} + 0(\delta^4) \tag{A4}$$

Comparing these two sets of equations, the exponent in the order-δ^2 term of (A2) must be $j = (3 + \sigma)m - 2$, and the similarity functions are related by the equations

$$\psi_o = \frac{\theta_o'}{(1+\sigma)\eta^\sigma} \quad , \qquad \psi_o\phi_o = \frac{1}{\eta^\sigma}\left(\frac{\eta\theta_o'}{1+\sigma} - \theta_o\right)$$

$$\psi_2 + \nu_o\psi_o = \frac{B\theta_2'}{m^2\eta^\sigma} \tag{A5}$$

$$\phi_o\psi_2 + \psi_o\phi_2 = \frac{B}{m^2\eta^\sigma}\left[\eta\theta_2' - \frac{(3+\sigma)m-2}{m}\theta_2\right]$$

The boundary condition on the stream function similarity functions are

$$\theta_o(\eta_b) = 0, \quad \theta_o(1) = 1$$

$$\tag{A6}$$

$$\theta_2(\eta_b) = 0, \quad \theta_2(1) = 1$$

Solving equations (A5) for the constant B and evaluating the similarity functions at $\eta = 1$, using equations (46) and (A6), gives

$$B = -\frac{2m^2}{\gamma-1}a_2$$

so that

$$\hat{\psi}(\xi,\eta) = \frac{\theta_o}{1+\sigma}\xi^{(1+\sigma)m} - \delta^2\frac{2a_2}{\gamma-1}\theta_2 m^2\xi^{(3+\sigma)m-2} \tag{A7}$$

In addition, equations (A5) can be solved for

$$\psi_o = \frac{\theta_o'}{(1+\sigma)\eta^\sigma} \quad , \quad \phi_o = \eta - (1+\sigma)\frac{\theta_o}{\theta_o'}$$

$$\psi_2 = -\frac{1}{\eta^\sigma}\left[\frac{\nu_o}{1+\sigma}\theta_o' + \frac{2}{\gamma-1}a_2\theta_2'\right] \tag{A8}$$

$$\phi_2 = \eta\nu_o - \frac{1+\sigma}{\theta_o'}\left\{\nu_o\theta_o + \frac{2a_2}{\gamma-1}\left[(1+\sigma)\frac{\theta_o\theta_2'}{\theta_o'} - \frac{(3+\sigma)m-2}{m}\theta_2\right]\right\}$$

Or, conversely,

$$\theta_o = (\eta - \phi_o)\psi_o\eta^\sigma$$

$$\tag{A9}$$

$$\theta_2 = -\frac{(\gamma-1)m\eta^\sigma}{2a_2[(3+\sigma)m-2]}[(\eta - \phi_o)\psi_2 + \psi_o(\eta\nu_o - \phi_2)]$$

As Mirels (10) showed for the zeroth-order case, the pressure can be related to the stream function by using the energy equation. Defining an entropy function $\omega \equiv p/\rho^\gamma$, the energy equation (3) in terms of the stream function becomes

$$\frac{\partial\hat{\psi}}{\partial r}\frac{\partial\omega}{\partial x} - \frac{\partial\hat{\psi}}{\partial x}\frac{\partial\omega}{\partial r} = 0. \tag{A10}$$

This has as a solution (to order δ^2)

$$\omega = \frac{2}{\gamma+1}\left(\frac{\gamma-1}{\gamma+1}\right)^\gamma \theta_o^{-\beta}\left[m^2\xi^{-2(1-m)} + \delta^2\frac{2a_2}{\gamma-1}(1+\sigma)\beta\frac{\theta_2}{\theta_o}m^4\xi^{-4(1-m)}\right] \tag{A11}$$

where the zeroth-order term is Mirels' zeroth-order solution (10) and the order-δ^2 term was found by trial and error. The parameter β is defined by $\beta = \dfrac{2(1-m)}{(1+\sigma)m}$ and varies from zero to one as m varies from one to $\dfrac{2}{3+\sigma}$, the lower limit for similarity solutions. The stream function expression for the pressure can be found from the entropy function, since the expression for the density is already given by equations (A8). Thus the density and pressure are

$$\rho^\gamma = \psi_o^\gamma [1 + \delta^2 \gamma \frac{\psi_2}{\psi_o} m^2 \xi^{-2(1-m)} + 0(\delta^4)]$$

$$= \left[\frac{\theta_o'}{(1+\sigma)\eta^\sigma}\right]^\gamma \left[1 - \delta^2 \gamma (\nu_o + \frac{2(1+\sigma)}{\gamma-1} a_2 \frac{\theta_2'}{\theta_o'})\right] + 0(\delta^4)$$

and

$$p = \rho^\gamma \omega$$

$$= \frac{2}{\gamma+1} (\frac{\gamma-1}{\gamma+1})^\gamma (\frac{1}{1+\sigma})^\gamma \frac{(\theta_o')^\gamma}{\eta^{\sigma\gamma}\theta_o^\beta} m^2 \xi^{-2(1-m)} \qquad \text{(A12)}$$

$$\times \left\{1 + \delta^2 \left[\frac{2(1+\sigma)}{\gamma-1} a_2 (\beta \frac{\theta_2}{\theta_o} - \gamma \frac{\theta_2'}{\theta_o'}) - \gamma\nu_o\right] m^2 \xi^{-2(1-m)}\right\} + 0(\delta^4)$$

On comparison with the similarity form of the normalized pressure (equation (8)), this equation gives the relations

$$F_o(\eta) = \frac{2}{\gamma+1} \left(\frac{\gamma-1}{\gamma+1}\right)^\gamma \left(\frac{1}{1+\sigma}\right)^\gamma \frac{(\theta_o')^\gamma}{\eta^{\sigma\gamma}\theta_o^\beta}$$

and

$$F_2(\eta) = \left[\frac{2(1+\sigma)}{\gamma-1} a_2 \left(\beta \frac{\theta_2}{\theta_o} - \gamma \frac{\theta_2'}{\theta_o'}\right) - \gamma\nu_o(\eta)\right] F_o(\eta)$$

(A13)

where, again, the zeroth-order function is Mirels'.

B. Zeroth-Order Approximate Solution

In reference 10, Mirels shows that, using equations (A8) and (A13) for ψ_o, ϕ_o, and F_o, the zeroth-order lateral momentum equation (11) can be approximated for $\theta_o(\eta) \ll .1$ by

$$\frac{\theta_o''}{\theta_o'} - \frac{\beta}{\gamma}\frac{\theta_o'}{\theta_o} - \frac{\sigma}{\eta} \approx 0$$

(A14)

He also gives the solution to this approximation:

$$\theta_o(\eta) \approx K_o \left(\eta^{1+\sigma} - \eta_b^{1+\sigma}\right)^{\frac{\gamma}{\gamma-\beta}}$$

(A15)

where

$$K_o = \left[\frac{\gamma+1}{2} \left(\frac{\gamma+1}{\gamma-1}\right)^\gamma \left(\frac{\gamma-\beta}{\gamma}\right)^\gamma F_o(\eta_b)\right]^{\frac{1}{\gamma-\beta}}$$

(A16)

Mirels uses this solution to make an improved approximation for the lateral momentum equation and an improved approximate solution

$$\theta_o(\eta) \approx K_o(\eta^{1+\sigma} - \eta_b^{1+\sigma})^{\frac{\gamma}{\gamma-\beta}} [1 + \frac{\beta}{2(2\gamma-\beta)} \frac{\eta_b^{1-\sigma}}{F_o(\eta_b)} \theta_o] \qquad (A17)$$

Putting this second approximation back into equations (A8) and (A13), he obtains the relations

$$\eta - \phi_o \approx \frac{\gamma-\beta}{\gamma} \frac{\eta^{1+\sigma} - \eta_b^{1+\sigma}}{\eta^{\sigma}} [1 - \frac{\beta\eta_b^{1-\sigma} \theta_o}{2(2\gamma-\beta)F_o(\eta_b)}]$$

$$\psi_o \approx \frac{\gamma}{\gamma-\beta} K_o(\eta^{1+\sigma} - \eta_b^{1+\sigma})^{\frac{\beta}{\gamma-\beta}} [1 + \frac{\beta\eta_b^{1-\sigma} \theta_o}{(2\gamma-\beta)F_o(\eta_b)}] \qquad (A18)$$

$$F_o \approx F_o(\eta_b) + \frac{\beta}{2} \eta_b^{1-\sigma} \theta_o$$

Using equations (A8) again, he obtains from these relations:

$$(\frac{\eta_b}{\eta})^{1+\sigma} \approx 1 - \frac{\gamma}{\gamma-\beta} (\frac{\eta-\phi_o}{\eta})[1 + \frac{\beta(\eta-\phi_o)}{2(2\gamma-\beta)} \frac{\psi_o}{F_o} (\frac{\eta_b}{\eta})^{1-\sigma}]$$

and $\qquad\qquad\qquad\qquad\qquad\qquad\qquad\qquad\qquad\qquad$ (A19)

$$F_o(\eta_b) \approx F_o(\eta) - \frac{\beta}{2} \eta_b(\eta-\phi_o)\psi_o(\frac{\eta}{\eta_b})^{\sigma}$$

These relations are correct to the order of θ_o^2 and therefore apply near the body surface, where $\theta_o(\eta_b) = 0$ (equation (A6)). Using (A15), terms of order θ_o^2 are less than terms of order-δ^2 when $\eta-\eta_b < \dfrac{(\delta/K_o)^{\frac{\gamma-\beta}{\gamma}}}{(1+\sigma)\eta_b^{\sigma}}$. At the point where equations (A19) are used in the numerical solution to determine the values of η_b and $F_o(\eta_b)$, the

integration has come so close to the body that

$\eta - \eta_b \ll \dfrac{(\delta/K_o)^{\frac{\gamma-\beta}{\gamma}}}{(1+\sigma)\eta_b^{\sigma}}$. Thus the error in relations (A17) to

(A19) at that point is much less than the order-δ^4 error

of the equations being integrated, and the zeroth-order

approximate solution for F_o, ψ_o and ϕ_o (relations (A18))

may be used the rest of the way to the body surface.

The zeroth-order longitudinal momentum equation can be

used to obtain an approximate solution for $v_o(\eta)$ in the

region near the body. Noting the implication for $v_o(\eta_b)$

from the body boundary conditions (equation (22)), a trial

solution is made in the form

$$v_o(\eta) = D\,\frac{F_o(\eta)}{\psi_o(\eta)}$$

$$v_o'(\eta) = D\,\frac{F_o}{\psi_o}\left(\frac{F_o'}{F_o} - \frac{\psi_o'}{\psi_o}\right) \tag{A20}$$

Putting this into the longitudinal momentum equation (11)

gives

$$D(\eta - \phi_o)\left(\frac{F_o'}{F_o} - \frac{\psi_o'}{\psi_o}\right) + \eta\,\frac{F_o'}{F_o} + 2\left(\frac{1-m}{m}\right)(D + 1) = 0.$$

Solving for D and substituting from equations (A8) and

(A13):

$$D = -\frac{\beta + \frac{\gamma}{1+\sigma}\left(\frac{\theta_o''}{\theta_o'} - \frac{\beta}{\gamma}\frac{\theta_o'}{\theta_o} - \frac{\sigma}{\eta}\right)\eta}{\beta\left(\frac{\gamma-1}{\gamma}\right) + (\gamma-1)\left(\frac{\theta_o''}{\theta_o'} - \frac{\beta}{\gamma}\frac{\theta_o'}{\theta_o} - \frac{\sigma}{\eta}\right)\frac{\theta_o}{\theta_o'}}$$

But D is a constant, so an approximation must be made; adopting Mirels' first approximation (equation (A14)) reduces D to $-\frac{\gamma}{\gamma-1}$, so that the relation (A20) for ν_o becomes (to order θ_o, $\theta_o \ll 1$)

$$\nu_o(\eta) = -\frac{\gamma}{\gamma-1}\frac{F_o(\eta)}{\psi_o(\eta)} = -\frac{2}{\gamma^2-1}\left(\frac{\gamma-1}{\gamma+1}\right)^{\gamma}\left(\frac{1}{1+\sigma}\right)^{\gamma}\frac{(\theta_o')^{\gamma}}{\eta^{\sigma\gamma}\theta_o^{\beta}} \qquad \text{(A21)}$$

C. Order-δ^2 Functions

In principle, expressions (A8), (A13) and (A21) could be put into the order-δ^2 lateral momentum equation (13) to obtain a first-order differential equation for the order-δ^2 similarity stream function θ_2. However, the equation would contain a very large number of terms and would require a considerable amount of approximation to be made in order to reduce it to a form for which a solution could be obtained. The approximation process is complicated by the facts that θ_o occurs to non-integral powers and that many terms contain β, which itself takes on very small values in the range of interest. Considering that the solution is only to be applied in a very small region near the body surface and that θ_2 is already of order-δ^2, the additional

accuracy which might be obtained probably does not justify the additional effort required to produce an approximate solution in this way. Instead, the simple linear extrapolation techniques described in Section III.B are used to carry the order-δ^2 similarity functions the short distance to the body surface.